Interactions in Collective Fish Swimming

Intesaaf Ashraf

Université Sorbonne Paris Cité

Thèse de doctorat

de l'Université Sorbonne Paris Cité

Préparée à l'Université Paris Diderot

Ecole doctorale [n°564 : Physique en Île-de-France]

Laboratoire de physique et mécanique des milieux hétérogènes (PMMH) UMR 7636

Interactions in Collective Fish Swimming

Auteur : ASHRAF Intesaaf

Spécialité doctorale "Mécanique des Fluides"

Directeurs de thèse : Ramiro Godoy-Diana & Benjamin Thiria

Présentée et soutenue publiquement par

ASHRAF Intesaaf

le 4 Avril 2018, PMMH

Jury :

Président du jury: José Halloy (Professseur, Université Paris Diderot)
Rapporteur: Charlotte K. Hemelrijk (Professseur, University of Groningen)
Rapporteur: Christian Jost (Maitre de Conférences - Université Toulouse III)
Examinateur: Francisco Huera-Huarte (Professseur, Universitat Politécnica de Catalunya)
Directeur de thèse: Ramiro Godoy-Diana (Chargé de recherches, CNRS, ESPCI Paris)
Directeur de thèse (invité): Benjamin Thiria (Maitre de Conférences, Université Paris Diderot, ESPCI Paris)

Titre : Interactions des poissons en nage collective.

Résumé : Le banc de poisson est un exemple typique d'auto organisation de groupe. Ce système implique des interactions complexes d'individus dans un milieu fluide et fait l'objets de nombreuses recherches multidisciplinaire théoriques, numériques ou expérimentales. Plusieurs hypothèses ont déjà été formulées pour expliquer la formation de ces bancs: la fuite face à des prédateurs, l'optimisation dans la recherche de nutriments ou encore l'économie d'énergie. Dans la plupart des recherches, les travaux se concentrent sur ce que les poissons devraient faire pour optimiser une tâche plutôt que sur des observations directes. Cela conduit à des différences dans les conclusions issus du travail des physiciens théoriciens ou ingénieurs avec ce qui est observé dans la nature par les biologistes.

Dans ce travail, nous apportons, basées sur des observations directes tetra Hemigrammus bleheri, de nouveaux éléments sur les interactions des poissons lors de la nage collective comme le phénomène de burst-and-coast ou la synchronisation des cinématiques entre plus proches voisins.

Enfin, nous démontrons que les bancs de Hemigrammus bleheri privilégient la configuration en ligne plutôt que celle en diamant souvent mise en avant dans la littérature.

Mots clefs : Economie d'énergie, Nage collective, Poisson.

Title : Interactions in Collective Fish Swimming

Abstract : Fish school is the classical example of self-emergent system of collective behavior in animal locomotion, which involves complex interactions between individuals and has drawn fascination of numerous multidisciplinary analytical, numerical and experimental researches. Various reasons have been cited for the formation of fish school such as evading predators, enhancing foraging success or advantage in terms of energy consumption. However, most of the works primary focus on what fish should do in a school instead of what fish really do, leading to discrepancies between the works of theoretical physicists and engineers and what is observed in the nature by biologists. This thesis is an attempt to bridge this gap.

In this work, we investigate the swimming dynamics of the red nose tetra fish Hemigrammus bleheri in a controlled experiment. The tetra fish are observed to swim using a burst-and-coast strategy, which could be for the purpose of active flow sensing.We also address the case of red nose tetra fish Hemigrammus bleheri swimming in groups in a uniform flow, giving special attention to the basic interactions and cooperative swimming of a single pair of fish. We first bring evidence of synchronization of the two fish, where the swimming modes are dominated by "out of phase" and "in phase" configurations. At last, we challenge the

question of energy benefit by discussing the channelling effect versus the vortex interaction hypothesis (Weihs, Nature 241:290-291, 1973) about diamond shape. We provide the experimental observation that fish prefer inline formation or phalanx formation over the diamond shape while swimming in a school.

Keywords : Collective fish, Fish, energy saving.

Contents

Abstract **i**

1 Introduction **1**
1.1 Fish swimming 4
1.1.1 Body and caudal fin swimming 6
1.1.2 Median and/or paired fin swimming (MPF) 10
1.2 Information transfer in the collective swimming of fish 12
1.3 Collective fish swimming 14
1.4 Objective and outlines of the thesis 26

2 Material and methods **27**
2.1 Water channel 27
2.2 Animals and housing 29
2.3 Image acquisition 29
2.3.1 Automated two-dimensional (2D) planar tracking of fish . . 30
2.3.2 Three-dimensional (3D) tracking of fish 30
2.4 Fish kinematics 36
2.4.1 Frequency and amplitude 36
2.4.2 Phase velocity 37
2.4.3 Burst-and-coast period 37
2.4.4 Internal frequency 37
2.5 Data statistics 39
2.6 Experimental procedure 39

3 Burst and coast kinematics in steady swimming in the fish *Hemigrammus bleheri* **40**
3.1 Abstract 40
3.2 Introduction 41
3.3 Experimental procedure 43
3.4 Results 43
3.5 Discussion 45

4 Synchronisation and collective swimming patterns in fish *Hemigrammus bleheri* **49**
4.1 Abstract 49
4.2 Introduction 50
4.3 Results 52
4.3.1 Two fish experiment 52
Spatial pattern 54
Synchronisation 55

4.3.2 Three fish experiment 60
4.4 Discussion 63
4.5 Concluding remarks 67

5 Simple phalanx pattern leads to energy saving in cohesive fish schooling 68
5.1 Abstract 68
5.2 Introduction 69
5.3 Results 72
5.4 Discussion 78

6 Conclusion and perspective 81

A Supplementary materials to the paper "Synchronisation and collective swimming patterns in fish *Hemigrammus bleheri*" 87

References 96

Chapter 1

Introduction

Collective motion is defined as the coordinated motion of groups of animals [1]. It is one of the most common and widespread animal behaviours observed in nature. It can be observed in school of fishes, swarm of insects, flock of birds, colony of ants or herd of mammals. Some of the observed collective motions are shown in Fig. 1.1. The group size can vary from a few individuals to thousands. Complex social interactions are hidden behind these collective motions. Various factors, such as the needs of each species, internal health of individuals, predation level, ways of life and food resources, lead to different levels of cohesive organisation [2, 3]. Collective motion can be due to the presence of one or more leaders or just because of a bottom-up, self-organised and self-emergent group driven by phenomenological behavioural rules.

In case of a group in which all the individuals follow a leader, the group is strongly organised, ordered, centralised in nature and controlled by a leader or group of leaders [4]. For example, dwarf mongooses (*Helogale parvula*), feral dogs (*Canis lupus familiaris*), and wolves (*Canis lupus*) are led by a leader or group of leaders [5]. Hence, information transfers in the group are centralised in nature and depend on a leader or group of leaders. As a result, collective response in case of any events is very poor, unless detected directly by the leader or group of leaders [4]. For example, whole elephant herds depend completely on the old female elephant's memories to lead them to distant water and food resources during droughts. The survival rate

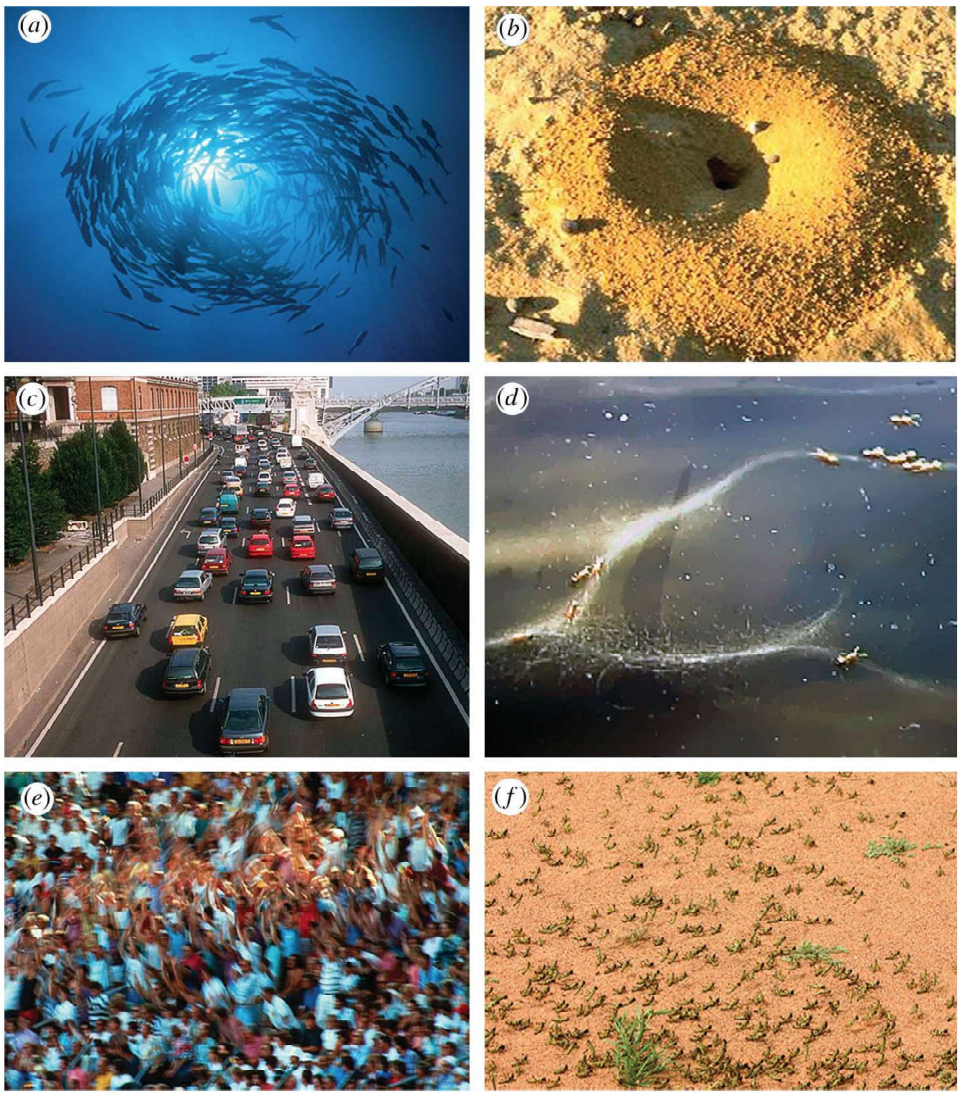

FIGURE 1.1: Examples of collective motion: (a) Fish milling, (b) the entrance crater to a nest of the ant (*Messor barbarus*), (c) traffic flow in Paris, (d) a bifurcation in a Pharaoh's ant trail, (e) mexican wave at an American football game, (f) a band of marching locusts [7].

of young calves depends completely on the leadership of surviving older female elephants [6].

In the case of self-organised or self-emergent groups, the efficiency of the collective response depends on how individuals transfer information. This information transfer can be direct or indirect. Direct information transfer takes place between individuals in direct sensory contact, while the indirect information transfer process

is governed by behavioural correlation. It is basically a process of an indirect information transfer, initiated by intermediate individuals with direct sensory interaction. During this process two animals, outside the range of direct interaction, may still interact with each other via intermediate interacting animals. Therefore, behavioural correlation is a key factor for the group's ability to respond collectively to any change of events in the environment [4]. Any environmental perturbations or sudden change of events will cause a change in the behaviour of the whole group. The another important characteristic of collective motions in self-emergent groups is that, although they depend on the density of individuals, the pattern formations are independent of the specific individuals. The histories and motivations of individuals in a group are not required to predict and define the collective motion of the group. The group exhibits strong coherence in its spatial formation and displays highly co-ordinated movements and manoeuvres, either spontaneously or in response to a predator attack. However, interactions and information transfer between the individuals in the group are vital for the stability of the collective behaviour. The mode of information transfer can be chemical (as in case of ants), visual, acoustic, hydrodynamic and so on. The flow of information transfer can be uneven; for example, a specific individual may be better at finding a food source, or all individuals may copy the anti-predatory response by following an individual who has detected the predator.

Collective motion is one of the major challenges in unifying the laws of nature. As a result, this has always been an aspiration and motivation for physicists, biologists, mathematicians and engineers. However, recent advancements in high-speed camera technology, computer vision by which automated tracking from video can be achieved, GPS system and so on have brought collective motion to the centre stage. A multidisciplinary research effort is ongoing to elucidate and harness different applications of this motion. Fish schools serve as a classical example of collective animal motion having self-organisation and emergent behaviour. The fish communicate actively via diverse signals, such as sounds, smells, body gestures and colour changes. However, most of the information transfer in collective fish swimming takes place

in passive ways where each individual responds to the position and movement of the nearest neighbours through visual and hydrodynamics [8]. This study aims to enhance our understanding of interactions in collective fish swimming. In this introduction, we will conduct a brief literature survey of fish swimming, describing their mode of information transfer and collective swimming.

1.1 Fish swimming

There is no animal better than fishes to represent efficient swimming, with an evolution and adaptation of 500 million years [9], although it should be noted that not all adaptations have been driven by the purpose of swimming only, like the wide nose of the hammerhead shark. Other key factors, such as foraging and protection against predators, have also been involved. Still, fishes are the most efficient swimmers. Their locomotion involves complex fluid-structure interactions that use various fins and morphological features (see Fig. 1.2). A fish swims by the expansion and contraction of complex network of skeletal muscle blocks, known as myomeres [10, 11], which drive the body and fin undulations. The myomeres are commonly zig-zag, "W" or "V" shaped.

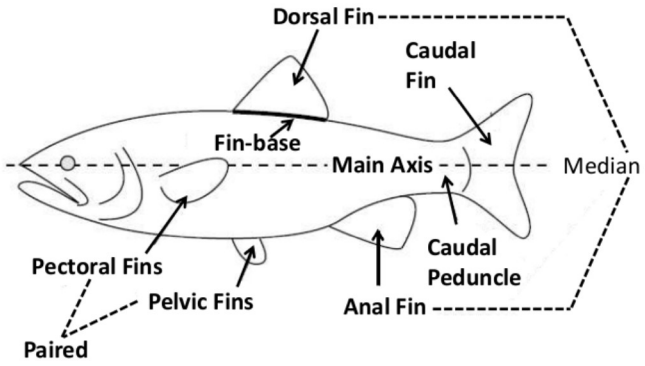

FIGURE 1.2: Fins and features of a fish [12]. Together, the anal and dorsal fins are referred to as median fins, whereas pectoral and pelvic fins are referred to as paired fins.

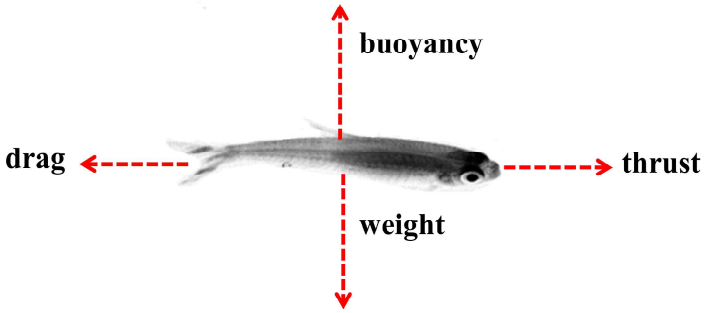

FIGURE 1.3: Average forces acting on a fish.

Fish swim by using momentum transfer to the surrounding water. On average, there are four different forces acting on a fish, namely drag, thrust, buoyancy and weight as explained in Fig. 1.3. For a propelling fish, the net or average thrust should be greater than the total resistance or drag force. Most fishes are generally neutrally buoyant. For negatively buoyant fish, the fish must supplement the buoyancy with an additional force in the vertical direction to balance the vertical forces. This is primarily achieved by flapping the pectoral fins [13]. Adult fish swim in the inertial regime, that is, with a Reynolds number, $Re = UL/\nu$, greater than 1000. Here, U and L are the speed and length scale of the fish and ν is the kinematic viscosity of the surrounding water of the fish. To swim in the inertial regime, fish employ two different thrust generation mechanisms, as follows (Fig. 1.4): (1) the added-mass or reactive mechanism and (2) the lift-based mechanism. In the added-mass mechanism, the body or fin of the fish accelerate the adjacent or nearby fluid [14, 15]. This produces a reactive (added-mass) force, which is perpendicular to each propulsive element. The reactive force has a component in the thrust direction, as shown in Fig. 1.4(a) [14–16]. The added mass mechanism has been the focus of numerous analytical [14, 17–23], numerical [24–28] and experimental studies [29–34]. In the lift-based mechanism, the swimmer oscillates the tail/fin. As a result, the lift force is generated and has a force component in the forward direction, which provides thrust, as shown in Fig. 1.4(b) [16, 35]. The lift-based mechanism is primarily used by

oscillatory swimmers, such as tuna and sharks. This mechanism can be visualised by the heaving and pitching of the swimming surface, hydrofoils or fins [36–39].

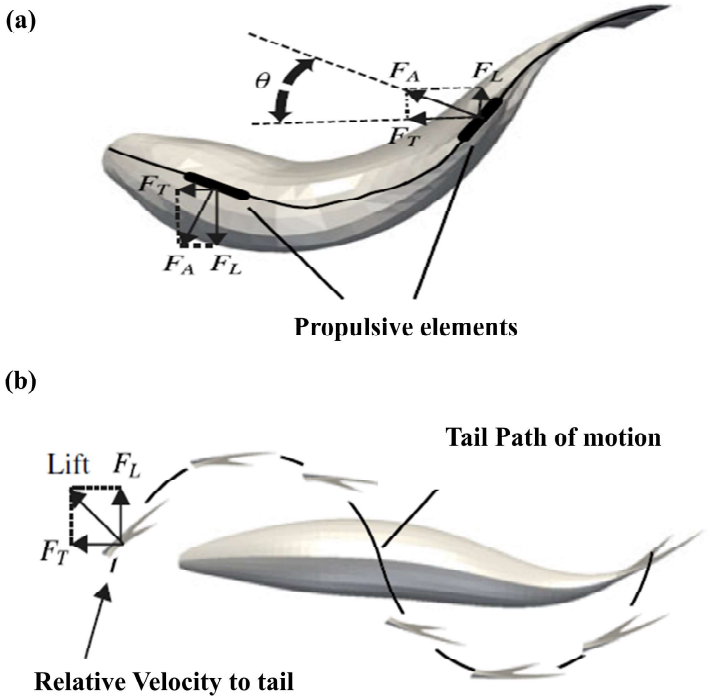

FIGURE 1.4: Propulsion mechanisms in aquatic swimming. (a) Thrust generation by the added-mass (reactive) mechanism. (b) Thrust generation by the lift-based (circulatory, vorticity) mechanism. F_A is the added-mass force, θ is the angle between the propulsive element and swimming direction, F_T is the thrust force and F_L is the lateral force [16].

Based on physiological mechanics, swimming modes can generally be divided into two basic groups. These are termed body and caudal Fin (BCF) and median and/or paired Fin (MPF) propulsion [40].

1.1.1 Body and caudal fin swimming

BCF swimming uses body undulations toward the caudal fin (tail) and the tail may also undulate, thereby propelling the fish. Almost 88% of fishes use BCF propulsion [41, 42]. The BCF mode of locomotion is further divided into five categories based

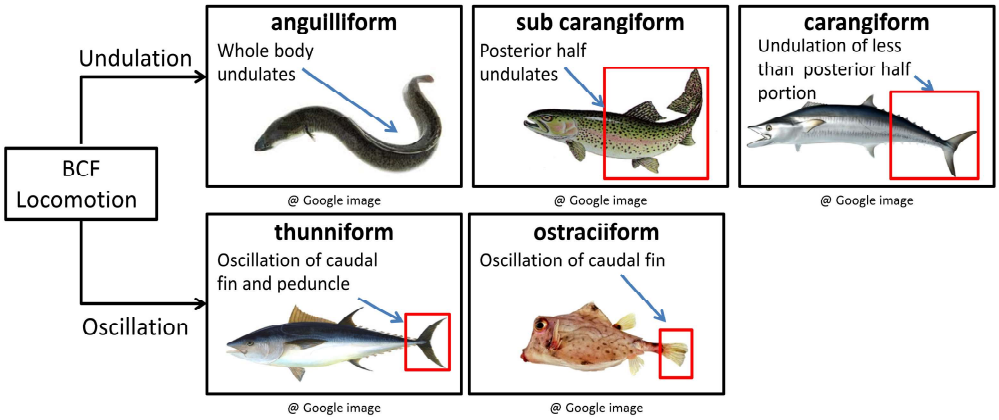

FIGURE 1.5: Classification of the BCF Mode[12]

on the fraction of their body that is displaced during propulsion, as follows: (1) anguilliform, (2) carangiform, (3) subcarangiform (4) thunniform and (5) ostraciiform (Fig. 1.5).

Irrespective of the thrust generation mechanism, the wake structure of fish swimming is charaterised by the formation of reverse Bénard-von Kármán (BvK) vortex street. A two-dimensional (2D) schematic of Bénard-von Kármán (BvK) vortex street behind a 2D cylinder and reverse Bénard-von Kármán (rBvK) vortex street behind a 2D fish in a steady swimming is illustrated in Fig. 1.6(a and c). For a 2D cylinder, there is a net momemtum or velocity deficit in the wake (see Fig. 1.6(b)). In contrast, for a 2D fish, there is a velocity excess or momentum gain. When a fish is in steady swimming, no net drag or thrust is exerted on an average basis (see Fig. 1.6(d)). However, for a cruising fish, the wake has to provide excess thrust on an average basis. It should be noted that the wake of a real fish is three-dimensional (3D), and it is far more complex and disorganised as compared with organised vortices of a 2D swimmer. Therefore, Fig. 1.6 is merely a respresentation of differences in the wake structure of a bluff body and swimmer in a broader and simplistic sense, but it is not an actual representation.

In the ***anguilliform mode***, the whole body participates in a large amplitude of undulation. The body contains at least one complete wavelength of oscillation; eels

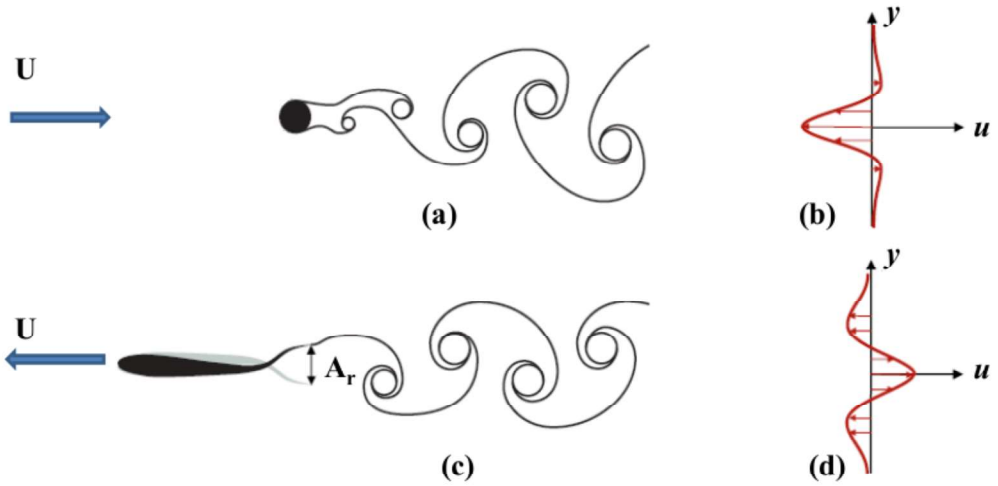

FIGURE 1.6: (a) Bénard–von Karman (BvK) vortex street behind a circular cylinder and (b) reverse Bénard–von Karman (rBvK) vortex street behind a steady swimming fish. The average velocity profile, u, of the wake of a two-dimensional (2D) cylinder (c) average velocity profile, u, of wake of a 2D steady swimming fish [43].

exemplify this mode. Müller et al. [29] and Tytell et al. [30] reported that anguilliform swimmers shed two vortices per half tail-beat cycle, which is self-organised into two distinct rows of vortices, also known as a double-row wake. However, when Carling et al. [44] carried out two-dimensional (2D) simulations of eel swimming and were unable to find the wake structure that reproduce the experimental results of Müller et al. [29] and Tytell et al. [30]. Nevertheless, this discrepancy was resolved by Kern et al. [25], who demonstrated that the two-dimensional (2D) simulations performed by Carling et al. [44] were unable to capture the actual three-dimensional (3D) flow.

In the ***Subcarangiform mode***, fish swim with the posterior portion of the body. The body contains less than one wavelength of undulation near the fish tail. The fish head also yaws with the motion of swimming. The aspect ratio of tail is $1.5:2$. Cods, basses and trouts use subcarangiform locomotion. In the ***Carangiform mode***, the body is stiffer and faster moving than in subcarangiform and anguilliform modes. In most fishes, the lateral undulation is restricted to the posterior one-third of the body. This mode of swimming is used by many fishes, such as mackerel. As

carangiform swimmers typically swim at high speeds, they are characterised by very high Reynolds numbers, Re>10^4 [45]. Müller et al. [46] studied the structure of the wake behind a continuously swimming mullet and reported that fish shed one vortex per half tail beat. Borazjani et al. [47] reported the formation of an attached vortex at the leading edge of the caudal fin in the case of a mackerel swimming with various tail shapes. Recently, Maertens et al. [48] showed that the Strouhal number, $St = fA_r/U$, and maximum angle of attack are principal parameters that effect efficiency. Here, f is the tail-beat frequency, A_r is the peak-to-peak tail amplitude of the fish and U is the swimming speed of the fish. These researchers also observed the wake bifurcation at a high Strouhal number. However, it should be noted that for both the anguilliform mode and carangiform mode of swimming, the wake structure primarily depends on the Reynolds number and Strouhal number [27, 47].

Thunniform swimming is a primary mode of locomotion for numerous fast swimmers and predators, such as tuna and sharks. Thunniform swimmers are generally at the higher end of the marine food chain and have a large, strong front body [13]. In this mode of swimming, swimmers propel themselves by propagation of the travelling wave of the body toward the tail along with the combination of oscillatory motion of the caudal fin. In thunniform swimmers, the undulation is limited to the rear third of the body and reaches the maximal amplitude at the end of the tail peduncle [49, 50]. Wolfgang et al. [51] performed the 3D simulation of a giant danio swimming together with a 2D particle image velocimetry (PIV) experimental study. They proposed that the tail fin has a secondary role in the generation of wake vortices. The vorticity is generated by the undulations of the body and upstream of the tail. The body-generated vorticity is favourably affected by the motion of the tail. The trailing edge vortex of the tail is merged and amplified with body-generated vortex. The undulation of the fish body and caudal fin motion are synchronised, which allows the vorticity formation and evolution to be actively controlled. Recently, Li et al. [50] performed a three dimensional numerical study of tuna fish under self-propulsion.

They reported that the moving part of the body also contributes to thrust. The kinematics of the anguilliform, subcarangiform, carangiform and thunniform mode are summarised in Fig. 1.7.

The ***Ostraciiform*** type of locomotion is found in box and trunk fishes (family Ostraciidae), in which the body is not flexible, and hence, it cannot undergo lateral undulation. Therefore, only the tail fin oscillates and provides propulsion [53]. These fishes live in complex habitats and can perform extremely impressive manoeuvring. For example, a box fish can perform 180 lateral turning manoeuvres during forward motion with almost no turning radius [54, 55].

1.1.2 Median and/or paired fin swimming (MPF)

Many fish use undulations or oscillations of pectoral, pelvic, anal, dorsal or combinations of them to generate the propulsion. This type of propulsion is termed MPF propulsion. BCF styles allow for greater acceleration and speed, while MPF provides better maneuverability [12]. The MPF mode is further classified as (a) rajiform, (b) mobuliform, (c) diodontiform, (d) amiiform, (e) gymnotiform , (f) balistiform, (g) mobuliform, (h) tetraodontiform and (i) labriform [12].

Rajiform locomotion is a characteristic of skates *Rajidae* and most stingrays *Dasyatidae* [40]. They produce thrust by vertical undulations of their pectoral fins [56, 57]. Bottom II et al. [16] performed the three dimensional (3D) large-eddy simulations of a self-propelled stingray *Potamotrygon orbignyi* and showed that the horse shoe vortex produces a low-pressure region in the frontal region, which enhances the hydrodynamic thrust. ***Mobuliform locomotion*** utilises the oscillation of the pectoral fins, by flapping up and down [58]. The pelagic rays (*eagle rays and manta rays*) swim using this style. Fish et al. [58] reported that manta rays have propulsive efficiency of around 89%. However, the key observation was that most of the thrust is generated bydistant end of the fin and flexibility plays a major role in their high efficiency.

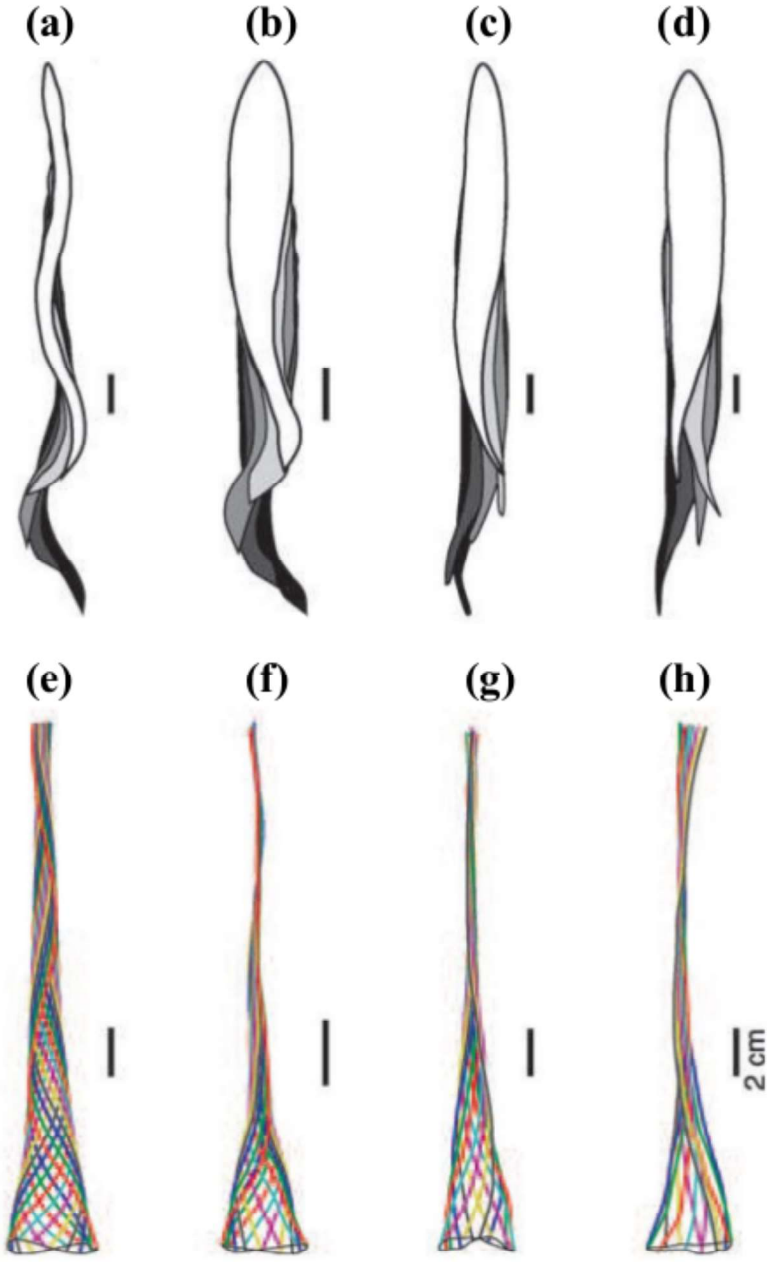

FIGURE 1.7: Kinematics of different BCF modes of swimming. (a) Anguilliform mode based on Anguilla, (b) Subcarangiform mode based on Lepomis, (c) Carangiform mode based on Scomber, and (d) Thunniform mode based on Euthynnus. (e) Midline envelope of Anguilliform swimming, (f) Midline envelope of subcarangiform swimming, (g) Midline envelope of Carangiform swimming, and (h) Midline envelope of thunniform swimming. The swimming speed is 1.8 BL/s [52].

In ***Diodontiform locomotion*** swimming, the fish generates propulsion by undulating its pectoral fins. Porcupine fish (*Diodon nicthemerus*) use this mode of propulsion. The ***Amiiform locomotion*** is characterised by undulations of a long dorsal fin, while the body axis is kept straight and stable. This mode can be observed in the bowfin. The ***Gymnotiform locomotion*** involves undulation of a long anal fin, essentially upside down. It can be seen in the knifefish, *Gymnotiformes*. In ***Balistiform locomotion***, both the anal and dorsal fins undulate. It is characteristic of the family balistidae *triggerfishes*. In ***Tetraodontiform mode***, the fish oscillate both the dorsal and anal fins. The oscillation is permormed as a unit either in phase or out of phase. The ocean sunfish displays this mode. The ***labriform mode***, generally seen in the wrasses *labriformes*, generates thrust by oscillatory movements of the pectoral fins. Propulsion is generated either by a resistive or lift mechanism [12].

1.2 Information transfer in the collective swimming of fish

As described previously, fish schools are self-organised and self-emergent. As in case of any self-organised group, information transfer and interactions are vital mechanism, they are not only important for collective motion, but also key for their formation and survival. Fish interact and transfer information through their sensory organs. The key sensory organs in fish are olfaction, hearing, vision and lateral line system. However, it has been commonly accepted that only the lateral line and vision are important for collective swimming behaviours [59, 60].

It has been shown by numerous studies that, under conditions of total darkness, fish in schools tend to disperse and opt for solitary swimming, while in the light fish have been observed to be mutually attracted and form polarised schools [61, 62]. Therefore, it has been assumed that vision is compulsory for maintaining collective

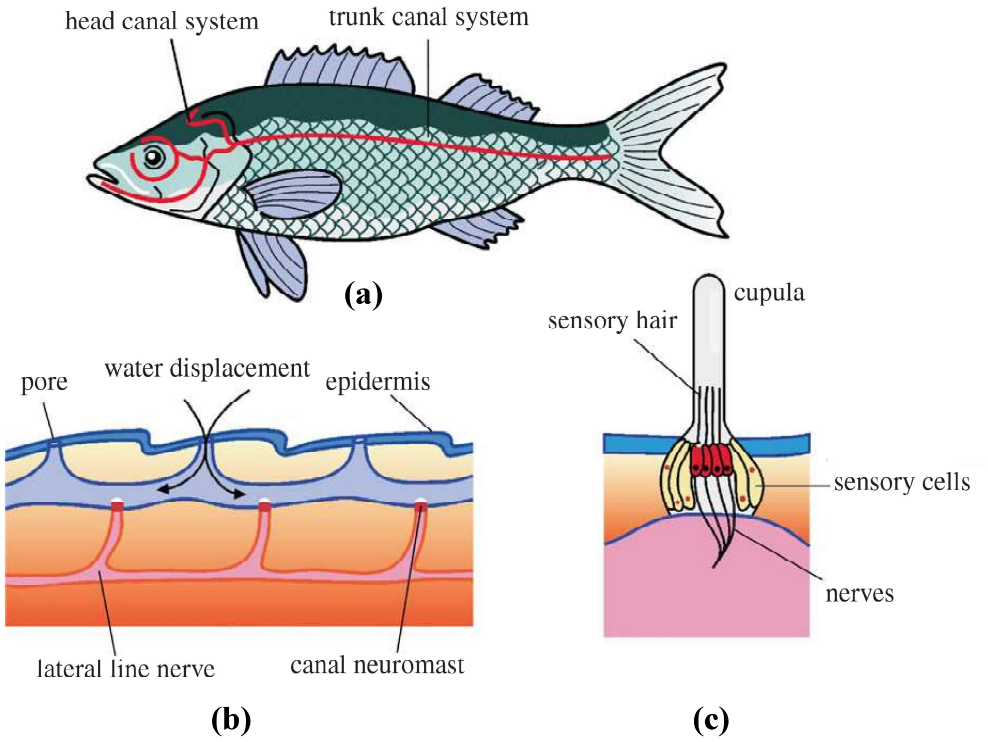

FIGURE 1.8: (a) Lateral line system in a fish, (b) canal neuromast (CN) and (c) superficial neuromast (SN) [63].

swimming behaviour. However, Pitcher et al. [59] successfully demonstrated that vision is not required to school. They showed that five blind saithe successfully formed a school with twenty five normal saithe. They also demonstrated the importance of the lateral line system in fish schools.

The lateral line is an extremely vital sensory organ in fishes that is used to detect any movements, vibrations or any distortions in the surrounding environment. Fish utilise it for depth or water pressure detection, prey and predator detection, sensing water current and wall or surface or rock detection. It consists of the collection of small functional units or hair cells, known as neuromasts. It is a sensory structure that is either located superficially on the skin, called a superficial neuromast (SN), or under the skin and inside a fluid-filled canal, called a canal neuromast (CN), that is usually open to the environment through a series of pores [64] (Fig. 1.8). The neuromast is a mechanoreceptive organ that detects water movements and hydrodynamic

signals. The lateral system plays a key role in the cohesive and collective swimming behaviours of fish [65]. Faucher et al. [60] showed that when fish are totally deprived of the lateral system (both trunk and head), they cannot maintain a shoal. In that case, the average nearest neighbour distance (NND) increases and fish swim far from each other as compared with fish with a full lateral line system. Similarly, frequent collisions between fish were also observed in the absence of the lateral line system. This study convincingly demonstrated that the lateral system is a crucial factor for the collective swimming behaviour.

1.3 Collective fish swimming

A lot of fishes spend their whole life in a school, while some spend part of their life in school. Approximately 25% of adult fishes exhibit schooling behaviour, whereas around 50% of fish species demonstrate schooling tendency during the larvae and juvenile stages [61]. Collective swimming in fish has been described by the shoaling or schooling behaviours. According to Pavlov [66], shoaling is simply the spatial arrangement of a group of fishes attracted toward each other by virtue of some stimuli, such as food, temperature or olfactory stimuli. In shoaling, fishes lack unitary organisation and co-ordination. Schooling is defined as collective swimming in which individual fishes are oriented in the same direction, maintain a certain distance from each other and demonstrate co-ordinated and correlated swimming [66–69]. Fish schools are not driven by a leader but instead, they are self-organised. The schools frequently make sharp turns or movement or accelerate or decelerate, and each individual in the school reacts to those events or changes. However, there is a certain delay in the response time of each individual in a school to those changes or events [67, 68].

Fish schools are generally associated with many benefits to the individuals. Collective swimming provides an individual platform for social life and interaction. In fact, some species cannot survive alone and tend to die within few days due to social

isolation stress [70]. However, the school disintegration trend has also been observed in various species. Some of the reasons for this disintegration are a heterogeneous habitat [71], reproductive period [72] or immense competition for resources [73]. The fish school also provides protection against predators [74–78]. Swimming in a school provides additional eyes or sensory mechanisms to detect and sense any source of danger. Magurran [79] transported guppies from source rivers with high predation levels to rivers with low predation levels. After passage of 34 and 16 years respectively, it was observed that the offspring of the transplanted fish had a low level of schooling tendency compared with their counterparts from the source river, as shown in Fig. 1.9 [79]. Reznick et al. [80] measured various life history traits in the transplanted fish in a low predation level area and observed that the offspring of transplanted fish achieved maturity at a later stage and larger size and produced larger offspring. Similarly, Huizinga et al. [81] reported that guppies living at a high predation level showed more cohesive behaviour compared with guppies living at a low predation level. Although, these studies focused only on one population group, but they validated the fact that collective shoaling or schooling provides some degree of security in case of a high predation level. Olson [82] used operation research theory [83] to study fish schooling and concluded that the probability of being eaten for a fish living in a school is considerably low (0.0005 in a fish school of 20000 individuals and prey size of 20 individuals), as compared with lone fish (0.11). Similarly, Neill et al. [84] showed that the increasing size of prey fish groups decreases the success rate of the predators' attacks on the prey. The success rate is higher for solitary swimmers. Similarly, Zheng et al. [69] showed that the probability of any member of a fish school being eaten by a predator depends strongly on their cohesiveness and collective evasion behaviour of the fish.

The fish school provides protection to individuals in both the passive and active modes. In the passive mode of defence or period before an attack from any predators, the fish in the school benefit from the increased rate of vigilance and predator detection and recognition. In the active mode of defence or period during an attack

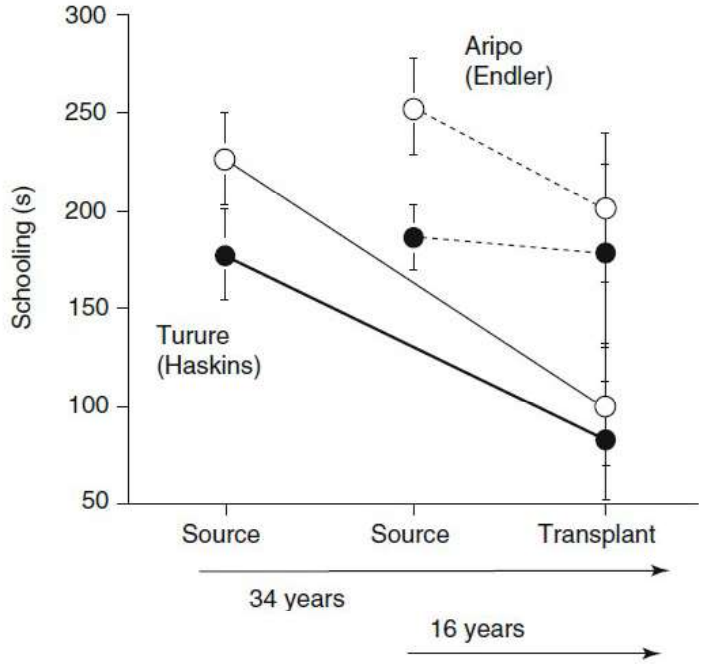

FIGURE 1.9: Evolution of antipredator behaviour in Trinidadian guppies [79]. Males are represented by black circles, while females are represented by white circles.

by predators, the schooling behaviour also helps in escaping the predators. When a predator encounters a large number of fishes swimming in a school, swimming fast and performing quick manoeuvres, it easily get confused. As a result, the predator finds it difficult to focus on single prey [69, 85, 86]. Another benefit of schooling is that it increases the foraging success considerably [87–93] as well as the chances of finding partner for reproduction.

The most fascinating part of the collective behaviour in the fishes is that they are self-organised and self-emergent. Despite being a leaderless group, they move cohesively, in a common direction, while they avoid splitting up or colliding with each other. Taking a clue from these behaviours, several mathematical models have been proposed to address the problem of fish schooling, such as the Aoki-Couzin model [94]. These mathematical models have been developed on focusing only on three simple phenomenological behavioural rules, commonly known as the 3A's rule: avoidance, alignment and attraction [96–101]. Each fish must avoid colliding with

neighbours to align itself with its neighbours and finally, join the group and avoid being outside the group. Therefore, a fish school is divided into three behavioural zones, as demonstrated in Fig. 1.10 [102, 103]. When fishes are in the repulsion zone, they will repel each other to avoid collision. In the orientation zone, fishes tend to swim together. Finally, when they are in the attraction zone, they will attract and become closer to each other. However, every model is not based on the 3A's rule in its entirety. For example, the Vicsek model is only based on alignment [95]. In the Vicsek's model, at every time step, each swimmer moves in the average direction of motion of its neighbours along with some noise. The mistakes fish make while evaluating the direction of motion of their neighbours are considered as the noise. When the noise magnitude increases, the system goes through a phase transition from an ordered state, in which all the fish move in the same direction, to a disordered state, in which all the fish move in random and uncorrelated directions. The Viscek model can only be used to model a fish school; in contrast, the Aoki-Couzin model [94] comprises the whole 3A's rule and can model all the commonly observed collective behaviour structures in nature, that is, schooling, swarming and milling .

The most common collective fish swimming patterns observed in nature are summarised in Fig. 1.11. The key parameters that are used to describe the collective motion of fishes are polarisation, angular momentum and nearest neighbours distance (NND). The "polarisation" is taken as a measure to quantify the degree to which fish in the school are aligned in the same direction. This is defined as $P = \frac{1}{N}\left|.\sum_{i=1}^{N}\frac{v_i}{v}\right|$ [96], where v_i is the unit direction vector of the fish i in a group of size N [96, 104]. The global normalised angular momentum or milling number is defined as $M = \frac{1}{N}\left|.\sum_{i=1}^{N}\frac{\overrightarrow{r_i}\times\overrightarrow{v_i}}{|\overrightarrow{r_i}|v}\right|$ [96], where r_i is the radius of orientation. The NND is used to quantify the cohesiveness of a fish school [105]. Swarming is generally observed associated with feeding behaviour, where the group remains cohesive with low level of polarisation and low angular momentum [96, 106], as shown in Fig. 1.11(a). In the school state, P tends to 1, and individuals are oriented in the same direction [96, 106], as shown in Fig. 1.11(b). In the milling state, individuals perpetually rotate

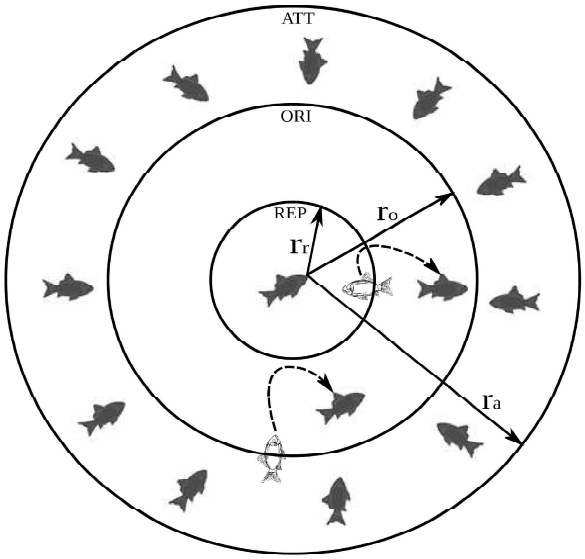

FIGURE 1.10: Behavioural zones in a fish school. REP is the repulsion zone, ORI is the orientation zone and ATT is the attraction zone; r_r denotes the radius of the repulsion zone, r_a denotes the radii of the attraction zone and r_o denotes the radii of the orientation zone [103].

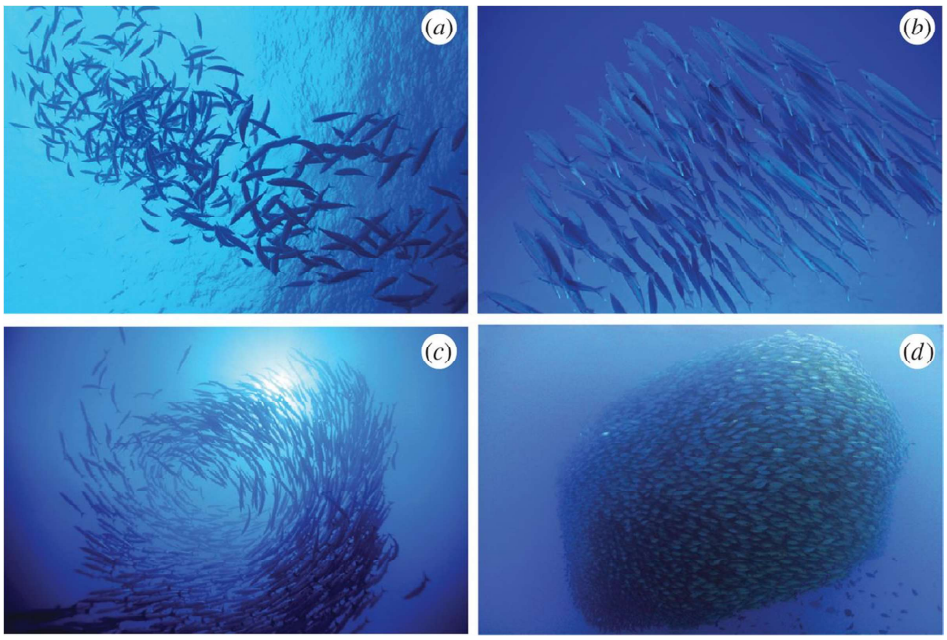

FIGURE 1.11: Collective motion patterns in fish schools. (a) Swarming, (b) fish school, (c) milling pattern, (d) structure pattern [1].

around an empty core [106], as shown in Fig. 1.11(c). M tends to 1 in the case of milling state [96, 106]. Figure 1.11(d) represents a special case, known as a structure pattern, which is generally taken as a last and desperate act of defence against predators.

Recently, Calovi et al. [96] and Gautrais et al. [99] applied the behavioural rules and models to fish shoaling in a tank by tracking individual fish. Filella et al. [101] coupled the behavioural rules with far-field hydrodynamics in 2D self-propelled particles (SPP) in a potential flow and reported a new turning phase pattern as a result of coupling the hydrodynamics in the SPP model (Fig. 1.12 and Fig. 1.13). Gazzola et al. [107] studied the fish school as SPP by using the Biot-Savart law equipped with hydrodynamics interactions and adaptive decision making. All these mathematical models are indeed elegant, novel and universal. However, they have rarely been validated with actual fish schools. In addition, these mathematical models do not consider the vortex structure and three dimensional effects. In these models, swimmers are massless and intertialess. The models also disregard the morphological features and kinematic traits of real fish. Therefore, actual hydrodynamic interactions cannot be explained by these models.

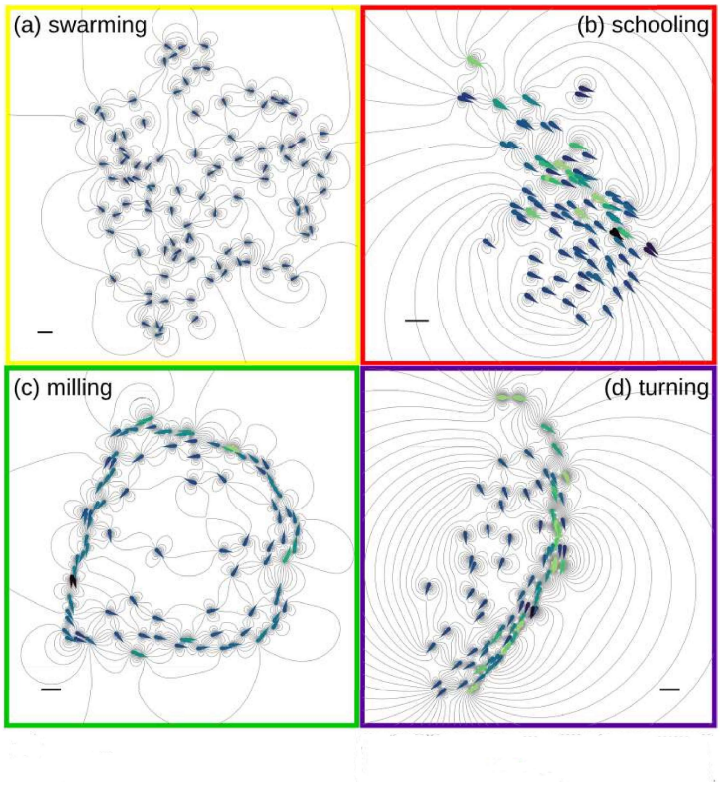

FIGURE 1.12: Different collective swimming phases observed by Filella et al. [101]. (a) swarming, (b) schooling, (c) milling, (d) turning

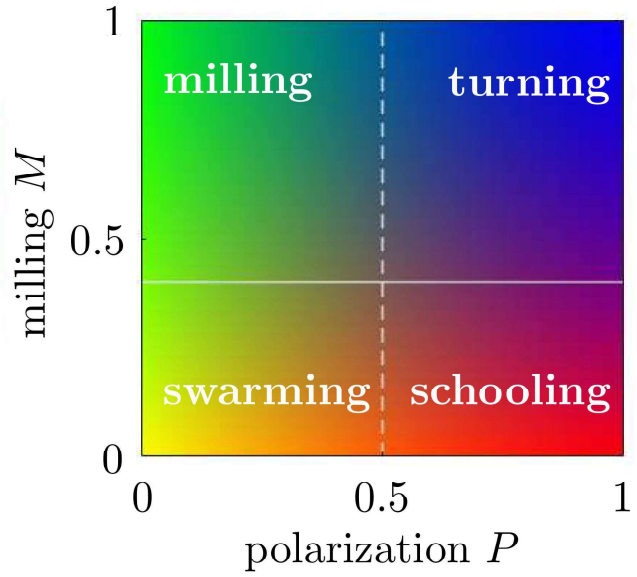

FIGURE 1.13: Phase diagram using the value of the polarisation P and milling M [101].

Hydrodynamic interactions play a key role in a fish school. There are several studies that have demonstrated the role of hydrodynamic interactions and the energetic benefits associated with it in fish schools. Fields [108] observed that the tail beat frequency of Pacific mackerel (*Scomber- Japonicus*) swimming in a school is lower compared with a lone swimming fish. Similarly, Herskin et al. [109] showed that the tail beat frequency of sea bass, Dicentrarchus labrax (L.), swimming at the front of school is 9-14 % higher compared with that of fish swimming at the rear of the school. In addition, the oxygen consumption rate is 9-23% lower for fish at the rear position of school. These benefits were primarily attributed to the hydrodynamics interaction between swimmers. Historically, Breder [110] was the first to postulate that the vortex shed by fish can play a vital role in their organisation. Belyayev et al. [111] suggested that swimming in groups can help in the reduction of drag. However, Weihs [112] was the first to postulate the mathematical model of an ideal fish school. Weihs [112] presented a two dimensional and inviscid model commonly known as the diamond shape, as shown in Fig. 1.14. According to this model, fish should swim at regular and fixed positions relative to one another to maximise the hydrodynamic efficiency of the school. He presented that rear fish should swim midways between two front fishes. Consequently, in this midway position, fish will be able to capture the vortices shed by the front fish. This will lead to a reduction of fish swimming velocity relative to the flow velocity in the swimming direction. The two front fish will benefit from each other through the channelling or wall effect. Still, according to Weihs [112], the required force for the entire school in a diamond shape will be reduced by two to three times as compared with solitary swimming.

Since then, not only has this theory has been widely reported in the literature, but it has also led to carry out new numerous experimental, analytical and computational studies [113–118]. Weihs theory is elegant but its major shortcoming is that it is hardly observed in nature [119, 120]. Partridge et al. [119] experimentally tested Weihs' theory over schools of saithe (*Pollacius virens*), herring (*Clupea harengus*),

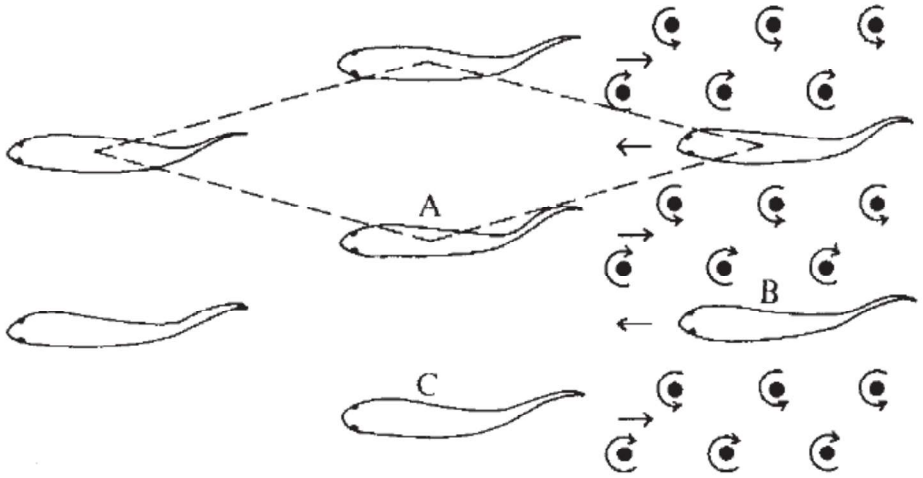

FIGURE 1.14: Ideal diamond shape formation according to Weihs [112].

and cod (*Gadus morhua*). The observations were the total opposite of the pridictions by Weihs' theory. No diamond shapes were observed. Similarly, Newlands et al. [121] used aerial observation to characterise the schools of Atlantic bluefin tuna *Thunnus thynnus L.* in the open ocean. They reported seven different shapes, as follows: (A) cartwheel (also known as mill or torus), (B) surface sheet, (C) dome or 'packed dome', (D) soldier (also known as phalanx), (E) mixed, (F) ball, and (G) oriented, as shown in Fig. 1.15. It was revealed that Atlantic bluefin tuna *Thunnus thynnus L.* prefer oriented, dome and soldier formations.

A similar observation was reported by Partridge et al. [122]. The reason for the difference between what is observed in nature and the idealised diamond shape can be attributed to the overly simplistic two-dimensional (2D) and inviscid model. Another limitation of the diamond pattern is that its effectiveness imposes the strong constraint of maintaining a precise position and perfect synchronised kinematics of the individuals in the school. This is somewhat impractical to achieve.

It should be noted that the theory of utilising the wake or fluid structure is not completely misplaced, and it can be easily seen in nature, as in dolphins doing bow riding or wake riding [123]. In bow riding, dolphins use the high pressure generated

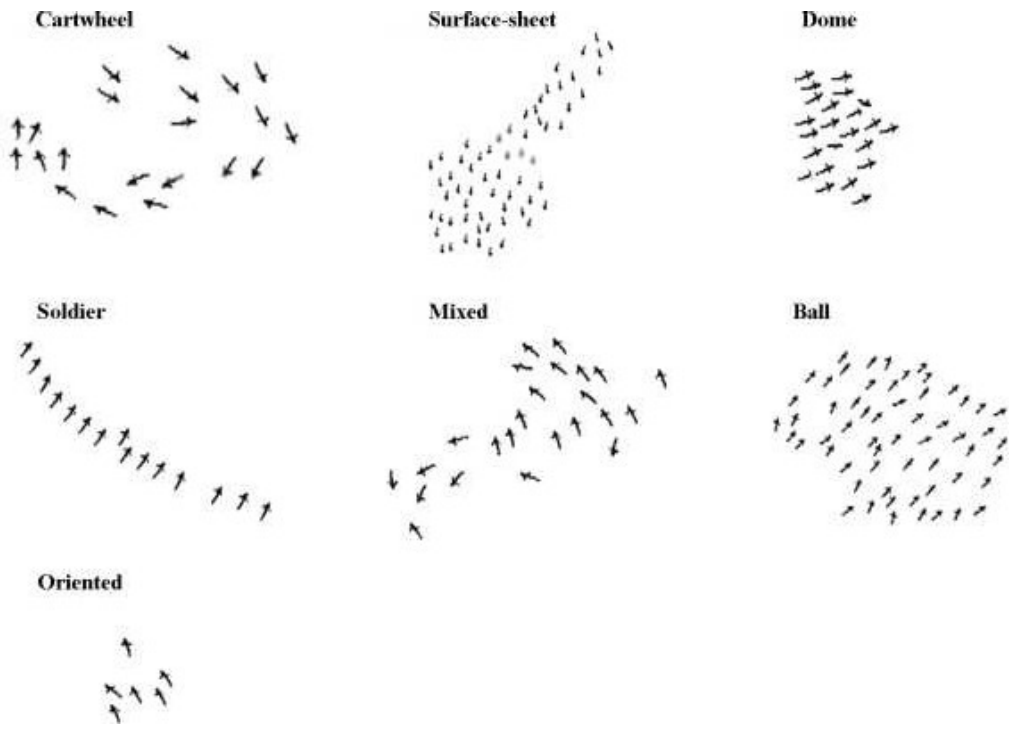

FIGURE 1.15: (A) Cartwheel (also known as mill or torus), (B) surface-sheet, (C) dome or 'packed dome', (D) soldier (also known as phalanx), (E) mixed, (F) ball and (G) oriented shapes[121].

in the anterior region of large individuals, such as ships, to 'push' in the forward direction without being in actual physical contact [124]. During wake riding, dolphins swim along and surf in the waves created by the back of boats and ships in the same manner as human surfers, which significantly reduces the cost of locomotion [125]. Similarly, whales are known to achieve propulsive power saving by absorbing energy from ocean waves [126]. According to Bose et al. [126], if the tail-foil oscillation is synchronous with the wave stream and the wavelength is less than four times the body length of the whale, then the whale can easily save up to 25% of its required propulsive power in head seas and 33% in following seas. Recently, Liao et al. [114] presented that the rainbow trout (*Oncorhynchus mykiss*) alter their body kinematics while swimming behind in the Bénard-von Kármán (BvK) street of a D-cylinder. It was shown that trout swimming in Bénard-von Kármán (BvK) street generate larger body amplitudes and curvatures compared with trout swimming in the absence of Bénard Von Kármán (BvK) street . It was also shown that the tail-beat frequency of

the rainbow trout matches the vortex shedding frequency of the Bénard-von Kármán (BvK) wake.

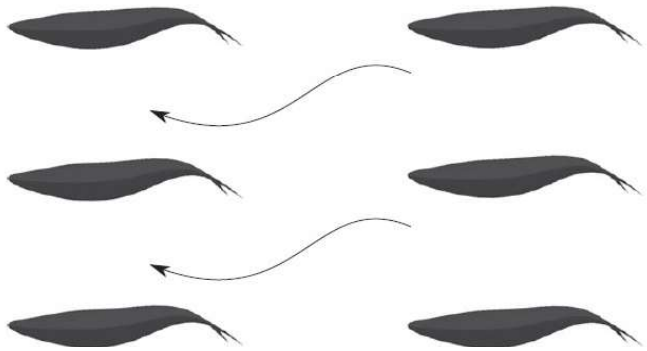

FIGURE 1.16: Enhancement of flow between swimmers in a rectangular pattern due to the channelling effect [127].

Another possible mechanism for positive hydrodynamic interactions during collective swimming is the *channelling effect* [112, 127, 128]. Here, when fishes in school swim close to each other, lateral hydrodynamic interactions take place between them. Due to this interaction, there is enhancement of flow between the swimmers, as shown in Fig. 1.16 [127]. The reason behind this enhancement of flow is that, when swimmers swim together and close to each other, it prevents their wake from being freely expanded in the lateral direction. Since the wake cannot expand in the lateral direction, the velocities in the axial direction must increase to satisfy the law of conservation of mass. This phenomenon is equivalent to the wake blockage effect, a commonly observed phenomenon in wind tunnels and water channel experiments [127]. This favourable flow provides additional momentum to the fish in the swimming direction. As a result, a fish in the school will require less muscle activity with respect to solitary swimming. Alternatively, if a fish spends the same amount of energy, then it will swim faster because of the channelling effect [127]. Hemelrijk et al. [128] showed that the rear fish or follower can dodge the incoming jet flow due to the swimming of the front fish by the sideways movement of their heads, and they can capture energy from the shedding vortex upstream. Therefore, with the

sideways movement of the fish heads, even fish swimming in a line or a rectangular configuration can be hydrodynamically beneficial and improve the swimming performance of the school. In addition, recently, it has also been reported that the wake of synchronised 3D swimmers is highly disorganised and noncoherent, with a lot of small vortical structures [127], which is in stark contrast with the organised, coherent structures of the wake of a 2D solitary swimmer, as shown in Fig. 1.17. Therefore, capturing those disorganised and noncoherent vortices is highly impractical.

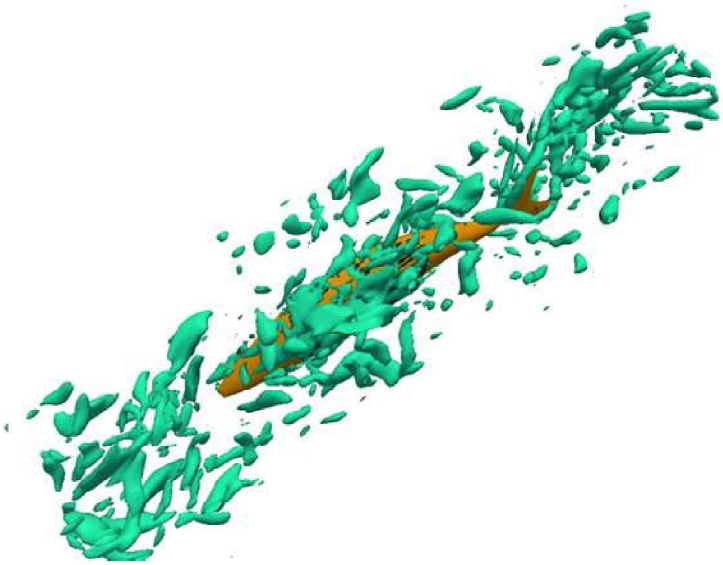

FIGURE 1.17: Three-dimensional (3D) wake structure by using q-criterion for a fish school in a rectangular pattern at lateral distances, $w = 0.3$ [127]. This clearly demostrates that the actual 3D wake structure of a fish is far more complex and non-coherent than the two-dimensional (2D) wake structure, as proposed in numerous studies.

The channelling effect does not impose any strict spatial organisation [128, 129]. A similar strategy is employed by young dolphin calves to swim with their fast-swimming mothers [124, 130], commonly known as drafting.

1.4 Objective and outlines of the thesis

The major objective of this thesis is improving our understanding of collective fish swimming based on direct observations. To achieve this objective, we need an experimental setup along with computational and image processing tools capable of carrying out the experiments. This setup is presented in detail in chapter 2. In addition, the details of the computational and image processing tools, fish and experimental protocols used to conduct all the experimentation are also presented. Thereafter, the objective is to proceed towards experimentation in a logical order from the most simple, that is, single fish swimming to the most complex ones, that is, group of fish swimming together. The experimental results are presented from chapter 3 to chapter 5. In chapter 3, we characterise the swimming dynamics of a single fish as a function of swimming velocities. In chapter 4, we explain the observation of synchronisation and its correlation with swimming speed in the fish pair. After studying the collective swimming of the fish pair, we add further complexities to the problem by increasing the number of fish in the group, from triplet to nontet as reported in chapter 5. In this chapter, we report the pattern formation observation in different groups of fish (pair to nontet) as a function of swimming speed and energy benefit associated with the collective swimming. Based on our observations, we also provide a brief conclusion along with future perspectives.

Chapter 2

Material and methods

The experimental setup consists of a water channel, imaging system and in-house code to track fish and extract kinematics.

2.1 Water channel

A shallow water tunnel with a test section of 2.2cm in depth and a swimming area of 20$cm\times$ 15cm was used for the experiments, as shown in Fig. 2.1. The test section is covered from the top by using acrylic plate. The flow rate Q can be varied from 4 to 22 litres per minute, resulting in an average velocity of $U = Q/S$, where S is the cross-section, in the range between 2.7cm/s to 15cm/s. To characterise the flow in the channel, particle image velocimetry (PIV) measurements were carried out in the mid-plane of the channel. Figures. 2.2(a) and 2.2(b) show the velocity flow field at $U = 2.7cm/s$ and $U = 15cm/s$ respectively. The mean turbulence intensity(TI) is found to be between $3-5\%$ and it seems to be independent of the flow rate. Figures. 2.3(a) and 2.3(b) show the velocity profile in the mid-section of the channel, which also remains unchanged for the different flow rates. We also note that the velocity profile is rather flat, with the wall effect region limited to a distance smaller than 3mm. The minimum distance between the fish and wall, in the most confined case (the nontet case), is $\approx$7 times the size of the wall effect region. This distance is more than 14 times the size of the wall effect region for the other groups. The wall effect is therefore negligible, as are the flow profile and turbulence intensity observations.

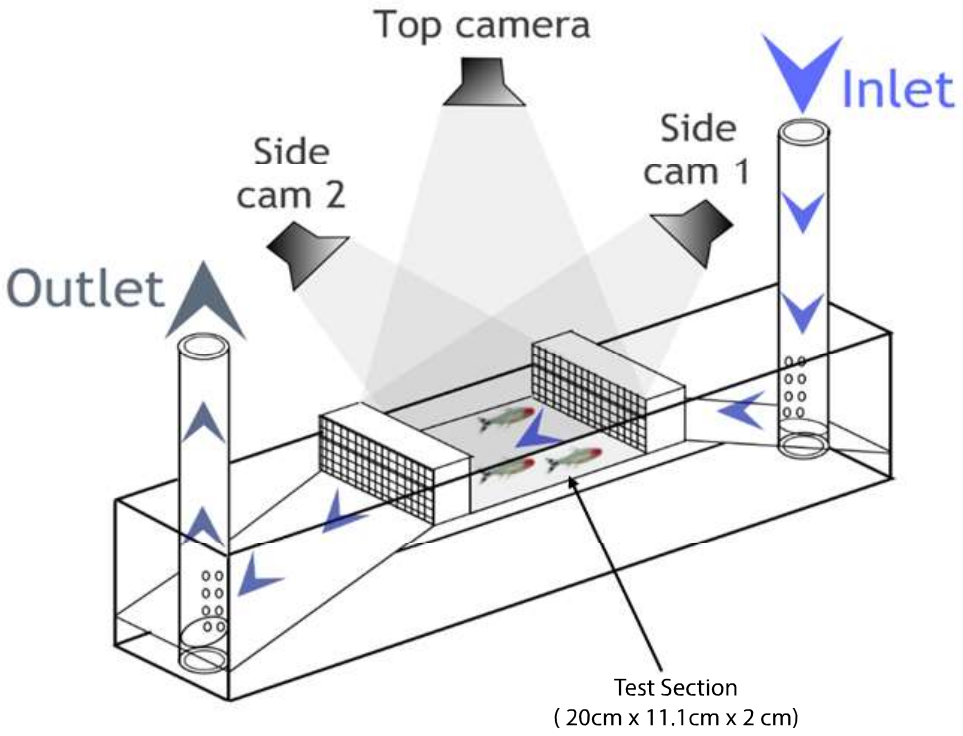

FIGURE 2.1: Schematic diagram of the swimming channel. An external pump drives the flow, which is directed toward the test section after a convergent ramp and through a honeycomb section to minimise swirling motions. The test section is covered from the top by using acrylic plate. The two side cameras and one top camera is installed to track the fish.

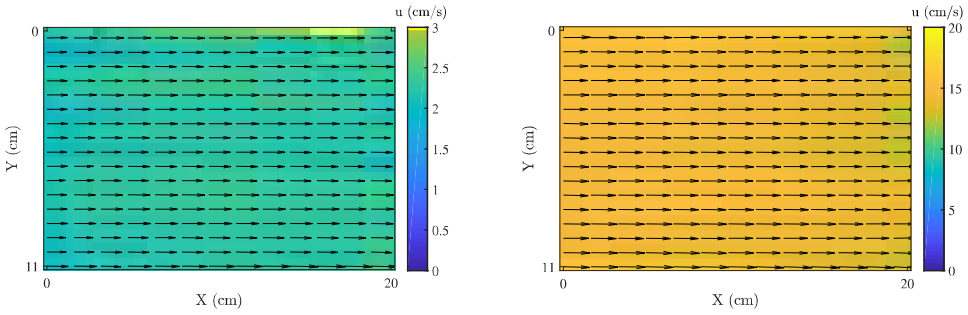

(a) (b)

FIGURE 2.2: Flow in the channel at the average flow velocity, (a) $U = 2.7cm/s$ and (b) $U = 15cm/s$ respectively.

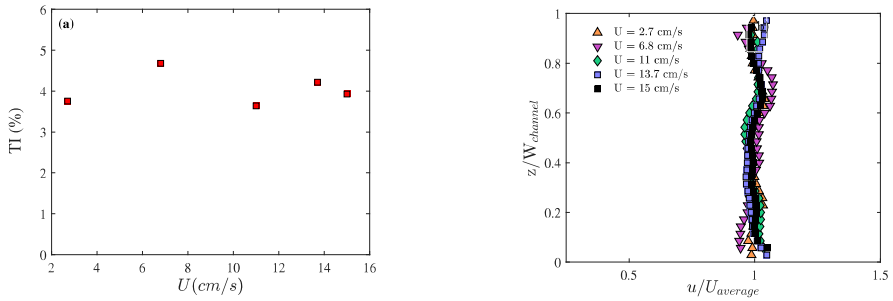

(a) (b)

FIGURE 2.3: (a) Velocity profile, u(y), in the x-direction at the mid-height and mid-section of the channel, which is flat and does not change with the flow rate. (b) Turbulence intensity (TI) as a function of the average flow velocity in the channel. It can be seen that the turbulence in the flow remains fairly constant over the flow rate range explored and stays below 5%.

2.2 Animals and housing

Hemigrammus bleheri (also known as red nose tetra fish, $\sim 3.5-4cm$ long $\times 0.5-0.6cm$ in width) was chosen for experiments. This species was chosen because it is known to be an excellent shoaling and cohesive fish with a well developed lateral line system [60]. *Hemigrammus bleheri* swim in the carangiform and subcarangiform mode of locomotion.

The fish were procured from a local aquarium supplier (anthias.fr, France). The fish were fed 5-6 times a week with commercial flake food. The fish were reared in a $100L$ tank with controlled water at a temperature between $26-27\,^{\circ}C$. The experiments performed in this study were conducted under the authorisation of the Buffon Ethical Committee (registered to the French National Ethical Committee for Animal Experiments no. 40).

2.3 Image acquisition

For both 2D and 3D visualisation, the images were acquired using Basler make camera from top view visualisations at 100 frames per second (fps). An in-house code,

written in Matlab, was used for 2D and 3D tracking of the fish. This is explained in detail below.

2.3.1 Automated two-dimensional (2D) planar tracking of fish

The automated tracking involves the following major steps:

1. Image acquisition using a high-speed camera.
2. Background estimation: The background image is estimated by selecting a region around the fish and erasing it using the $Matlab^{TM}$ function 'roifill'. It smoothly interpolates inward from the pixel values on the boundary of fish by solving Laplace's equation, without modifying the boundary pixels.
3. Subtraction of the background from acquired images.
4. Binarisation of substracted images.
5. Boundaries estimation of fish: The $Matlab^{TM}$ function 'bwboundaries' is used to calculate the fish boundary from the binary images.
6. Midline calculation from the boundaries.

All the steps are illustrated in Fig. 2.4.

2.3.2 Three-dimensional (3D) tracking of fish

For the 3D tracking of fish, direct linear transformation (DLT) was employed. DLT is a method by which the perspective 2D image coordinate system is converted into a 3D object coordinate system [131]. A 3D reconstruction by DLT comprises two steps, which are calibration and reconstruction. Each step is described in detail below:

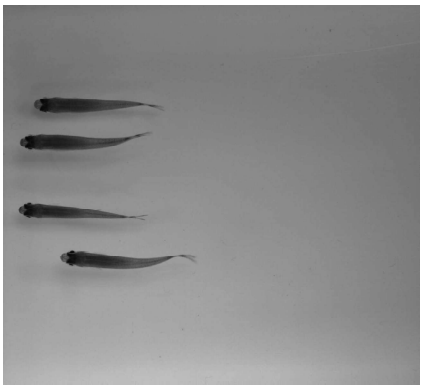

(a) Acquired image

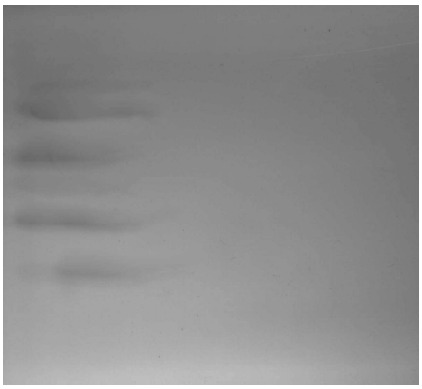

(b) Background estimation

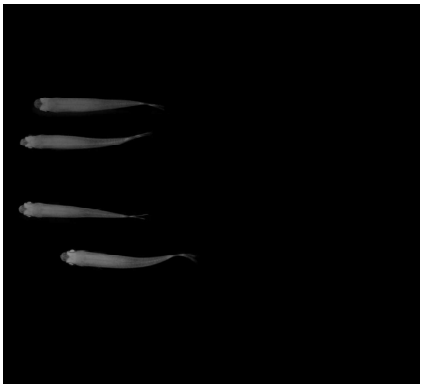

(c) Background subtraction

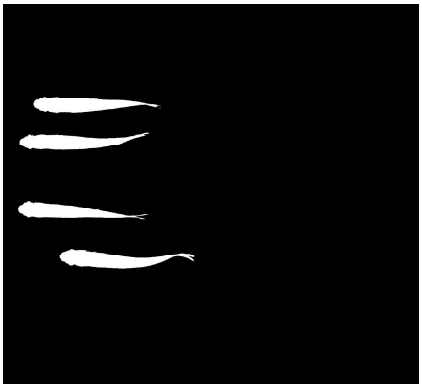

(d) Binarisation of the image

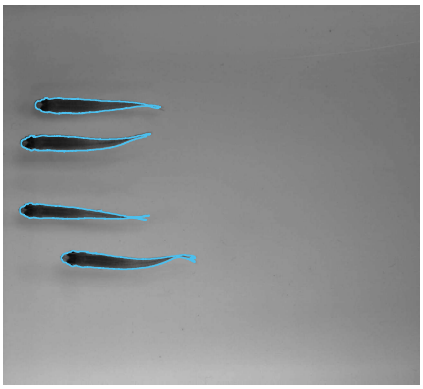

(e) Boundary points estimation

(f) Midline extraction

FIGURE 2.4: Process of automated fish tracking and midline estimation.

Calibration: It is carried out by using an object of known global co-ordinates and digitising the control points from each camera. The calibration object and digitised points are then used to obtain the DLT coefficients for each camera.

Let's assume the coordinates of known point O are [x, y, z]. We acquire a pair of images by using two stereo side cameras, as shown in Fig. 2.1. The left image is represented by coordinate system [U_L, V_L], whereas the right image is represented by [U_R, V_R]. Here, u_L,v_L,u_R and v_R are coordinates of the object in left and right images respectively. The image points [u_L, v_L] and [u_R, v_R] and the object point [x, y, z] can be related through a series of constants [132], as follows:

$$\begin{aligned} u_L &= \frac{L_1x + L_2y + L_3z + L_4}{L_9x + L_{10}y + L_{11}z + 1} \\ v_L &= \frac{L_5x + L_6y + L_7z + L_8}{L_9x + L_{10}y + L_{11}z + 1} \\ u_R &= \frac{R_1x + R_2y + R_3z + R_4}{R_9x + R_{10}y + R_{11}z + 1} \\ v_R &= \frac{R_5x + R_6y + R_7z + R_8}{R_9x + R_{10}y + R_{11}z + 1} \end{aligned} \tag{2.1}$$

As we can see, with one calibration point, we have 7 knowns, 22 unknowns and four equations. To find 22 unknowns, we need 22 equations. Therefore, we need atleast six points to solve the above equations. However, more control points are used for the following reasons [133]:

1. Additional points leads to an over-determined solution of the camera calibration coefficients. This helps in improving the accuracy of least squares minimisation.

2. Control or calibration points should be distributed all over the volume of interest for accurate 3D reconstruction.

Therefore, we use more than 100 calibration points of coordinates distributed uniformly all over the test section of channel. For the number of calibration points, $N \geq 6$, the left camera cordinates can be related to a 3D object coordinated by equation 2.2. Similarly, for the right camera, it can be represented by equation 2.3.

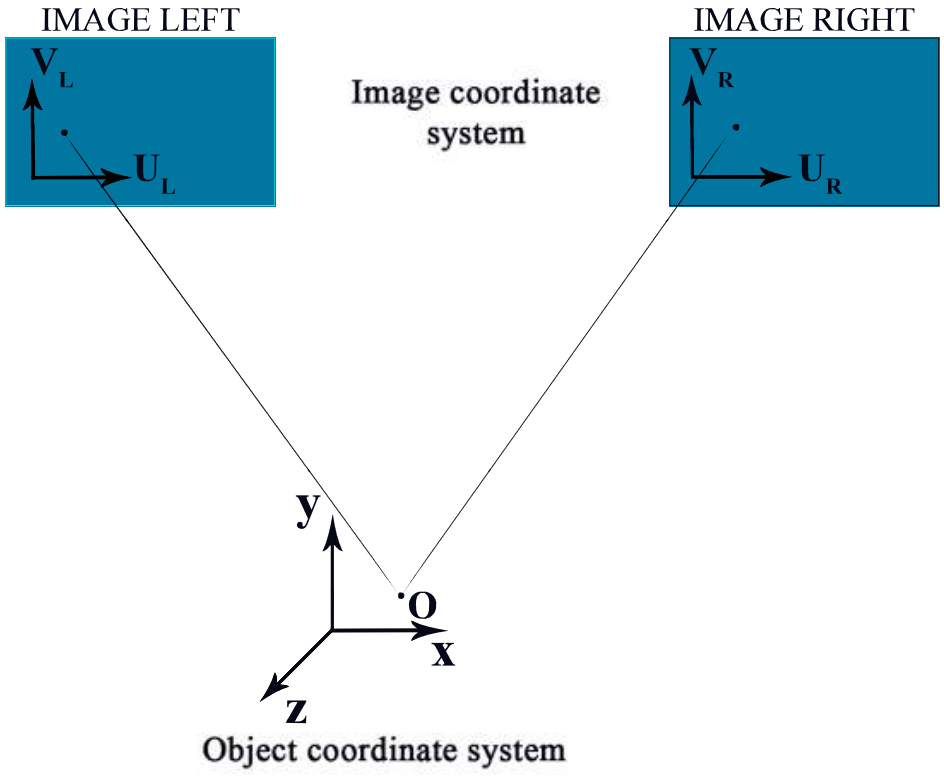

FIGURE 2.5: Stereoscopic imaging system for three-dimensional (3D) tracking.

$$\begin{bmatrix} x_1 & y_1 & z_1 & 1 & 0 & 0 & 0 & 0 & -U_{L_1}x_1 & -U_{L_1}y_1 & -U_{L_1}z_1 \\ 0 & 0 & 0 & 0 & x_1 & y_1 & z_1 & 1 & -V_{L_1}x_1 & -V_{L_1}y_1 & -V_{L_1}z_1 \\ x_2 & y_2 & z_2 & 1 & 0 & 0 & 0 & 0 & -U_{L_2}x_2 & -U_{L_2}y_2 & -U_{L_2}z_2 \\ 0 & 0 & 0 & 0 & x_2 & y_2 & z_2 & 1 & -V_{L_2}x_2 & -V_{L_2}y_2 & -V_{L_2}z_2 \\ \vdots & \vdots & \vdots & \vdots & \vdots & \vdots & \vdots & \vdots & \vdots & \vdots & \vdots \\ x_N & y_N & z_N & 1 & 0 & 0 & 0 & 0 & -U_{L_N}x_N & -U_{L_N}y_N & -U_{L_N}z_N \\ 0 & 0 & 0 & 0 & x_N & y_N & z_N & 1 & -V_{L_N}x_N & -V_{L_N}y_N & -V_{L_N}z_N \end{bmatrix} \begin{bmatrix} L_1 \\ L_2 \\ L_3 \\ L_4 \\ L_5 \\ L_6 \\ L_7 \\ L_8 \\ L_9 \\ L_{10} \\ L_{11} \end{bmatrix} = \begin{bmatrix} U_{L_1} \\ V_{L_1} \\ U_{L_2} \\ V_{L_2} \\ \vdots \\ U_{L_N} \\ V_{L_N} \end{bmatrix} \tag{2.2}$$

$$\begin{bmatrix} x_1 & y_1 & z_1 & 1 & 0 & 0 & 0 & 0 & -U_{R_1}x_1 & -U_{R_1}y_1 & -U_{R_1}z_1 \\ 0 & 0 & 0 & 0 & x_1 & y_1 & z_1 & 1 & -V_{R_1}x_1 & -V_{R_1}y_1 & -V_{R_1}z_1 \\ x_2 & y_2 & z_2 & 1 & 0 & 0 & 0 & 0 & -U_{R_2}x_2 & -U_{R_2}y_2 & -U_{R_2}z_2 \\ 0 & 0 & 0 & 0 & x_2 & y_2 & z_2 & 1 & -V_{R_2}x_2 & -V_{R_2}y_2 & -V_{R_2}z_2 \\ \vdots & \vdots & \vdots & \vdots & \vdots & \vdots & \vdots & \vdots & \vdots & \vdots & \vdots \\ x_N & y_N & z_N & 1 & 0 & 0 & 0 & 0 & -U_{R_N}x_N & -U_{R_N}y_N & -U_{R_N}z_N \\ 0 & 0 & 0 & 0 & x_N & y_N & z_N & 1 & -V_{R_N}x_N & -V_{R_N}y_N & -V_{R_N}z_N \end{bmatrix} \begin{bmatrix} R_1 \\ R_2 \\ R_3 \\ R_4 \\ R_5 \\ R_6 \\ R_7 \\ R_8 \\ R_9 \\ R_{10} \\ R_{11} \end{bmatrix} = \begin{bmatrix} U_{R_1} \\ V_{R_1} \\ U_{R_2} \\ V_{R_2} \\ \vdots \\ U_{R_N} \\ V_{R_N} \end{bmatrix} \tag{2.3}$$

Reconstruction: After calibration, digitisation of unknown point(s) is carried out in the calibrated volume by applying the DLT to obtain the global 3D coordinates. The 3D reconstruction of the target object point is obtained by rearranging equation 2.1, as follows :

$$\begin{bmatrix} U_L - L_4 \\ V_L - L_8 \\ U_R - R_4 \\ V_R - R_8 \end{bmatrix} = \begin{bmatrix} L_1 - u_L L_9 & L_2 - u_L L_{10} & L_3 - u_L L_{11} \\ L_5 - v_L L_9 & L_6 - v_L L_{10} & L_7 - U_L L_{11} \\ R_1 - u_R R_9 & R_2 - u_R R_{10} & R_3 - u_R R_{11} \\ R_5 - v_R R_9 & R_6 - v_R R_{10} & R_7 - U_R R_{11} \end{bmatrix} \begin{bmatrix} x \\ y \\ z \end{bmatrix} \tag{2.4}$$

or

$$\begin{bmatrix} I \end{bmatrix} = \begin{bmatrix} A \end{bmatrix} \begin{bmatrix} X \end{bmatrix} \tag{2.5}$$

whereas

$$\begin{bmatrix} X \end{bmatrix} = \begin{bmatrix} x & y & z \end{bmatrix}^T \tag{2.6}$$

Using least square estimation (LSE), the X can be estimated as

$$\left[X\right] = \left[A^T A\right]^{-1} A^T I \tag{2.7}$$

The DLT coefficient calculation and reconstruction is carried out using the source code of DLTdv software written by Hedrick [133]. The two sides cameras are used, as shown in Fig. 2.1 and the 2D points obtained from side camera images are converted into 3D coordinates using DLT Reconstruction. We designed a calibration test pattern and took its images with both sides cameras, at different known heights in the test section, as shown in Fig. 2.6. The pattern is 19 cm long and 11 cm large, so it fits perfectly in the test section, and consists of series of black dots or control points, which is spaced at a distance of 0.5cm from each other. The DLT method uses this set of control points, whose 2D image space coordinates are known, to calculate DLT coefficicient. Once we have DLT coefficients, the 2D image space coordinates is converted into 3D object space coordinates by using DLT reconstruction, as explained in the above section. The stereo angle for our setup is 110° and the number of calibration points is > 100. The calibration and fish tracking is completely automated. The mean error in calculation is $\pm$ 1mm.

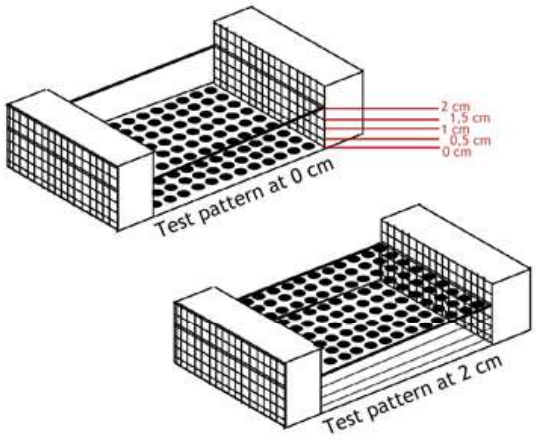

FIGURE 2.6: DLT calibration method in experimental setup. As shown, the images with test pattern are taken at different height of known coordinates.

Although DLT is extremely simple and relatively accurate, it does suffer from

reconstruction inaccuracy. The primary cause of DLT's inaccuracy is that it does not take nonlinear lens distortions into account. To take care of this effect, the camera calibration toolbox [134] written by Jean-Yves Bouguet (CalTech) is used. This is done to acquire images before the DLT calculations.

2.4 Fish kinematics

The fish undulates its body and passes a travelling wave from anterior part of the body towards the tail. The fish body undulation is given by

$$y(x,t) = A(x)e^{k_c x - \omega t} \tag{2.8}$$

whereas k_c is the wave number of the travelling wave, ω is the angular frequency of the tail beat, t is time and $A(x) = A_r e^{\alpha(x-1)}$ is the envelope [22]. Therefore, after extracting the midline from automated 2D fish tracking, the fish kinematics values are calculated. The key kinematics values are described below:

2.4.1 Frequency and amplitude

The key kinematics parameter of fish swimming is the frequency and amplitude of the tail beat. The frequency, f, is calculated by finding the time difference between the nearest peaks, as explained in 2.7. Similarly, the amplitude, A_r is taken as the peak-to-peak value of the tail movement. The tail-beating kinematics were extracted for each fish.

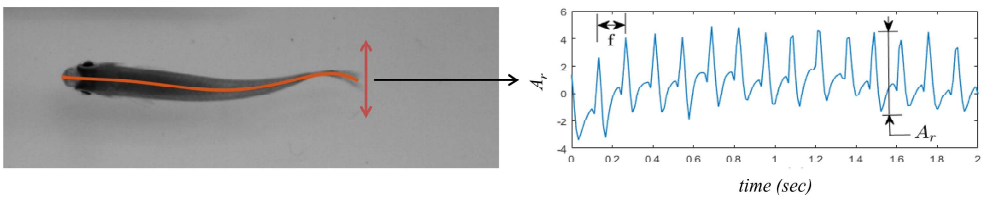

FIGURE 2.7: Fish tail tip frequency, f and amplitude, A_r estimation.

2.4.2 Phase velocity

The phase velocity v_ϕ is the speed of the travelling wave, passing from the fish body. It is calculated by finding the peak of the midline of the fish at two different time steps as $v_\phi = (x_2 - x_1)/(t_2 - t_1) = \omega/k_c = 2\pi/\lambda$ (see Fig. 2.8), where λ is the wavelength of the travelling wave.

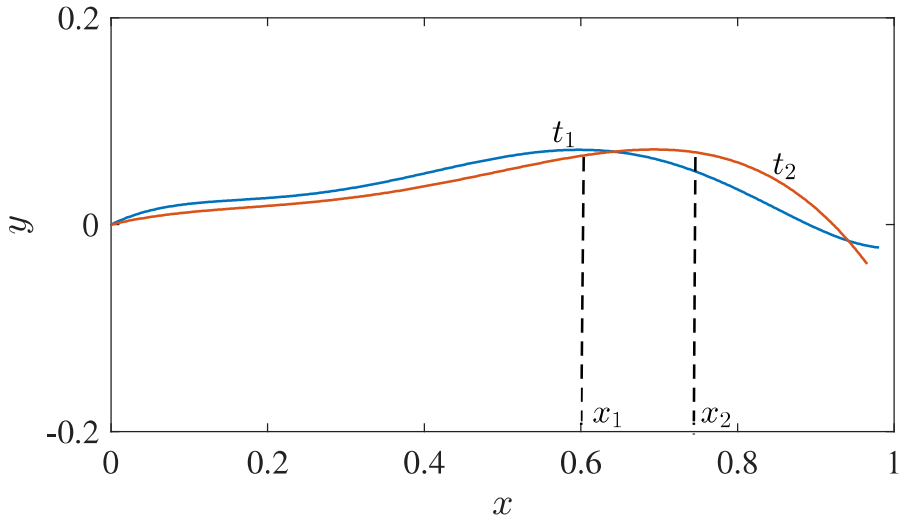

FIGURE 2.8: Phase velocity, v_ϕ estimation.

2.4.3 Burst-and-coast period

The burst-and-coast dynamic is characterised by a burst period and a coast period. The burst period, T_b, is the duration during which the fish is actively moving its tail; in contrast, the coast period, T_c, the fish tail is gliding or held stationary. The bout period, T_P, is the summation of the consecutive burst period and coast period, that is, $T_P = T_b + T_c$, as shown in Fig. 2.9. It is done automatically by a script written on $Matlab^{TM}$.

2.4.4 Internal frequency

The internal frequency, F_i, is the tail-beating frequency in a burst, which is characteristic of each individual fish. It is calculated by estimating the width of each burst

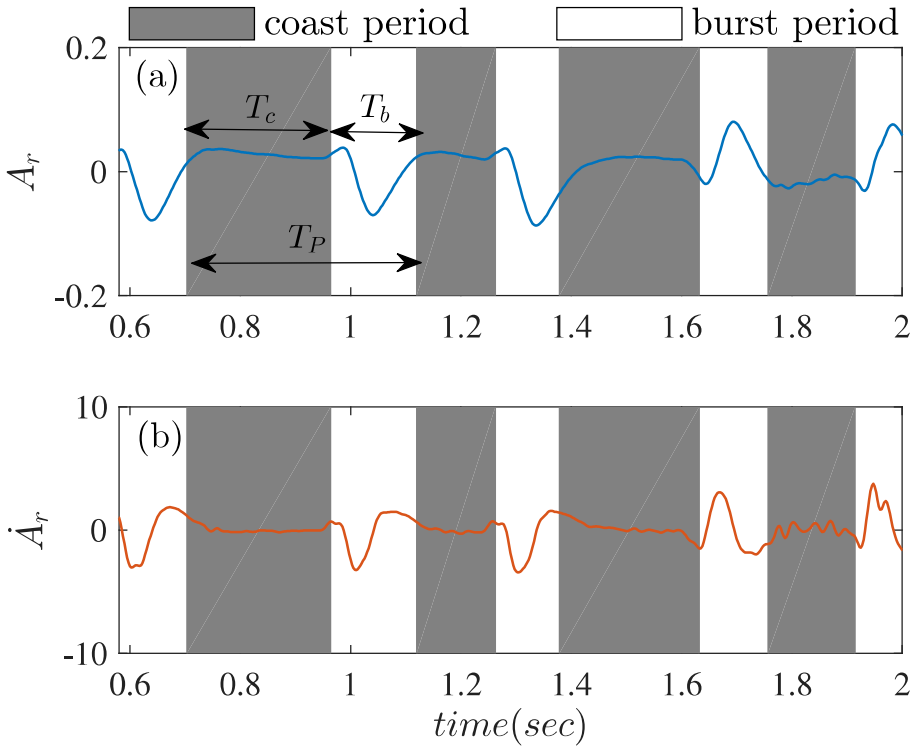

FIGURE 2.9: Burst-and-coast time period estimation: (a) amplitude profile, A_r, (b) velocity profile, $\dot{A}_r$, of tail-beat undulation.

at the half prominence level, as shown in Fig. 2.10.

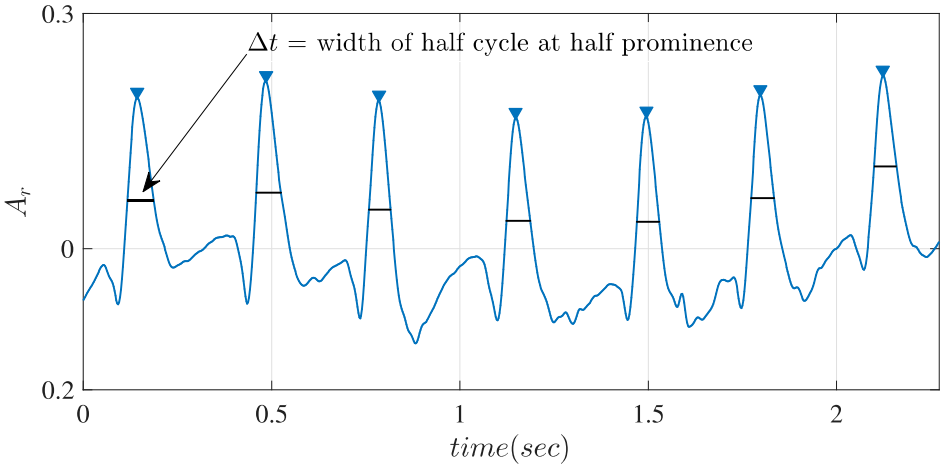

FIGURE 2.10: Internal frequency, F_i, estimation.

2.5 Data statistics

The average and standard deviation (SD) are computed for each kinematic parameters, and for each fish in case of a single fish swimming and each group in case of a school at every swimming velocities. All plotted quantities are thus averaged value and error bars are standard deviation.

2.6 Experimental procedure

Before starting each run, the fish were transferred with a hand net from the rearing tank to the test section of the channel without any flow. The fish were left idle for around 1 hour in the channel, to habituate them to the shallow test section. After each test with a fish group, the fish were allowed to relax for over $20-30$ minutes in the channel without flow.

Chapter 3

Burst and coast kinematics in steady swimming in the fish *Hemigrammus bleheri*

3.1 Abstract

In this work, we investigate the swimming dynamics of the red nose tetra fish *Hemigrammus bleheri* in a controlled experiment. Fish swimming alone are observed with video recordings while swimming against the flow in a shallow channel with average velocities ranging from 0.36 to 3 body lengths per second (BL/s). We track the motion of the midline of the fish and characterise the tail-beating kinematics, as well as the changes in the body curvature dynamics as a function of the imposed swimming velocity. The tetra fish are observed to swim using a burst-and-coast strategy. We show that the average bout period $T_P = T_B + T_C$, that is, the duration of a burst event (T_B) and its successive coast event (T_C) remains relatively constant over the range of velocities tested. The fish accommodate to an increasing swimming velocity imposed in the channel by increasing the ratio of the burst duration to the bout period, T_B / T_P, while the tail-beat frequency during the burst event remains relatively constant for each individual.

3.2 Introduction

Intermittent locomotion is a widely observed phenomenon in birds, aquatic mammals and fishes. In birds, it is characterised by active climbing and passive descent gliding [135], while in aquatic mammals and fishes, burst-and-coast (or kick-and-glide) swimming behaviour is used by several species [136, 137]. Burst-and-coast swimming is widely considered to provide an energy advantage [136, 138, 139]. Using a theoretical model, Weihs [138] showed that burst-and-coast swimming could diminish as much as 50% of the energy expenditure when compared with continuous swimming at the same mean velocity. The model was tested, and it accurately predicted the experimental values for cod and saithe [139]. The effectiveness of burst-and-coast from the perspective of the energy advantage depends on the fish geometry; for instance, an optimal fineness ratio — the body length versus the transverse sectional diameter of the animal — of about 5 was obtained by Blake [140] using a simple hydromechanical model. Burst-and-coast swimming has also been analysed experimentally [141] and numerically [142] using simplified mechanical models. Floryan et al. [33] experimentally investigated the intermittent swimming of a 2D rigid airfoil, pitching about its leading edge. They observed that the mean thrust and power increased with increasing duty cycle, all the way up to continuous motion. Chung [142] performed two dimensional (2D) numerical simulations, showing energy savings associated with burst-and-coast swimming and connecting these to the different wake structures observed between burst-and-coast and continuous swimming.

Several other studies have investigated burst-and-coast swimming. For larval and adult zebra danios, Muller et al. [143] provided a detailed quantitative analysis of the flow patterns using particle image velocimetry, while McHenry et al. [144] studied their coasting performance over the life history and proposed a mathematical model of coasting mechanics to explain the effect of the Reynolds number on the swimming style. Recently, Calovi et al. [151] proposed a mathematical model of

the burst-and-coast dynamics in the rummy-nose tetra (*Hemigrammus rhodostomus*) and showed that the swimmimg velocity decay exponentially after each burst with an average relaxation time of $\tau_0 \sim 0.80s$. Wu et al. [145] studied the kinematics and wakes of a koi carp *(Cyprinus carpio koi)* and estimated an energy saving in burst-and-coast swimming of $\sim 45\%$ as compared with continuous swimming. They also characterised the kinematics of the bursts, identifying half tail-beat (HT) and multiple tail-beat (MT) modes. All these studies have been performed in free swimming experiments. Another approach, commonly used to test the swimming ability of fishes in the laboratory, consists of using an imposed water current against which the fishes swim [146]. Burst-and-coast swimming in carp *Cyprinus carpio* was studied in such a configuration by Tudorache et al. [147], who characterised the transition between continuous swimming and burst-and-coast swimming as a function of the swimming velocity. More generally, the change in locomotor behaviour as a function of velocity depends on the preferred use of MPF or BCF propulsion. It also depends on the fish species, as well as the type of manoeuvre, such as hovering, steady swimming or fast starts [148]. In this paper, we analyse the swimming kinematics of the tetrafish *Hemigrammus bleheri* in a shallow swimming tunnel with a controlled flow rate. The fish spontaneously adopt a station-holding behaviour while swimming against the flow. Using high-frame rate video recordings, we show that the fishes use a burst-and-coast swimming gait over the whole range of swimming velocities tested. At high velocities though, the coasting time is reduced greatly so that the kinematics can be fairly described by a single tail-beating frequency —as has been considered in recent studies describing collective swimming in an equivalent experimental configuration [149, 150]. We characterise the burst-and coast dynamics by means of a midline kinematics in detail.

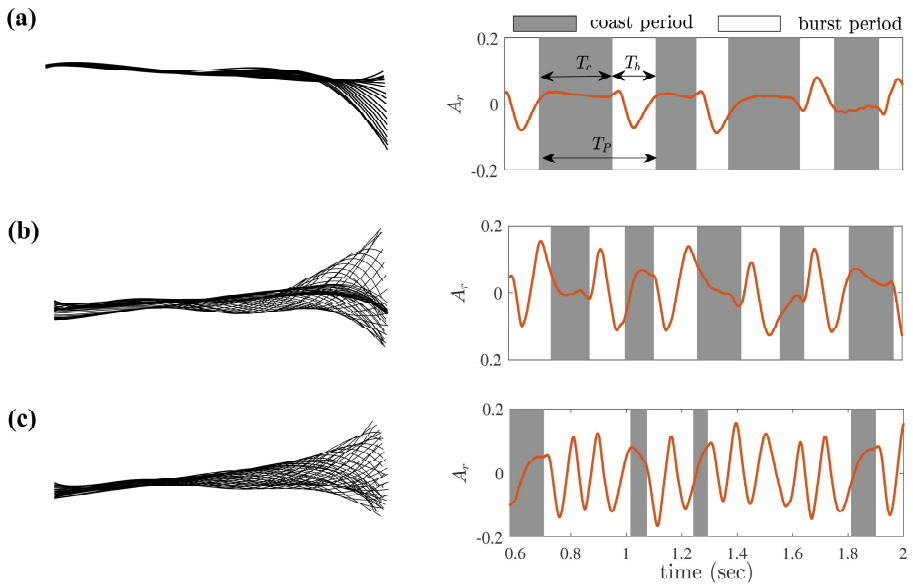

FIGURE 3.1: Midline kinematics (left) and time series of the tail tip amplitude, A_r, (right), for fish swimming at (a) 0.36 BL/s, (b) 1.26 BL/s, and (c) 3.0 BL/s. The burst-and-coast periods, T_B, and, T_C, in a swimming bout of duration, T_P, are indicated: grey bands in the background of the plots correspond to coasting time, white backgrounds correspond to bursting.

3.3 Experimental procedure

Before starting each run, the fish were transferred with a hand net from the rearing tank to the test section of the channel without any flow. The fish were left idle for around 1 hour in the channel for habituation. Each swimming experiment was carried out for 2.5 seconds. The experiments were performed on four different fishes with four observations for each velocity per fish. The fish were at least 2 cm away from the side walls during experiments.

3.4 Results

Figure 3.1 shows the midline kinematics and the time series of the tail-beating amplitude at the rear end of the caudal fin for three different swimming velocities. The evolution of the burst-and-coast dynamics is clearly observed: At each swimming bout of duration, T_P, the tail moves actively during the bursting time T_B and then

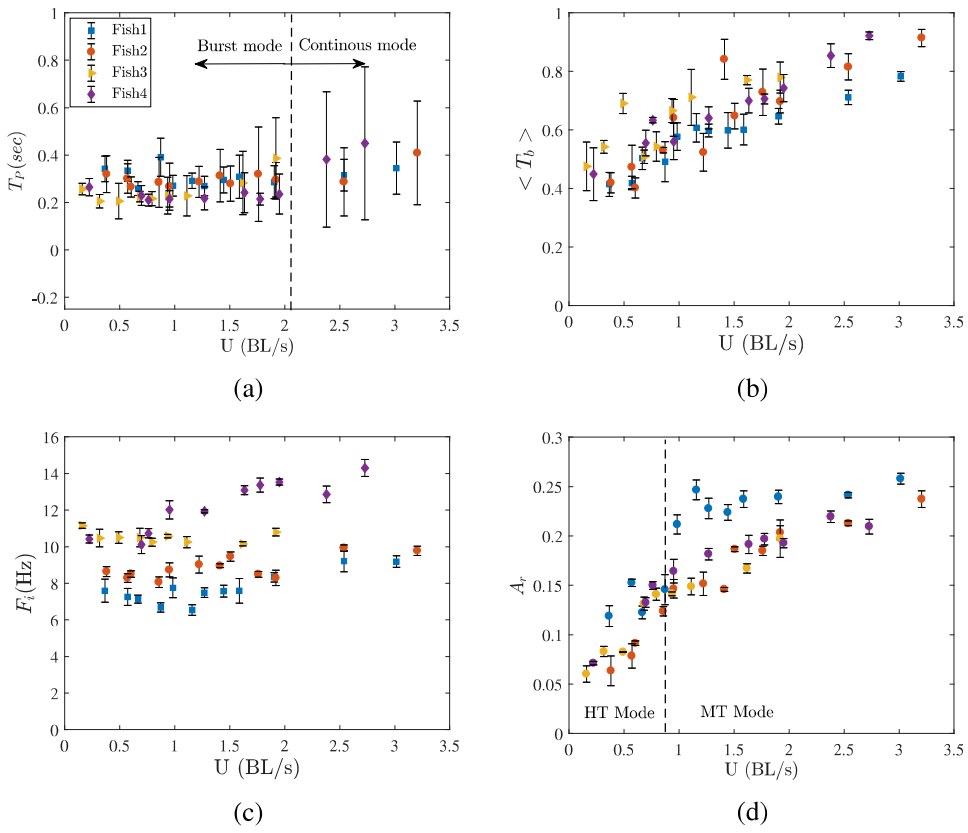

FIGURE 3.2: (a) Burst-and-coast event period, T_P, (b) duration of bursting with respect to the burst-and-coast event, where 1 means continuous flapping, (c) internal frequency (measured within a burst) and (d) tail-beat amplitude at the rear end of the caudal fin A_r, as a function of the average swimming velocity in body lengths per second.

stops during time, T_C, to finish the bout coasting before the next burst. At low velocities, the burst consists of only a half tail-beat, which determines the clear asymmetry observed in the midline kinematics. Following the nomenclature of Wu et al. [145], we call this half-tail-beat mode the HT mode. Increasing the swimming velocities determines, first, that a full back and forth tail-beat is performed for every burst; subsequently, for larger velocities, multiple tail-beats per burst occur. We refer to the last two cases as MT mode (multiple tail-beat mode).

The measurements of T_P and T_b for all the cases tested are summarised in Fig. 3.2(a) and (b) as a function of the swimming velocity. Remarkably, the average bout time remains fairly constant, although more fluctuations are observed at high

swimming velocities. The increasing percentage of the bout occupied by bursting appears clearly in Fig. 3.2(b). Two other measurements can be obtained from the tail-beat kinematics: On the one hand, the *internal frequency* F_i, that is, the tail-beating frequency within a burst, which is shown to be characteristic to each individual fish. However, for each fish, it remain relatively constant for different trials, regardless of the swimming velocity or duration of the burst (see Fig. 3.2 (c)). On the other hand, the tail-beat amplitude A_r increases rapidly for low velocities as the burst changes from the half tail-beat amplitude of the HT mode to the full tail-beat amplitude, flattening to a slightly increasing trend from velocities of $\sim$ 1 BL/s and higher.

3.5 Discussion

The results of the present experiments show that *Hemigrammus bleheri* fishes in station-holding swimming against an ambient flow adopt a burst-and-coast strategy. The average duration of a burst-and-coast bout remains constant, as the imposed swimming velocity is increased (see Fig. 3.2(a)) around a value of $\approx$ 0.3s. We found no measurements of this time in the literature for *Hemigrammus bleheri*, but it is lower than the free swimming values of $\approx$ 0.5s reported for another tetra fish, *Hemigrammus rhodostomus* [151] and $\approx$ 1s for the zebra fish *Danio rerio* [143], which are of similar size to *Hemigrammus bleheri*. The mechanism used by the fish to cope with the increasing current seems to mainly involve the increase of the bursting time within a bout (see Fig. 3.2 (b)). The characteristic tail-beat frequency of the burst event F_i remains relatively constant at different swimming velocities (see Fig. 3.2(c)), pointing to a time scale set by the muscle response time. The latter is also consistent with the observation of F_i changing between individuals. In contrast, the tail-beat amplitude, A_r, on the contrary does increase with increasing swimming velocity (see Fig. 3.2(d)), especially for velocities lower than 1 BL/s, due to the build-up of the full flapping cycle (the MT mode). Thus amplitude increase is related to increasing bursting time: To sustain low velocities, only a short bursting

time, T_B, is needed, and thus, only a half tail-beat can be accommodated; as the T_B increases, there is enough time to complete a full tail-beat, entering the so-called MT mode. Once the MT mode is in place, at velocities higher than 1 BL/s, the amplitude increases at a much lower rate.

We can go back to the measurements of the midline deformation, as shown in Fig. 3.1 to make conjectures on the mechanical processes that accompany the burst-and-coast kinematic observations. For $U < 1$, the undulation is restricted to the caudal region of the fish, as shown in Fig. 3.1(a). As U increases, the undulation starts shifting forward, showing that more muscles are recruited to power the swimming stroke —see Fig. 3.1(b-c). Muscle strain can be represented quantitatively using the midline curvature k [152, 153]. The curvature $k(x) = \frac{y''(x)}{(1+y'(x)^2))^{3/2}}$, where $y(x)$ is the curve representing the midline and primes represent spatial derivatives, is presented in Fig. 3.3(a), showing that a larger extent of muscle is recruited at higher velocities. This is further validated from Fig. 3.3(b) and 3.3(c), which represent the maximum curvature value K_{max} and average value K_{avg} of the midline, respectively. K_{max} and K_{avg} increase with the swimming velocities. As expected, the maximum curvature is found near the tail tip. These findings illustrate that fish swimming is extremely adaptive in nature. Similarly, in the case of trout swimming in an altered flow, such as in the wake of an upcoming obstacle, it was observed that fish interact with vortices and alter their body kinematics and curvature to match the shedding of vortices [114]. This shows that the fish not only sense the flow, but they also interact with it, adjusting their body kinematics accordingly. However, these adjustments are not limited to the tail-beat frequency and amplitude; the body movements and curvature are also adapted.

The burst-and-coast regime is widely viewed as an energy saving mechanism, but in light of the arguments made in the previous paragraph, another important use of the intermittent swimming could be the active flow sensing. As discussed in chapter 1, fish use the lateral line system to detect distortion in the flow signals due to their own swimming or nearby objects[154], which can be prey, a predator, simply a wall

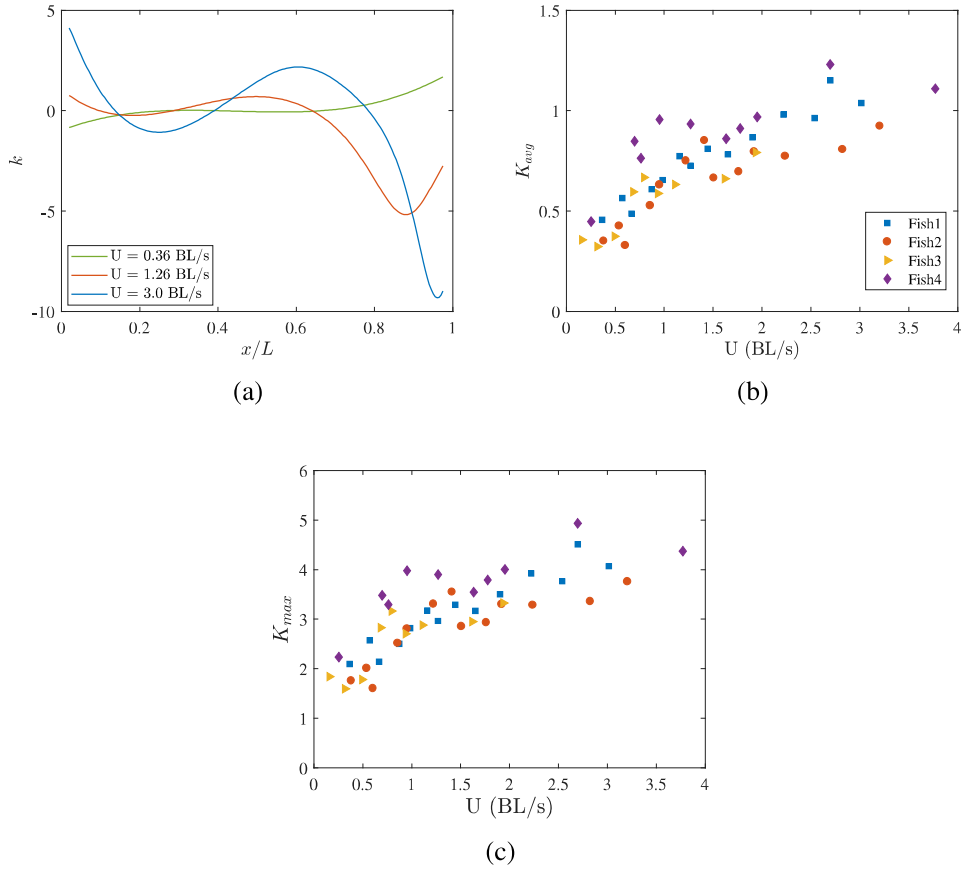

FIGURE 3.3: (a) Curvature at profile, (b) average curvature value & (c) maximum curvature value as a function of swimming velocity, U.

or another fish. The fish is more likely to be detected while in movement. Therefore, intermittent locomotion can reduce the probability of detection of both predators and preys [155, 156]. Feitl et al. [157] also demonstrated that intermittent locomotion offers sensory benefits in terms of predator detection over continuous locomotion. Therefore, the fish could use the strategy of burst-and-coast swimming to achieve these sensory benefits.

In our experiments, we observed a bout of constant duration. The exact reason for the constant bout is unknown to us. It seems that it may be related to the neurobiological clock of the fish, which may be optimised to achieve goals, such as fatigue recovery, stability of the sensory field or avoidance of detection by a sympatric predator or prey with in the fish's sensory zone. However, this needs to be investigated in

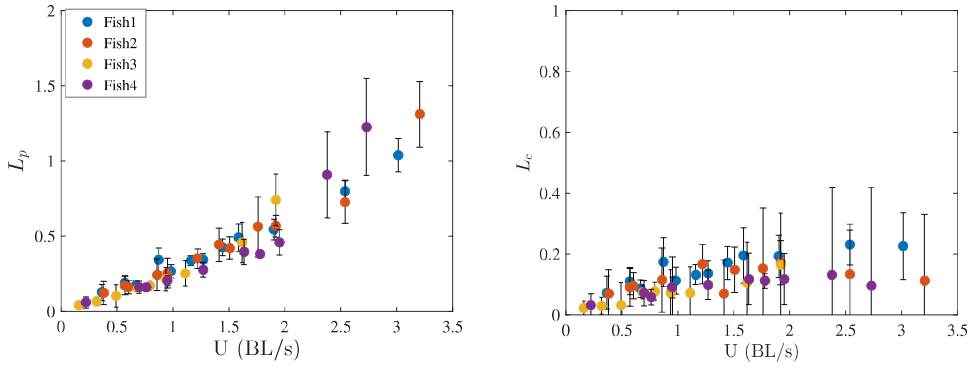

(a) (b)

FIGURE 3.4: (a) Length scale L_p during bout period (b) Length scale L_c during coast period as a function of swimming velocity, U.

future research works.

Using the measurements of burst-and-coast duration, we defined two length scales, $L_p = U* < T_p >$, and, $L_c = U* < T_c >$, of swimming during the bout period and coast period, respectively. As shown in Fig. 3.4, at low swimming velocities, both L_p and L_c are similar in magnitude, showing that the distances covered during burst-and-coast are approximately equal. However, L_p is much greater than L_c at higher swimming velocities, which demonstrate that, at high velocities, fish need to burst for a considerably longer period.

Chapter 4

Synchronisation and collective swimming patterns in fish *Hemigrammus bleheri*

Ce chapitre reprend l'article : Ashraf, I., Godoy-Diana, R., Halloy, J., Collignon, B., Thiria, B. (2016). Synchronization and collective swimming patterns in fish (Hemigrammus bleheri). *Journal of The Royal Society Interface*, **13(123)**, 20160734.

4.1 Abstract

In this work, we address the case of red nose tetra fish *Hemigrammus bleheri* swimming in groups in a uniform flow, giving special attention to the basic interactions and cooperative swimming of a single pair of fish. We first bring evidence of synchronisation of the two fish, where the swimming modes are dominated by "out of phase" and "in phase" configurations. We show that the transition to this synchronisation state is correlated with the swimming speed (i.e. the flow rate), and thus with the magnitude of the hydrodynamic pressure generated by the fish body during each swimming cycle. From a careful spatiotemporal analysis corresponding to those synchronised modes, we characterise the distances between the two individuals in a pair in the basic schooling pattern. We test the conclusions of the analysis of fish pairs with a second set of experiments using groups of three fish. By identifying the typical

spatial configurations, we explain how the nearest neighbour interactions constitute the building blocks of collective fish swimming.

4.2 Introduction

Collective behaviours of living animals in nature have recently been in the center of attention of a pluridisciplinary research effort, from biologists and neuroscientists to physicists and applied mathematicians [2, 3]. Complex social interactions are hidden behind the motions and reactions of aggregates of individuals, leading to different levels of cohesive organisation, that depend on each species' needs and ways of living. Fish schools are archetypes of these kind of cohesive social systems and they have been discussed over now several decades [61, 68]. Except from social life, benefits from swimming in groups are, for instance, a way to reduce risk from potential predators or to optimise food prospection [68, 158]. Schooling is also often evoked from an energy perspective [61, 112, 159] where the spatial organisation of individuals within the swimming group is said to optimise hydrodynamic interactions for a global power saving of the school. In any case, the formation and organisation of a group is built on local cooperation between individuals, which is achieved relying on different sensory systems such as vision or the flow sensing lateral line [65]. The specific characteristics of the subsystem composed of the interactions of an individual and its nearest neighbours, are thus the building blocks from which large and complex social groups are developed.

However, if strong efforts have been made by improving models, simulations and observations, the exact comprehension of the formation of swimming groups still need new insights. One of the main shortcomings is the lack of convergence between observations, assumptions and conclusions. For instance, real schooling data can be found in the literature from biologists, reporting tridimensional and unsteady behaviours for different configurations [65, 160] which might be considered far from the ideal two dimensional and energy-based approaches of physicists [112].

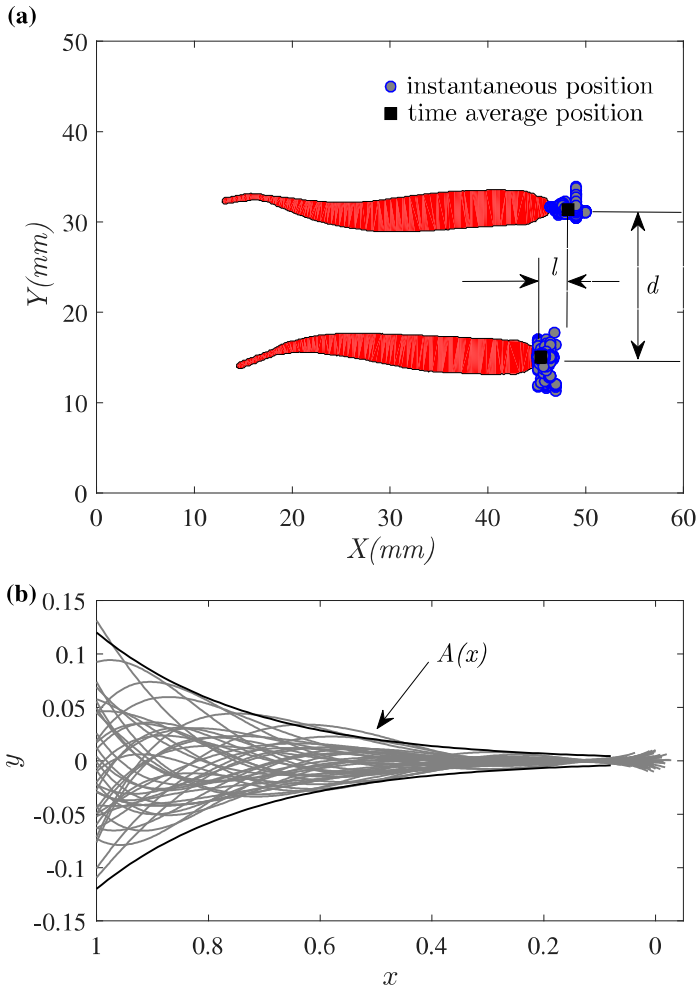

FIGURE 4.1: (a): Example of top visualisation of two swimming fish. The school pattern is defined by the two characteristic length scales d and l, representing the distance to the nearest neighbour(s) and the shift between leading and following individuals, respectively. (b): superimposed instantaneous swimming kinematics (middle lines) extracted from the visualisation. The black lines are the spatial envelop fitted with the analytical function $A(x) = A_r \exp\alpha(x-1)$ [22]. The head of the fish is located on the right, the tip of the caudal fin on the left.

In this work, we propose to study the basic mechanisms underlying the formation of a school combining a physical approach and real fish observations. The present work focuses specifically on the most simple subsystem of cooperation between individuals, namely the schooling of a fish pair. We aim here at characterising the transfer of information within the duet mainly using fluid dynamics considerations and direct visualisations of swimming fish. We show that, even for such a simple

configuration, the schooling pattern formed by the fish pair already presents certain repeatable features. In particular, we highlight a phenomenon of phase synchronisation and elementary pattern formation between swimmers, which are observed to keep the distance to nearest neighbours constant and to prefer an energetically favourable synchronisation pattern. Then, based on the two fish observations, we analyse the behaviour of fish trio and also present an opening account of it.

4.3 Results

A setup was especially designed for the collective swimming of red nose tetra fish *Hemigrammus bleheri* . It consists of a shallow water tunnel (2cm depth) in order to foment swimming of neighbouring individuals in the same plane; the two other dimensions of the tunnel are 20cm $\times$ 15cm (see Fig. 2.1), sufficiently large compared to the typical size of the fish ($\sim$ 4 cm long $\times$ 0.7 cm width). Water flow rates used in this work range from 4 to 22 litres per minute, corresponding to swimming velocities of 2.7 to 15 cm s^{-1}. For each test, the fish quickly start swimming at the flow velocity imposed on the water tunnel, i.e. they stay in a stationary position in the laboratory frame as can be seen from Fig. 4.1(a). The swimming velocity U is thus the average flow velocity based on the cross-sectional area of the test section and it can be set precisely by controlling the flow rate through the test section. The fish kinematics are recovered from top view visualisations, giving the spatio-temporal evolution $y(x,t)$.

4.3.1 Two fish experiment

We study the statistics of the fish kinematics over a population. For the two fish configuration, 14 different individuals (7 pairs) were studied. For each pair, experiments were performed for 10 different swimming velocities. Neither of the individuals in a pair is repeated in any other pair. From these data we first address global quantities of the collective swimming of two fish, namely, the evolution of the beating frequency f and amplitude A, the phase velocity v_ϕ of the bending wave that characterises the

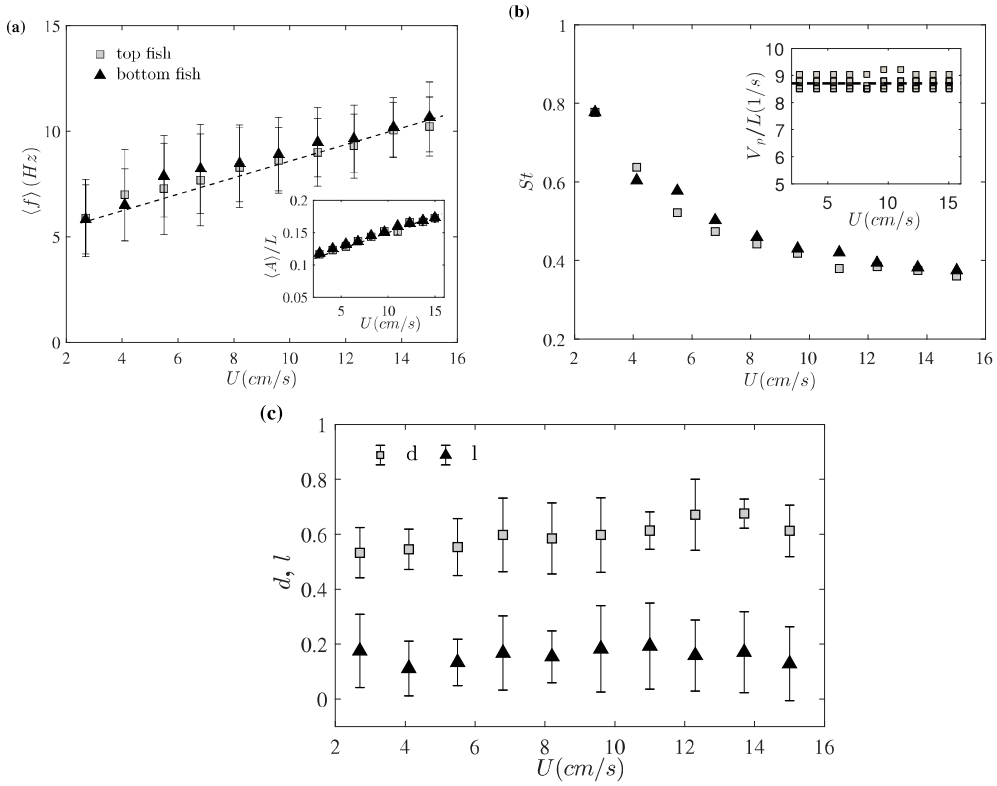

FIGURE 4.2: (a) Averaged beating frequency, f, and amplitude,A, (inset) for both top and bottom fish as a function of the swimming velocity averaged over the seven pairs studied. As can be seen here, fish frequencies are very close to each other and evolves linearly with U. L is the fish body length. (b) Strouhal number $St = \langle f \rangle \langle A \rangle / U$ and phase velocity v_ϕ (inset) as a function of the swimming speed U. (c) Typical lengths l and d defining the swimming pattern of a tandem of individuals as a function of the swimming speed. Again, the values are averaged over the seven pairs studied. The results show a constant value for both lengths, setting in average, a single spatial ordering for the tandem.

body deformation kinematics, and the evolution of the pattern chosen by the fish to swim together, as a function of the swimming velocity. For a tandem configuration, the swimming pattern is fully described by the two distances d and l as illustrated in Fig. 4.1. The results are displayed in Fig. 4.2 and correspond to averaged quantities over the seven different pairs of fish.

A few conclusions can be readily drawn form these first observations. First about the kinematics, we see that the frequencies of the top and bottom fish (Fig. 4.2(a)), respectively, are in average very close to each other and evolve linearly with the flow rate. There is of course a large scattering around the average values (up to 30 % represented by the error bars on the data), resulting from several experimental sources of uncertainty such as the selected pair or the size of the fish. In the inset of Fig. 4.2(a), the amplitude evolution as a function of the swimming velocity is also shown. In the same manner, the phase velocity v_ϕ (inset Fig. 4.2(b)) seems converging to a constant value, for all fish and all swimming velocities (again with a large scattering due the heterogeneity of the population). This is not surprising because v_ϕ is directly related to the elasticity modulus of the fish [161]. In Fig. 4.2(b) we plot the Strouhal number, defined in the usual way as the ratio of the flapping characteristic velocity Af and the swimming speed U. It can be readily seen that as the swimming velocity increases the Strouhal number tends to lower values, in the range of those corresponding to efficient swimming [162].

Spatial pattern

The most noticeable observation from this data certainly concerns the swimming pattern (or spatial arrangement) chosen by the tandem. This pattern is fully described by the two characteristic l and d, as described in Fig. 4.1. As can be observed in Fig. 4.2 (c), the parameters of the swimming pattern stay statistically constant over the large range of swimming velocities tested here; fish seem to choose a stable configuration independent of their gait. The distance d, which can be refereed to as the distance to the nearest neighbour (NND) is here measured around $0.5-0.6$

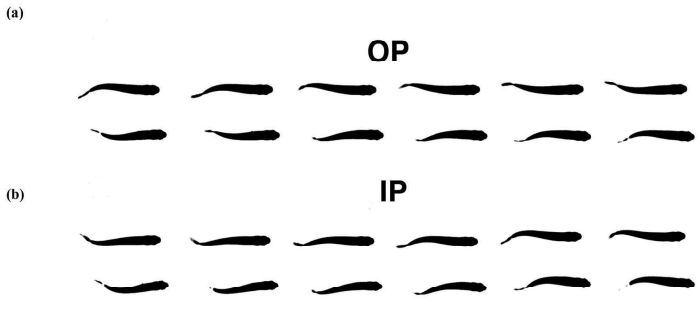

FIGURE 4.3: Top: The two different state of synchronisation observed for a pair of swimming *H. bleheri*. The OP state corresponds to a configuration where both fish swim out-of-phase (a), the IP state to a configuration where both fish swim in-phase (b).

fish body lengths. This value is consistent with observations that have been made on schooling fish with strong cohesion (as the red nose tetra fish) [163].

Synchronisation

The two cases shown in Fig. 3 are the two synchronisation modes considered: in-phase (IP, Fig. 3(b)) and out-of-phase (OP, Fig. 3(a)). To define synchronisation in a fish pair, we compared the tracks of the tail tips of the two fish using the tail beating of one fish as reference —the top fish in the representation of 4.1(a). For each tail flapping cycle of the reference fish, the signal of the neighbouring fish was analysed defining a phase difference signal $\delta\phi$ with one measurement point every cycle. Fig. 4.4(a) and Fig. 4.4(c) correspond, respectively, to the tail beat signals of a pair at slow (2.7 cm s^{-1}) and fast (15 cm s^{-1}) swimming velocities, while Fig. 4.4(b) and Fig. 4.4(d) correspond to the instantaneous phase difference between the tail beat signals of the top and bottom fish. The instantaneous phase can thus be defined as $\delta\phi = 2\pi\langle f\rangle\,\delta t$, where δt is the time difference between two nearest peaks in the two tail beat signals. To build the histograms in Fig. 4.5, we counted

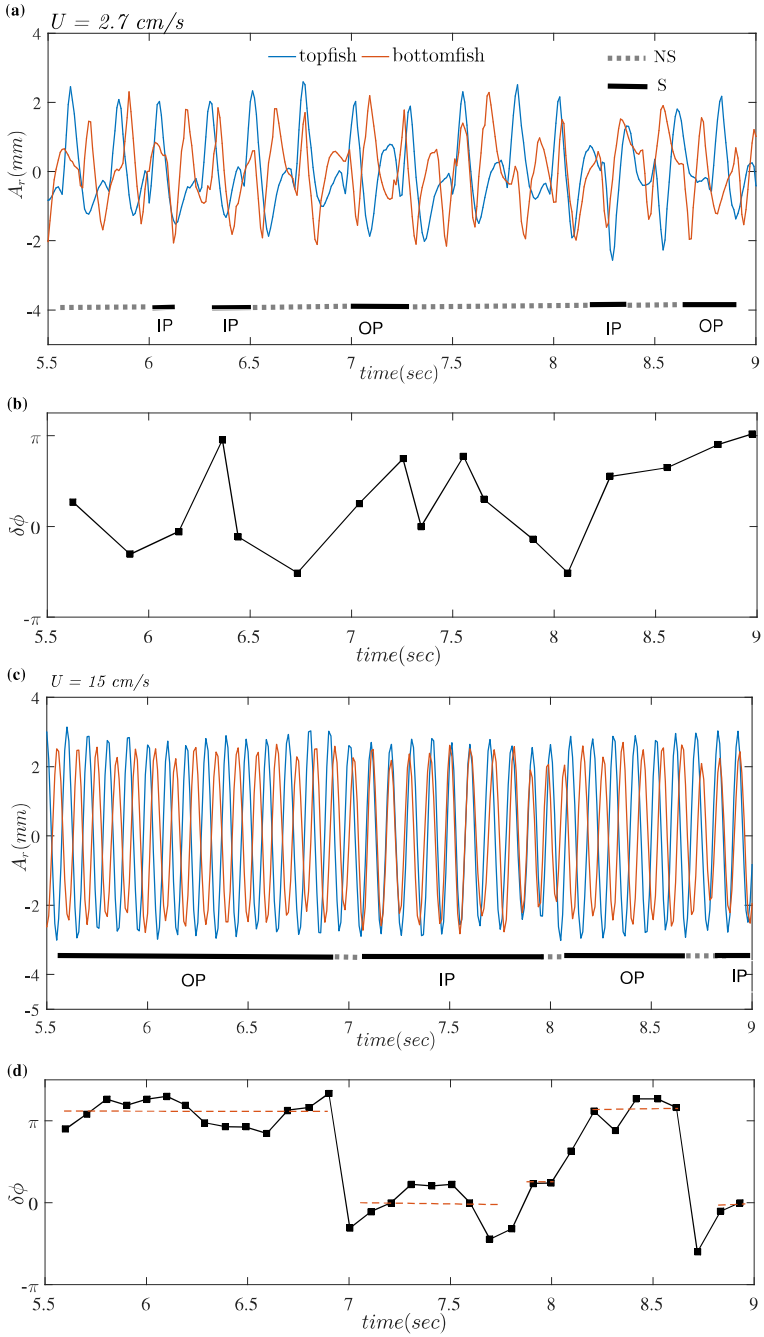

FIGURE 4.4: Two typical caudal fin tip kinematics for respectively slow (2.7 cm.s^{-1}, (a)) and fast (15 cm.s^{-1}, (b)) swimming velocities. Top and bottom fish are represented by blue and red lines, respectively. Phase difference plot for swimming velocities 2.7 cm s^{-1}, (b) and 15 cm s^{-1}, (d) respectively.

one synchronised state (**S**) for each full flapping cycle in which the two fish were observed to perform IP or OP swimming. In any other configuration – partially synchronised or fully desynchronised– the cycle was counted as non-synchronised (**NS**). IP or OP were defined, respectively, when the instantaneous phase difference is $0 \pm \pi/4$ and $\pi \pm \pi/4$. From Figs. 4.4(a) and 4.4(b), we can clearly see that at low speed there is basically no synchronised swimming except for a few cycles. On the contrary, when the fish are forced to swim faster synchronised states are preferred, as shown in Figs. 4.4(c) and 4.4(d).

Fig. 4.5 shows the cumulated statistics (averaged over the seven different pairs of fish) of the synchronised states as a function of the swimming velocity. The evolution is here straightforward: for relatively slow swimming velocity, the fish spend most of their time swimming independently in a **NS** state (see Fig. 4.4(a)). This tendency changes with increasing swimming velocity where more and more **S** states are observed in the distribution to get, in contrast, for fast velocities, to an almost fully synchronised state over the period of observation (which represents more than 80 tail beating cycles). The transition from independent to collective swimming is here clearly observed to be based on the fish gait, which strengthens the importance of the interactions betweens individuals. This synchronisation process recalls, for instance, the mechanisms of interpersonal coordination of side-by-side human walking [164–166], where it was shown that the rate of synchronisation was statistically correlated with the strength of sensory feedback mechanisms. And of course synchronisation is a widely observed phenomenon in collective motion (see e.g. the recent study by Yuan et al. [167] on the synchronisation of swimming *C. elegans*). It is worth noticing that the fish pair, when synchronised, favours the anti-phase state (OP). This point will be discussed further below.

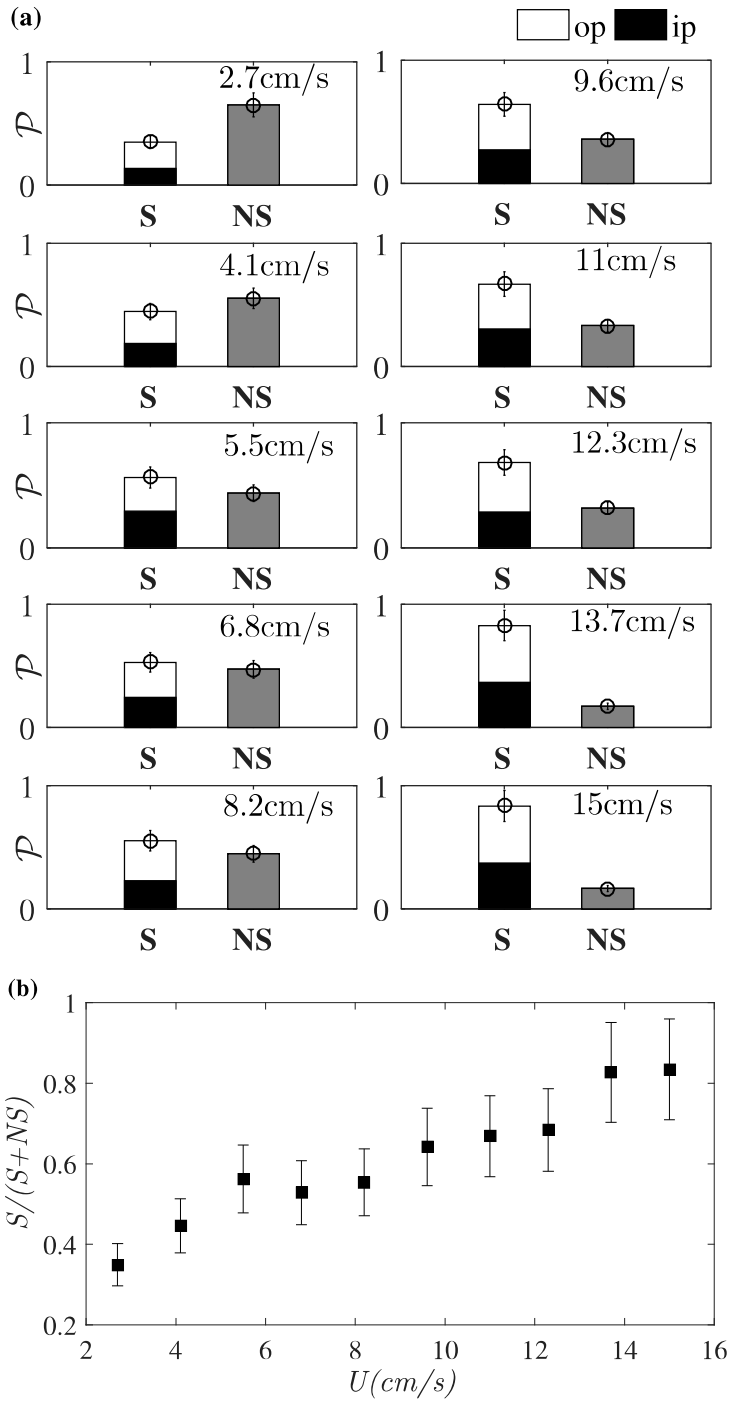

FIGURE 4.5: (a) Cumulated probability histograms of synchronisation over seven different fish pairs at different flow velocities. In each frame, the left bar represents the percentage of time where the fish were synchronised (**S**), in phase (black fill) or out of phase (white fill), over a 10 second recording of the swimming kinematics. The right bar is the time spent out of synchronisation (**NS**). The time series were analysed using the flapping frequency of one fish as the time base so that fish were considered synchronised at a given time only if they spent the full flapping period synchronised. (b) Plot showing the cumulative probability of synchronised state as a function of swimming speed.

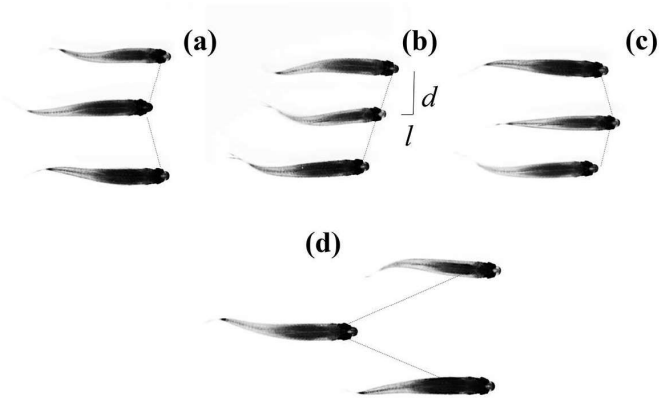

Probability	
a	0.22
b	0.26
c	0.36
d	0.16

FIGURE 4.6: Top row: Illustration of the three most probable swimming patterns for a three fish group of *H. bleheri*. Distances and angles between neighbours are kept constant. (a): two aligned fish are leading the pattern on the sides and the middle fish lies in the back. (b): one fish is leading the pattern on the side, the two other fish are shifted respectively from the other. (c): one fish is leading in the middle of the pattern, two aligned fish follow in the back. Bottom row: (d) occasionally observed schooling pattern evoking the diamond-like arrangement described in [112], two aligned fish are leading the pattern on the sides. This time the third fish is evolving in the wakes of the two firsts, changing the global organisation of the swimming pattern.

4.3.2 Three fish experiment

We conducted another set of experiments for seven groups of three fish in the same swimming conditions. The results are displayed in Figs. 4.6 to 4.8. Fig. 4.6 shows the patterns observed over the whole range of swimming speeds, summarising the geometric parameters of the shoaling pattern. The top row shows the three most probable observed patterns, the last case shown in 4.6(d) represents 16% of the observations for three fish schooling in the present work.

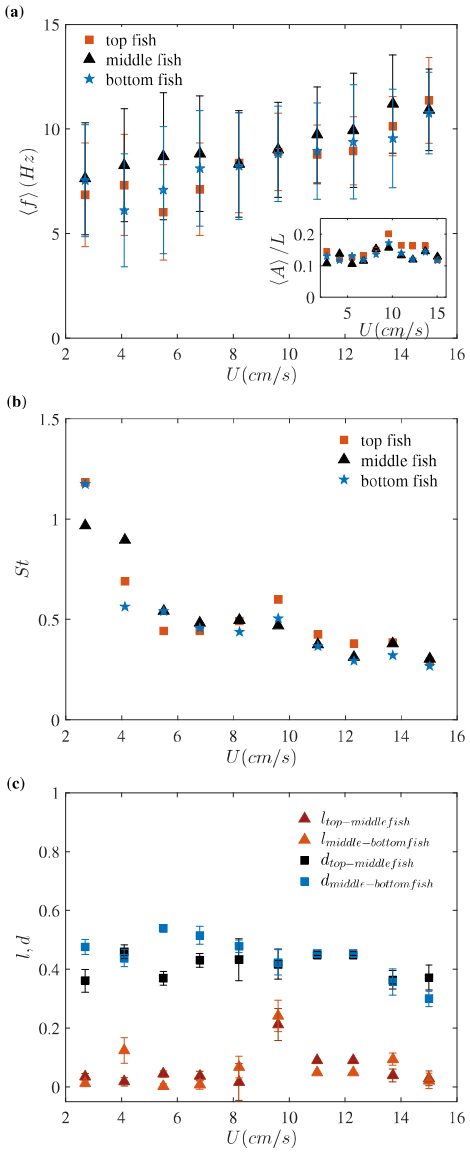

FIGURE 4.7: (a) Averaged beating frequency for the three fish (top, middle, bottom) as a function of the swimming velocity averaged over the seven trio of individuals studied, and amplitude in the inset. As for the two-fish case, respective frequencies are very close to each other and evolves linearly with U. (b) Strouhal number for the three fish (top, middle, bottom) as a function of the swimming velocity. (c) Typical distance to nearest neighbour and shift lengths l defining the swimming pattern of the trio of individuals as a function of the swimming speed. Again, the values are averaged over the seven pairs studied.

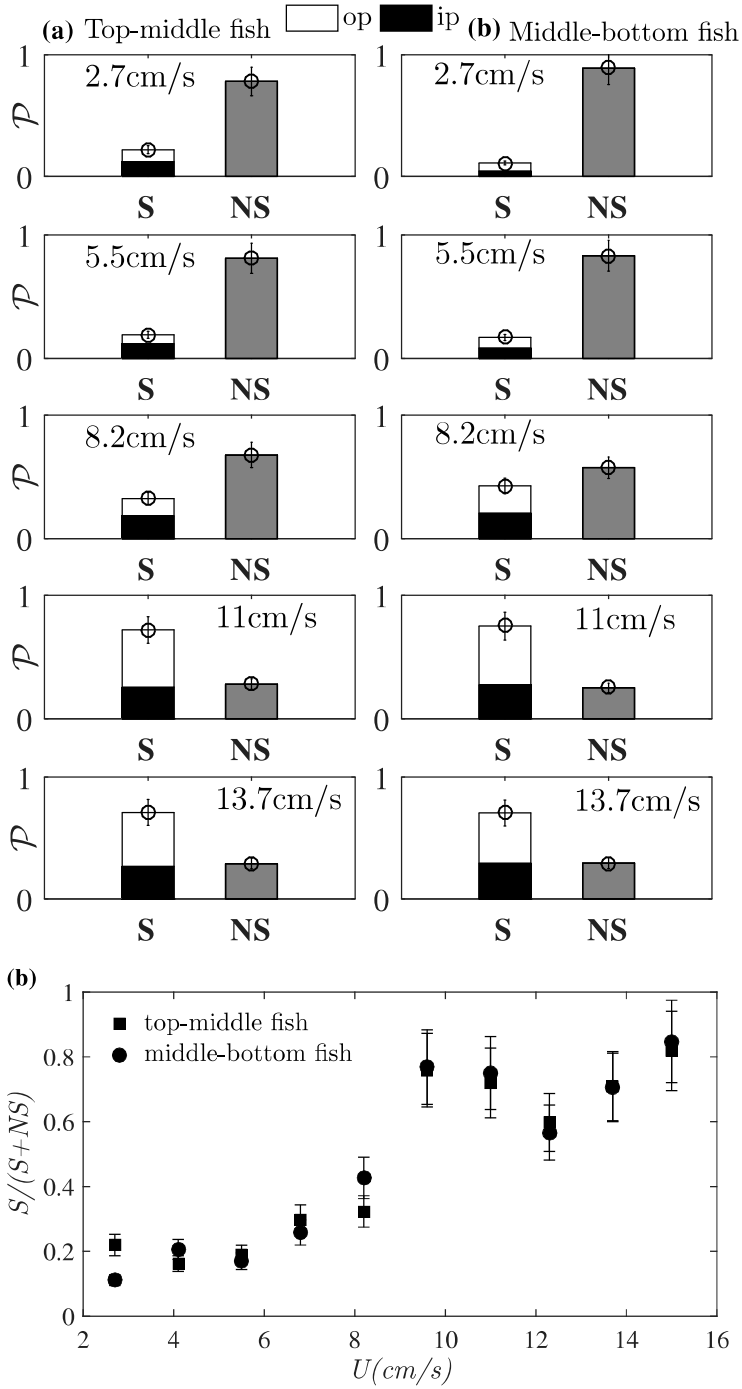

FIGURE 4.8: (a)-(b) Cumulated probability histograms of synchronisation over seven different fish trios at different flow velocities. In each frame, the left bar represents the percentage of time where the fish were synchronised (**S**), in phase (black fill) or out of phase (white fill), over a 10 second recording of the swimming kinematics. The right bar is the time spent out of synchronisation (**NS**). (c) Plot showing the cumulative probability of a synchronised state between (1) top and middle fish and (2) middle and bottom fish, as a function of swimming speed.

4.4 Discussion

Some physical arguments can be put forward in order to understand the basic interactions behind the schooling mechanism. The first concerns the synchronisation process as a direct consequence of the sensitivity of each individual to hydrodynamic pressure, through the lateral line. This lateral system has been shown to play an important role in the cohesive behaviour of swimming fish [65], and more particularly in a population of *H. bleheri* [60]. Together with vision, sensitivity to pressure fluctuations is thus the principal mode of interaction between neighbours in the present experiments. To a first approximation, the flow around a swimming fish can be described considering a two-dimensional elongated waving plate evolving in a potential flow [17, 168]. In that case, the local pressure on the fish body can be explicitly calculated for a prescribed kinematics. Here, the kinematics can be easily determined from the middle-line extracted from the visualisations. Following [22], we consider that the amplitude distribution of the swimmer is given by $A(x) = A_r \exp \alpha(x-1)$, where A_r is the amplitude of the displacement at the tail tip of the swimmer and α represents the growth rate of the local amplitude along the body (i.e. the head to tail amplitude ratio). This specific kinematics favours the contribution of the tail to the propulsion with respect to the head of the fish. Using Bernoulli's equation (see [22] and references therein for details), the pressure fluctuation $p(x)$ can be written

$$p(x) \sim -\mathcal{M}(\ddot{y} + 2U\dot{y}' + U^2 y''), \tag{4.1}$$

where $\mathcal{M}$ is the added mass coefficient defined as the product of the fluid density ρ_f and the the fish section $\mathcal{S}$ [22]; the dot and prime symbols stand for time and spatial derivatives, respectively. Thus, for a fish kinematics given by $y(x,t) = A(x) \exp \omega(x/v_\phi - t)$, where ω=2πf, we have

$$p(x) \sim -\mathcal{M} y(x) \left[\omega^2 - 2U \left(\omega\alpha + \frac{\omega^2}{v_\phi} \right) + U^2 \left(\frac{\omega}{v_\phi} + \alpha \right)^2 \right]. \tag{4.2}$$

Finally, considering that $\omega \sim U$ (see Fig. 4.2(a)), it follows that the magnitude of the pressure signal becomes greater with increasing frequency and that it gradually increases from head to tail. An example of the pressure field generated using the kinematics of the moving midline for $y(x,t)$ is shown in Fig. 4.9.

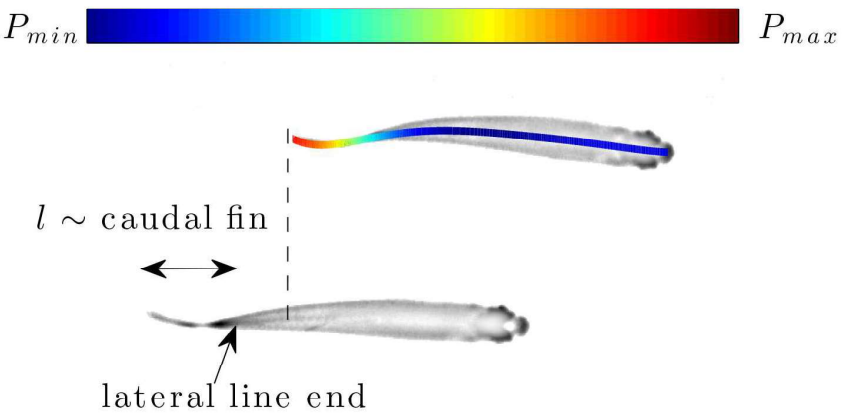

FIGURE 4.9: The pressure field produced by the undulating midline calculated using Eq. 4.2 is shown in colour for the top fish, illustrating that the maximum of pressure fluctuations occurs before the end of the lateral line of the neighbouring fish (at the root of the caudal fin) because of the pattern chosen by the fish pair.

Now, as shown in Fig. 4.2(c), fish keep constant their separating distance d while swimming, for the whole range of flow speeds studied. This means that, referring to the above scaling for the pressure, the intensity of the interaction between individuals grows drastically with the swimming velocity. Assuming that each swimming fish behaves as an independent oscillator, coupled to its neighbours by sensory feedback mechanisms (the feedback being here ensured by the lateral line), synchronisation thus takes place when the coupling mechanism constituted by the fluid pressure signal generated between the two individuals is sufficiently strong. This is consistent with models of synchronisation of non-correlated and noisy oscillators that have been extensively studied in the literature [169–171]. It can be also seen from Fig. 4.4(a) and Fig. 4.4(c) that the tail beat signals at high swimming speeds are periodic and

smooth as compared to those at low swimming speeds, which is another indication of the strong coupling of the two synchronous swimmers.

High swimming speed gaits are thus characterised by synchronised states in the side-by-side fish pair configuration. As evoked above, in this regime, the anti-phase pattern (OP) is favoured with respect to the opposite in-phase (IP) mode. These two swimming modes have been studied recently both experimentally [172, 173] and numerically [159] in the context of collective swimming of fish-like robots. The main conclusion of those works was that anti-phase swimming is an energy-saving mode for the swimmers. This conclusion was based on the generated wake difference (i.e. the energy dissipation rate) between both configurations. The (OP) mode, because of its mirror-symmetry between the two swimmers, was found to limit flow velocity fluctuations produced by the tail, hence improving efficiency. Transposed to real fish, the side-by-side configuration should benefit from the same effect. More specifically, the (OP) mode might be a collective strategy for fish swimming out of their usual gaits as, for instance, in the cases of high velocity imposed in this experiment. This conjecture is strengthened by the trend of the Strouhal number displayed in Fig. 4.2(b), which reaches its lowest values (indicating more efficient swimming) specifically in the regime of synchronisation. These observations suggest an adaptation of the gait for efficiency purposes.

The other feature of the basic pattern in the two fish experiments is the gap length l. As shown in Fig. 4.2(c), this distance remains statistically constant for all pairs and swimming speeds studied, fixing, with d, the geometric pattern for the two fish. The existence of this gap can be understood by the need to maintain a good transfer of information within the fish pair. As evoked above, *H. bleheri* use the lateral line to sense the presence of their nearest neighbours. This lateral line, for most species and in particular for *H. bleheri* and other *Hemigrammus* species, is located all along the fish sides but does not penetrate in the caudal fin [60, 174–176]. The zone near the caudal fin is however the region where pressure fluctuations are focusing, due to the specific swimming kinematics. In the case of a side-by-side configuration, a perfect

alignment of the two fish will not give an optimal configuration as the strongest produced pressure would be placed in face of an inert zone in terms of sensing. A small shift, roughly of the typical size of the caudal fin (measured at 0.16 ± 0.01 body length for the 14 fish), could nevertheless overcome this problem and give a more efficient communication between the two fish. Results plotted in Fig. 4.2(c) show shift distances l of the order of magnitude of caudal fin length, which strengthens the above statement. This consistent shift in the side-by-side configuration establishes a leader-follower hierarchy in the pair. Although beyond the reach of what could be observed in the present experiments, it would be interesting to see if this hierarchy is respected over long periods of swimming.

Under the light of the previous observations, assuming that highly shoaling fish hold the distance to their nearest neighbours [60, 65], the spatio-temporal pattern seems to be imposed by the transfer of pressure information from one individual to the other. An isolated pair of swimming *H. bleheri* is then characterised by aside-by-side pattern, shifted to install an efficient transfer between the pressure source (the swimming fish) and the sensor (through the lateral line). High speed swimming cases are characterised by phase synchronisation states (IP and OP states) which are not statistically equiprobable; in those specific regimes demanding high energy resources, the anti-phase synchronisation is favoured for its efficient nature.

The previous conclusions are of course to be put into perspective for larger populations of fish, and the goal of the experiments with three fish, that we have performed so far, was to test how the results from the two fish experiment could scale up. The three patterns 4.6(a-c) can be directly derived from the two fish interactions as they represent the possible combinations keeping l and d constant for the three fish. Those observations are quantitatively reported in Fig. 4.7. Also, synchronisation states still hold for the three fish arrangement. Statistics are displayed in Fig. 4.8 and bring strictly the same conclusion as for the side-by-side configuration of Fig. 4.2, giving strength to the basic one-to-one interactions illustrated between two fish.

There is, however, a noticeable difference between the two and three fish configurations. In addition to the preferred pattern illustrated in Fig. 4.6 (a), (b) and (c), the trio chooses sometimes the organisation exemplified in Fig. 4.6 (d). These organisation recalls the basic subsystem of the so-called "diamond shape" evoked in the pioneer work of [112]. Here, the fish in the middle lies in the wakes of the two leaders in the front, breaking the previously observed organisation of the swimming pattern. This last spatial configuration is still statistically infrequent to be considered as an alternative swimming strategy in itself. It is however worthy to note that even if this pattern is occasional, it seems stable over time.

4.5 Concluding remarks

Previous works have revealed the network of visual interactions in fish a group [177, 178] and its importance for the information transfer within the group. Here, we extend the analysis of inter-individual interactions to bio-mechanical mechanisms. The distance between nearest neighbours d is constant probably maintained by visual contacts. We observed in this work a persistent shift l in the other length scale that defines the basic spatial pattern between neighbouring fish, as well as a synchronisation state of the caudal fins oscillations. We argument that while the pattern geometry facilitates information transfer between neighbours, the observed synchronisation can be explained from an energy efficiency perspective. Indeed, the synchronisation increases with swimming speed, corresponding to a range of Strouhal numbers of efficient gaits. Further works, in the continuity of the present one, will be dedicated to study groups with larger numbers of swimmers to put into perspective the basic interactions shown here in a more complex network.

Chapter 5

Simple phalanx pattern leads to energy saving in cohesive fish schooling

Ce chapitre reprend l'article : Ashraf, I., Bradshaw, H., Ha, T. T., Halloy, J., Godoy-Diana, R., Thiria, B. (2017). Simple phalanx pattern leads to energy saving in cohesive fish schooling. *Proceedings of the National Academy of Sciences*, **114(36)**, 9599-9604.

5.1 Abstract

The question of how individuals in a population organise when living in groups arises for systems as different as a swarm of microorganisms or a flock of seagulls. The different patterns for moving collectively involve a wide spectrum of reasons, such as evading predators or optimising food prospection. Also, the schooling pattern has been often associated to an advantage in terms of energy consumption. In this study we use a popular aquarium fish, the red nose tetra fish *Hemigrammus bleheri*, which is known to swim in highly cohesive groups, to analyze the schooling dynamics. In our experiments, fish swim in a shallow water tunnel with controlled velocity, and stereoscopic video recordings are used to track the three-dimensional

positions of each individual in a school, as well as their tail-beating kinematics. Challenging the widespread idea of fish favouring a diamond pattern to swim more efficiently (Weihs, *Nature* **241**:290-291, 1973), we observe that when fish are forced to swim fast —well above their free-swimming typical velocity, and hence in a situation where efficient swimming would be favoured— the most frequent configuration is the "phalanx" or "soldier" formation, with all individuals swimming side-by-side. We explain this observation by considering the advantages of tail-beating synchronisation between neighbours, which we have also characterised. Most importantly, we show that schooling is advantageous as compared to swimming alone from an energy efficiency perspective.

5.2 Introduction

The dynamics of animal groups is driven by many different factors, such as foraging, social life or survival instinct against predators [179]. The collective movements are built from local interactions between the individuals constituting the group [2, 3]. Apart from behavioral aspects, the benefit from schooling has been often associated with group optimization in terms of hydrodynamic resistance [61]. A fish school represents a typical case of such cohesive and collaborative complex systems. The fluid dynamical mechanisms influencing the motion of fish in a school have been described in essence in the early study of Weihs [112]. He demonstrated, using a two-dimensional (2D) model, that if each fish maintains a specific position within the school, forming a diamond pattern, the hydrodynamic interactions will improve globally the swimming performance. The basic idea is that fish in a school optimize swimming by interacting constructively with the vortices shed by the local leading individuals; such constructive interactions require a precise synchronization between fish. This study has been followed by an extensive number of studies modeling or simulating fish school swimming configurations in order to validate Weihs' hypothesis [127, 128, 180]. It has been shown that by following this strategy, fish could

improve their efficiency by around 20% [48, 128]. However, the idea that a beneficial situation in terms of swimming power can be achieved for the group by maintaining a specific complex pattern remains, in some sense, a pure view from hydrodynamicists rather than an observation from nature. One of the shortcomings of the diamond pattern as a true description of natural systems lies in the strict 2D approach, which limits the comparison with real fish schools. There have certainly been several three-dimensional (3D) computational studies on a single fish swimming [25, 26, 48, 181–183], but very few exploring the case of fish swimming in groups [127]. Another limitation of the diamond pattern is that its effectiveness imposes the strong constraint of maintaining a precise position and a quasi-perfect synchronized kinematics of the individuals within the group [127]. To a certain extent, this interesting and elegant view of fish group dynamics may be too idealized for noisy and multiple-parameter-dependent real schools.

In the present study, we investigate the energy-saving mechanisms of a fish school using real fish in a controlled swimming experiment. We chose for this purpose to examine the case of the red nose tetra fish *Hemigrammus Bleheri*. This species is particularly cohesive [60], representing thus a characteristic system to analyze collaborating interactions. It has been used in a recent study focusing on the interactions of neighboring fish swimming in pairs and triads —which can be considered the elementary sub-systems of a fish school— that reported remarkable collaborative swimming features motivated by energy saving [149]. This study showed especially that tail-beat synchronization increases dramatically when fish are forced to swim fast, i.e. in more energy demanding gaits. How the nearest-neighbor dynamics scales up when considering larger schools is the question that we address in this paper, where we have analyzed groups of up to 9 individuals swimming at different speeds. The experimental apparatus allows to explore a wide range of swimming speeds, from less than one body-length-per-second (BL/s), which is roughly the natural free swimming gait of *H. Bleheri*, to high energy-consuming regimes (such as escaping or hunting) at up to 4 BL/s. Additionally, the swimming channel is relatively shallow

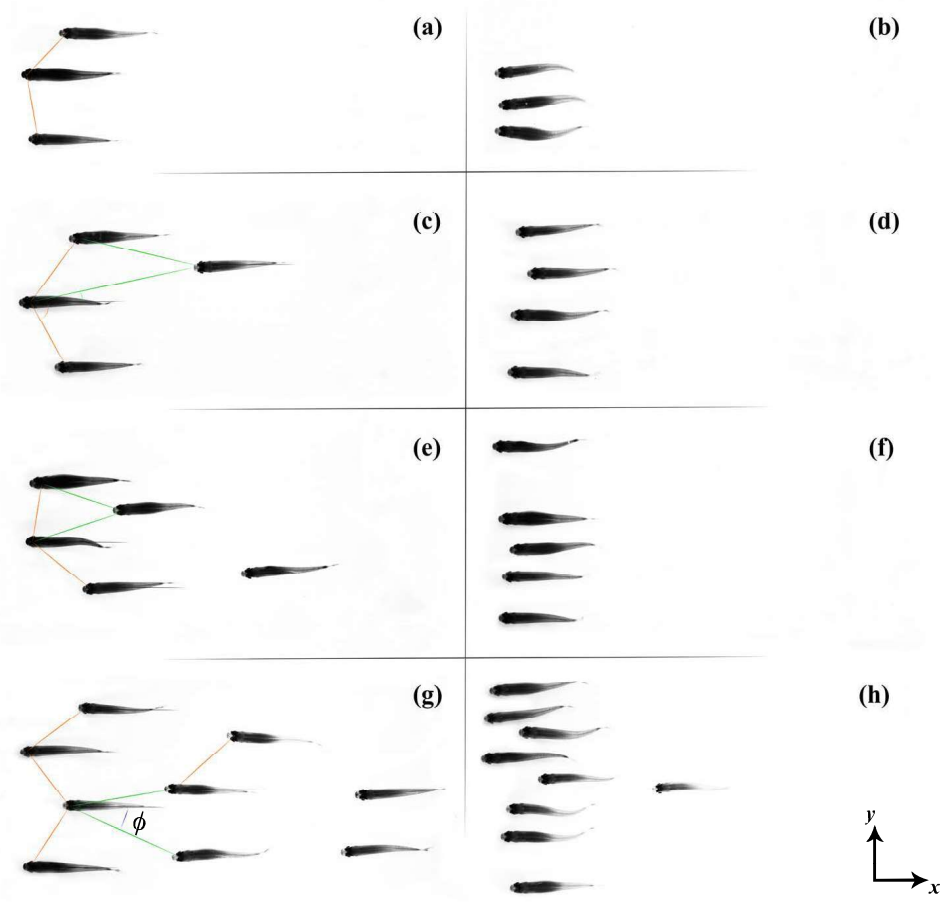

FIGURE 5.1: Characteristic swimming patterns for increasing fish group size at two different swimming speeds. Left column (a), (c), (e) (g): $U = 0.77BL.s^{-1}$. The school pattern is spread downstream with characteristic angles and distances to nearest neighbors (see text). Right column (b), (d), (f) (h): $U = 3.91BL.s^{-1}$. As more effort is required to hold a high swimming regime, the fish reorganize in a compact in-line formation. In this configuration, fish within the group are synchronized with their nearest neighbors, corresponding to collaborative efficient swimming modes.

such that it constrains the vertical spatial extent of the fish school, leading to quasi-two-dimensional patterns. We show that the most efficient swimming mode does not correspond to a diamond pattern but rather to in-line configurations where fish take advantage of side-by-side hydrodynamic interactions. We show in detail, by studying different group sizes, that the global dynamics of the school can be deduced by local basic fish-to-fish interactions. Synchronization between neighbors is shown to be one of the crucial physical mechanisms involved, correlated with the observation

of a decreased intensity of the tail-beating stroke when a fish is part of a school.

5.3 Results

A stereoscopic camera setup has been used to track the three-dimensional position (x, y, z) of each fish constituting the school as a function of time (see Materials & Methods section for details). In addition, the body deformation, characterized by the time-resolved kinematics of the body mid-line, is recovered from top view visualizations [as in 149], giving information for each individual on the tail-beating frequency and amplitude. The swimming velocity of the school is set by imposing a flow in a shallow water tunnel, ranging from 2.5 to 15 cm s^{-1}. Fig. 5.1 shows typical school structures of groups of different sizes (from 3 to 9 individuals) observed at low and high swimming velocities (0.8 BL/s and 3.9 BL/s, respectively). As can be seen, there is a strong contrast between these two limiting cases. The patterns observed at low velocities (left column) show the individuals spread along the direction of the stream, with the typical spreading length increasing with the group size (pair, triplet, quartet, quintet and nontet). The spatial patterns formed in this case can be identified as diamond configurations —see for instance Fig. 5.1 (g). The picture changes markedly for the cases with high swimming velocity. Regardless of the school size these are characterized by in-line configurations, described in the literature as *phalanx* [128] or *soldier* [121]. This type of swimming pattern is observed for instance for hunting/predatory bluefin tunas in the Atlantic ocean [122]. We also note that the typical nearest-neighbor distance (**NND**) is smaller than in the schools swimming at low velocity. The observations of Fig. 5.1 are supported by a statistical analysis over a large number of measurements (see Materials and Methods section) with single fish and schools of up to 9 individuals.

The averaged characteristics of the school are given in Fig. 5.2 as a function of the swimming velocity. Fig. 5.2 (a) shows the vertical spreading of the fish school using the distance to a reference fish in the school normalized by the fish height h_z,

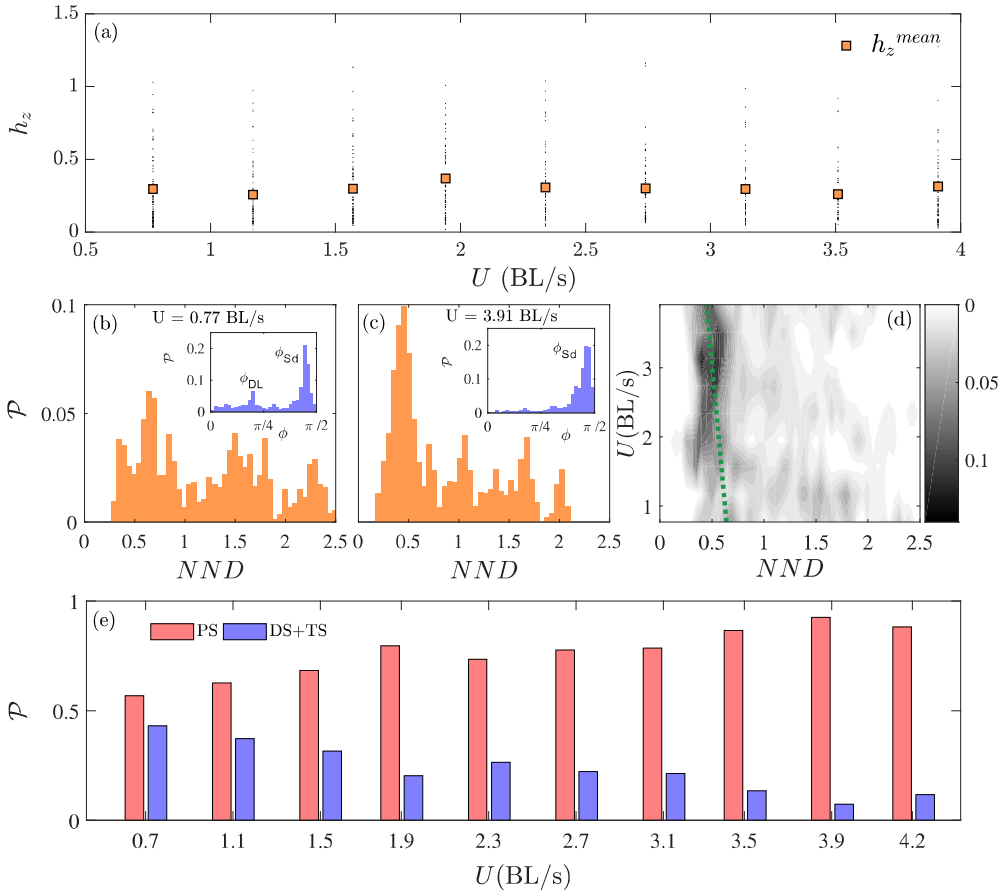

FIGURE 5.2: Statistical properties of the fish schools as a function of swimming speeds over the whole range of cases studied. (a) Variation of the z-position of fish (h_z is the depth normalized by the fish average body height) as a function of swimming speed. Small black dots represent the instantaneous z-position of each fish, whereas orange squares represent average z-position, averaged over all groups. (b) and (c): Probability density of the nearest neighbor distance **NND** for low and high swimming speeds respectively. Insets show the probability density of nearest neighbor angles ϕ. (d): Probability density map of **NND** as a function of the swimming speed. (e): Percentage of occurrences of diamond-shaped **DS** (or T-shaped **TS**) and phalanx-shaped **PS** patterns. High speed swimmers are mainly characterized by phalanx patterns and short **NND** in comparison to low speed regimes.

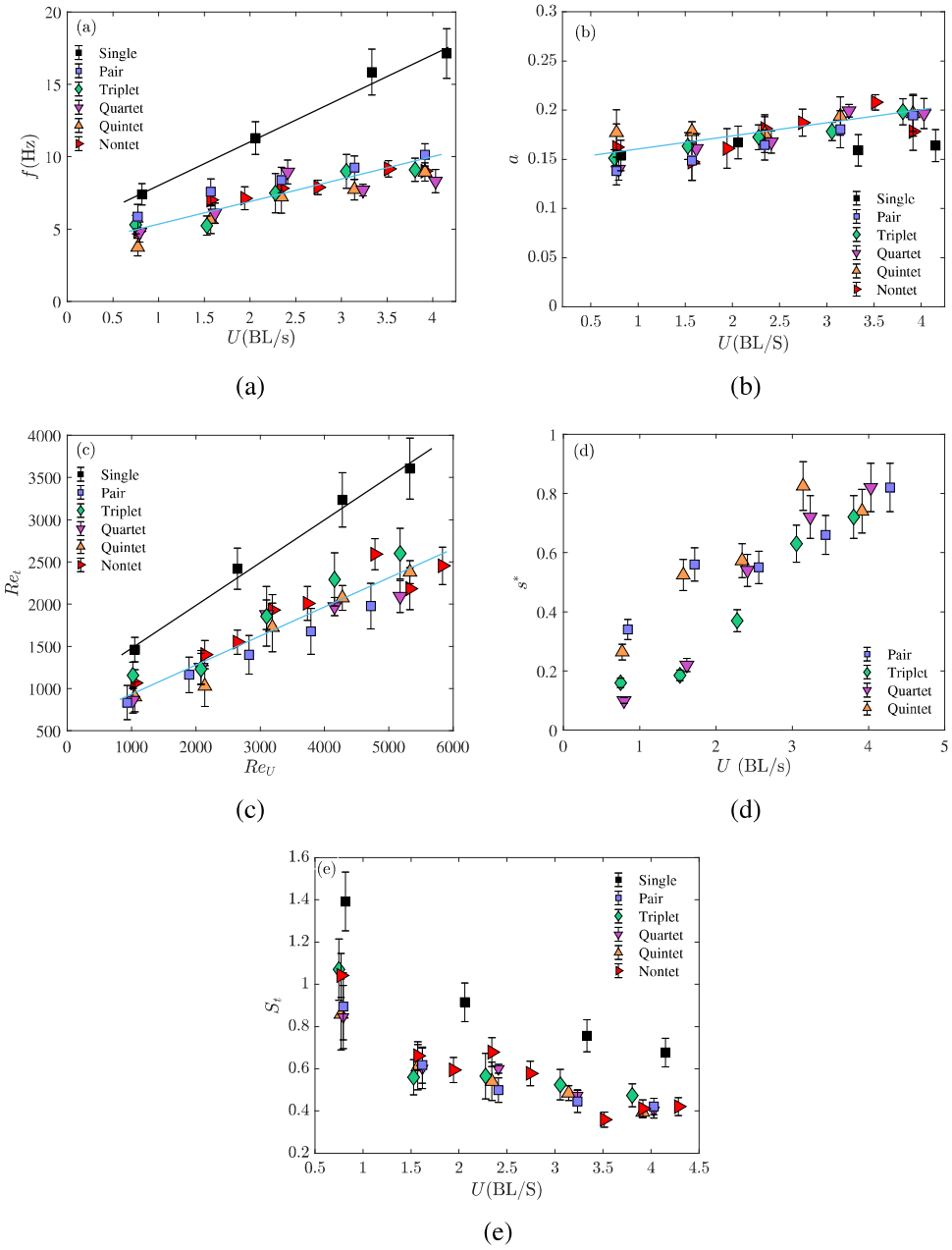

FIGURE 5.3: (a) Tail flapping frequency f (Hz), and (b) Tail flapping amplitude (non-dimensionalized by fish body length), as a function of the swimming velocity U (in body lengths per second). (c) Transverse Reynolds number, $Re_t = \langle f \rangle \langle A \rangle \langle L \rangle / \langle \nu \rangle$, as a function of the cruising Reynolds number, $Re_U = \langle U \rangle \langle L \rangle / \langle \nu \rangle$. (d) Evolution of the synchronisation parameter $s^* = S/(S+NS)$ that represents the cumulative probability of a synchronized state between nearest neighbors, as a function of the swimming velocity U. (e) Strouhal number, St, as a function of the swimming velocity U.

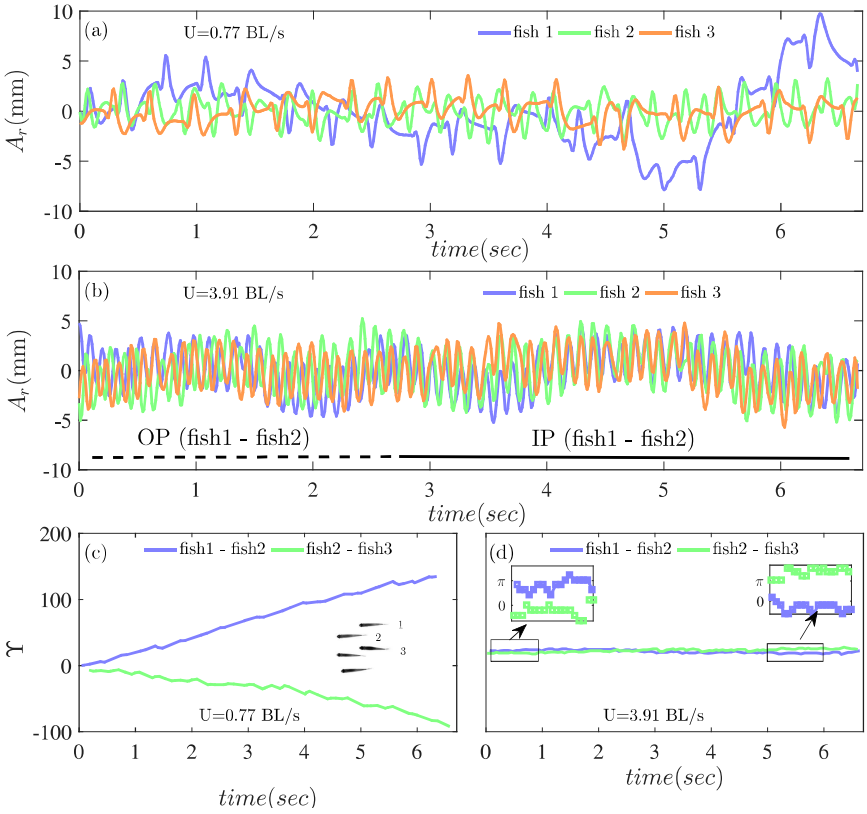

FIGURE 5.4: Examples of time series of the tail tip amplitude for one given individual (fish 2) within the school and its two nearest neighbors (fish 1 and fish 3). (a): For low swimming speed and (b): high swimming speed. The in-phase (IP) and out-of-phase (OP) swimming regimes are also shown. Evolution of the phase difference Υ between fish 2 and its two nearest neighbors (fish 1 and fish 3) showing (c) a non-synchronized state (*NS*) at low swimming speed and (d) strongly synchronized state (*S*) at high swimming speeds. The insets in (d) show zooms in the case of synchronised swimming that are either around 0 (for in-phase synchronization) or π (for out-of-phase synchronization).

showing that fish are on average placed at most at a quarter of fish height from their neighbors. The schools do have nonetheless a three-dimensional structure, which supports the observations reported in the literature where a slight spreading of the school pattern in the third dimension permits to enlarge the visual field of each member of the school [82, 184, 185]. Considering the horizontal positions, in Fig. 5.2 (b) we note that at low swimming velocities, the school patterns present two typical **NND** and angles as defined in Fig. 5.1 (left column). This characteristic pattern has already been identified in previous study on *H. Bleheri* fish triplets [149]. As can be observed, this reduced set of geometric parameters determines the most basic school consisting of a fish triplet and we use it here to describe the spatial pattern for larger groups of individuals. Results for high swimming velocities, where stronger effort is required to sustain a high swimming velocity, confirm that, statistically, there is only one typical angle characterizing the group pattern —see inset in Fig.5.2 (c)—, and that the typical **NND** becomes shorter —see the shift in the histogram in Fig. 5.2 (c) with respect to that in Fig. 5.2 (b)—. The histograms for all swimming velocities are compiled in the map shown in Fig. 5.2 (d), where the bright spot at high velocities shows the aforementioned trend (the green dashed line marks the shift in the most probable **NND**. All the experiments can be summarized in terms of statistical occurrences of diamond-shaped (**DS**, fish behind the leading rows are placed between the two nearest neighbors in front of them), T-shaped (**TS**, where one fish follows directly behind one of the leaders) or in-line "phalanx" (**PS**, with fish swimming side-by-side and closer to each other) configurations —see Fig. 5.2 (e). As can be noticed, **PS** configurations are dominant at high swimming velocity, independently of the school size. The central point is now to correlate the different spatial configurations of the schools with the observed tail-beating kinematics, which is how we probe the swimming efficiency of the school. Fig. 5.3 presents the kinematic measurements obtained from the midline tracking for all cases. The tail-beating frequency f and amplitude a are shown in Fig. 5.3 (a) and (b), respectively, as a function of the swimming velocity. As can be seen, no consequence of

swimming in a group is observed on the tail-beating amplitude, which only increases slightly when fish are swimming faster. However, there is a clear effect on the frequency: fish swimming alone use a higher frequency than those that have at least one neighbour. Moreover, this difference in tail-beating frequency increases with the swimming velocity. The frequency and amplitude observations can be summarized using the dimensionless representation of Fig. 5.3(e) (c) that shows the transverse Reynolds number $Re_t = faL/\nu$ as a function of the usual cruising Reynolds number $Re_U = UL/\nu$. The Re_t has also been named the *Swimming number* in a recent study on the scaling of macroscopic aquatic locomotion [186] and has been used in the literature to describe flapping based locomotion [see e.g. 187]. Because the amplitude is almost constant, the dimensionless Re_t vs. Re_U curve reproduces the results already described in the frequency curve.Another quantity usually used to describe animal swimming is the Strouhal number $St = fa/U$ [see e.g 162], which is related to swimming efficiency because it compares the input effort of the fish characterized by the flapping velocity fa to the output represented by the swimming velocity U. The values of St resulting from the present observations range between 0.3 and 1.5 (see Fig. 5.3). In accordance with the observations for the frequency and amplitude, the average Strouhal numbers for fish schools are lower than those for fish swimming alone at the same velocities. Combining the observations on the school patterns and those on the beating kinematics, we note that the most frequent patterns corresponding to efficient swimming —i.e. low values of Strouhal number— are characterized by a side-by-side phalanx configuration. The other remarkable feature observed in the fish schools is the change of synchronization of tail-beating kinematics between neighboring individuals within a group. The time series of the caudal fin tip motion for three neighboring fish in a group of five are reported in Fig. 5.4, at (a) low swimming velocity (close to the natural speed of free swimming) and (b) high swimming velocity (representing a high-energy-demanding situation). Fish swimming together at their free ranging speed do not show any sign of correlation in their respective kinematics; the phase differences in Fig. 5.4 (c), Υ between one individual

(fish 2) and its two nearest neighbors (fish1 and fish 3) show a constant drift (almost linear) with time, typical of uncorrelated dynamics [188]. Fast swimmers, on the contrary, show strong synchronized dynamics —see Fig. 5.4 (b)—, characterized by in-phase (**IP**) and out-of-phase (**OP**) modes. In contrast to the low speed regime, the synchronization is confirmed here by constant phase differences [188] all along the measurement time —see Fig. 5.4 (d) . The phase difference is calculated by a peak identification routine on each time series of the tail-beating amplitude. The synchronization effect for *H. Bleheri* was already pointed out in previous study with fish pairs [149], in which observations on a large set of experiments showed that more than 90 % of the fish pairs studied were synchronized when swimming at high speed. Fig. 5.3(d) presents the synchronization rate $s^* = S/(S+NS)$ as a function of the swimming velocity, where S and NS are the total number of synchronized and non-synchronized states, respectively. This demonstrates that high synchronization is a general behavior in schools sustaining high swimming gaits. It also supports the idea of considering local interactions within a subgroup of nearest neighbors as the minimal unit to describe the dynamics of larger schools.

5.4 Discussion

We have shown that schools of the cohesive fish species *Hemigrammus Bleheri* sustaining a high swimming speed gather in a phalanx configuration, rather than in the diamond pattern described as the most efficient by a 2D hydrodynamics idealized view. These phalanx configurations appear to be actually efficient, if one measures the advantage of schooling by the net decrease in the tail-beating frequency observed for fish swimming in a group, when compared to the case of a single fish swimming alone (see Fig. 5.3). The tail-beat frequency is directly correlated with the oxygen consumption rate of the fish, oxygen consumption being an indirect measure of metabolic rate and energy consumption [109, 189–196]. Therefore, the decrease

in tail-beat frequency can be considered as a decrease in energy consumption. Indeed, while at low velocities the benefit is barely observable, it is significant at the more energy-demanding higher velocity regimes, where almost all schooling occurs in phalanx formation. Moreover, the occurrence of the phalanx formation is correlated with the observation of local kinematic synchronization of each swimmer with its nearest neighbors.

Several arguments can be put forward to understand the formation of an efficient pattern in the *H. Bleheri* schools studied here. Swimming in a packed side-by-side phalanx configuration has been identified by 2D and 3D simulations as a good strategy to optimize thrust or efficiency using channelling effects, especially at small clearance ($\sim$ 0.5 BL) and in-phase synchronized kinematics of nearest neighbors [127–129]. In particular, Hemelrijk et al. [128] confirmed the advantage of phalanx and diamond shaped configuration over solitary swimming in terms of Froude efficiency. Daghooghi and Borazjani [127] underlined, based in full 3D simulations, that the wakes shed by the swimmers show strong differences with the 2D idealized view at the core of Weihs' description of the diamond pattern [112]. They reported that the primary vortices shed by the fish tail break down rapidly into smaller vortices, leading to a rather disorganized wake structure with very low chance for constructive vortex interaction. In the phalanx configuration on the other hand, the case of out-of-phase synchronization between neighbors —which has already been noted to be slightly preferred to in-phase synchronization in previous experiments with fish pairs [149]— can be expected to be beneficial in terms of propulsive performance owing to the jet-like profile produced by two neighboring fish. The latter mechanism has been demonstrated in the literature using numerical simulations [159] and experiments with model swimmers [173]. In summary, synchronization either in-phase or out-of-phase should give an advantage to fish swimming in groups, especially when nearest neighbors come closer to each other. The prevalence of phalanx configurations at high swimming velocities observed in the present experiments, together with their correlation to a high rate of kinematic synchronization between nearest neighbors,

confirms that these physical mechanisms are indeed at play in a real fish school.

Additionally, as evoked above, the possibility of taking advantage of a diamond pattern might be uncertain for actual swimming animals: fish must maintain a perfectly ordered configuration. These issues were already remarked by Weihs [112], and have been the center of criticisms in previous studies [85, 119, 184], because achieving the required conditions to maintain such idealized diamond patterns may be too constraining for a school. Choosing a phalanx pattern appears to be the selected strategy to optimize swimming performance, combining social and mechanical priorities together. It remains to be confirmed if the conclusions reached here for *H. Bleheri* is valid for other species and other experimental conditions.

Chapter 6

Conclusion and perspective

The purpose of our research was to investigate the interactions in collective fish swimming. We aimed to go further concerning what already exists in the literature on this topic. The chapter 1 clearly demonstrates that there are vast discrepancies between the different theoretical models of collective swimming and what is observed in the nature.This thesis puts an effort to bridge this gap by observing the collective fish swimming from direct observations in a control experimental setup. To achieve this, we built a specific experimental set-up where the experiments from single fish to schools of large fish can be carried out, with a flow rate parameter control. We successfully developed and implemented the fish tracking software to obtain the midline envelope and kinematics. We also implemented the stereoscopic 3D tracking system in this project.

In this project, red nose *Hemmigramus bleheri* was used as a fish species for the experiments. *Hemmigramus bleheri* was chosen because these fish species were found to be cohesive and excellent shoaling fish, and they readily respond to imposed water flow. In our experiments, we proceeded step by step. Before studying the interactions in the fish school, we started with a study on single fish swimming, then proceeded to consider the collective swimming of fish, from a fish pair to a group of nine fish (nontet). In the case of single fish swimming, we observed that the fish swam in a burst-and-coast regime at all experimental swimming velocities. This observation is consistent with what has been suggested in the literature, where fish utilises burst period for propulsion and coast period for active slow sensing [154].

As a result , the average bout period $T_P = T_B + T_C$, that is, the duration of a burst event (T_B) along with its successive coast event (T_C) remained relatively constant over the range of experimental swimming velocities. The fish employed the strategy of increasing the ratio of the burst duration to counter the increase in swimming velocities. We also observed that the fish kinematics and body curvature have a strong dependency on the swimming speed.

The experiments with fish pairs were performed to understand the interactions in their collective swimming. The two key observations were as follows: (1) pattern formation and (2) tail beat synchronisation. The individuals in fish pairs are found to be swimming side by side, and the characteristic distance between fish pair (as shown by Fig. 4.1(a)) is found to be independent of the swimming velocities. Synchronized swimming was observed in the fish pair, which is found to be linearly co-related with swimming velocities. This can be explained by understanding how fish feel, sense and interact with each other. The key sensory mechanisms in fish are the eyes, ears, lateral line system and smell. Among them, the lateral line is most important to maintain schooling and shoaling behaviour [60]. The fish lateral line is the neuromast, a sensory structure that act as a pressure sensors and allows fish to detect water motions [64]. Therefore, the lateral line is a mode of hydrodynamic sensing and interaction. Since the characteristic distances between fish pairs do not change with swimming velocities, the hydrodynamic interaction increases with the swimming velocities. As a result, the synchronisation tends to increase with swimming speed. The synchronised state is further classified into 'in-phase (IP)' and 'out of phase (OP)'. The OP mode is found to be favoured by fishes. The OP mode has been proven to be energy efficient as compared 'in-phase' mode [197]; thus, it is not surprising that fish preferred the 'out of phase' mode over 'in-phase' mode.

In our next experiments, we moved to more complex and larger schools of fish, that is, from triplets to nontets. We observed the dominance of the "phalanx" or "soldier" pattern formation at higher swimming speed; in contrast, at low swimming velocities, the diamond-shaped pattern is found to be prevalent. In the diamond

shape, the fish are spread over the entire test section and have an NND of around 1. However, in the case of "phalanx" or "soldier" formation, the fish school is extremely compact and NND is around 0.5. Theoretically, the diamond shape is considered as the most hydrodynamically efficient pattern [112]. However, it is less prevalent at high swimming velocities or high energy demand situations. This is in contrast with the generally assumed theory of the diamond shape. This is because the diamond is totally based on the constructive vortex interaction mechanism [112], which is practically impossible because vortex structure behind a real and 3D fish is complex, highly disorganised and non-coherent [48, 127]. In addition, the diamond-shaped structure puts a strong restriction on the spatial position of a fish in the school. Therefore, fish tends to adopt a simple startegy, that is, "phalanx" formation, in which they just need to be close enough for hydrodynamic interactions and can benefit hydrodynamically via the channeling' effect. This is further validated by the reduction in the tail-beat frequency of collective swimming compared with solitary swimming. Another key observation was the evolution of NND as a function of swimming. For a fish pair, it was found to be constant and independent of swimming speed. However, for larger group, there is a decrease in NND with increased velocity. This is because of the evolution of different swimming patterns for large schools. In the collective swimming of fish pairs, there is only one pattern, that is, side-by-side swimming; therefore, NND or characteristic distances are constant.

We have provided a new insight into our understanding of fish swimming and their collective behaviour, but the problem has not been definitively closed. These observations are for *Hemmigramus bleheri* only. The next step is to compare all these observations with different species especially species which have different mode of swimmimg such as anguilliform or thunniform (see chapter 1 for detail). It could be also interesting to study the fish anatomically to see what makes them behave a certain way and compare the outcomes with the study of fish in their natural environment. The environment is an important factor in the collective behaviour of fish. Thus, it would be interesting, for example, to put fish face to face with a predator or

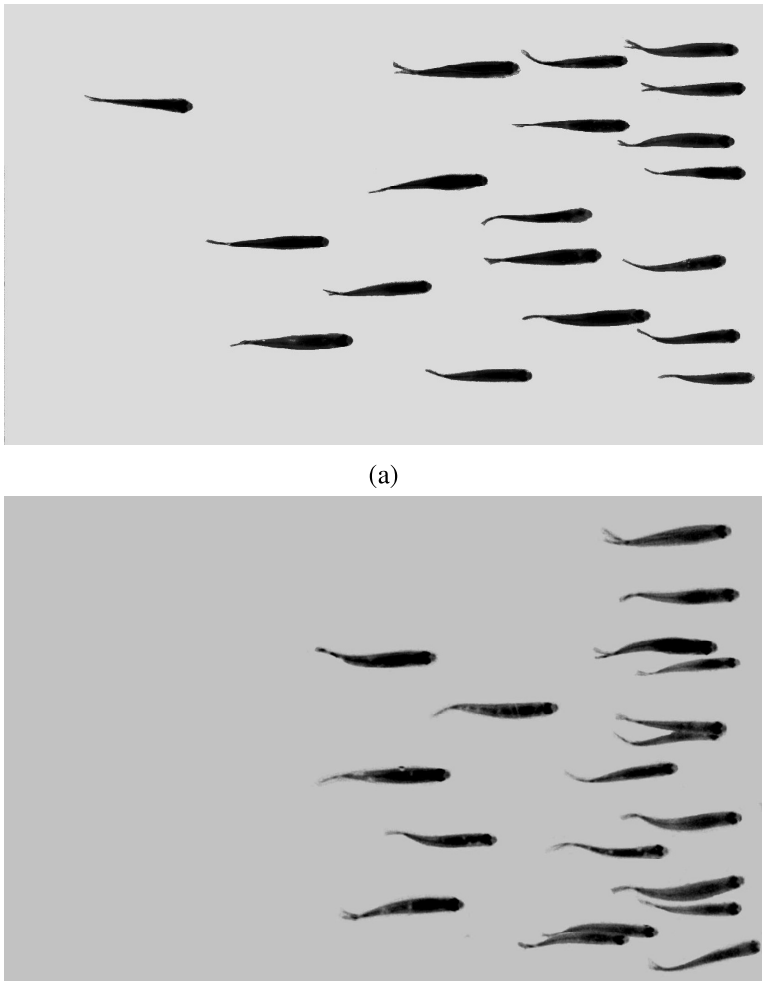

(a)

(b)

FIGURE 6.1: Fish school of size , $N = 19$, at swimming velocities of (a) $U = 1BL/s$ and (b) $U = 3.5BL/s$.

outsider, something that could provoke fear and show how they swim together when they are under stress and how they react when they are hiding and looking for food.

In this project, experiments and observation were performed for fish schools of two to nine fish. However, the findings of this project need to be examined in fish schools with large numbers of individuals. An effort was made in this direction. The preliminary result validated the findings of chapter 5 that the fish prefer phalanx formation over the ideal, diamond-shaped configuration at high swimming velocities, as shown in Fig. 6.1. But, more rigorous experimental observations are required. The key roadblock in the study of large schools is the accurate tracking of individual fish.

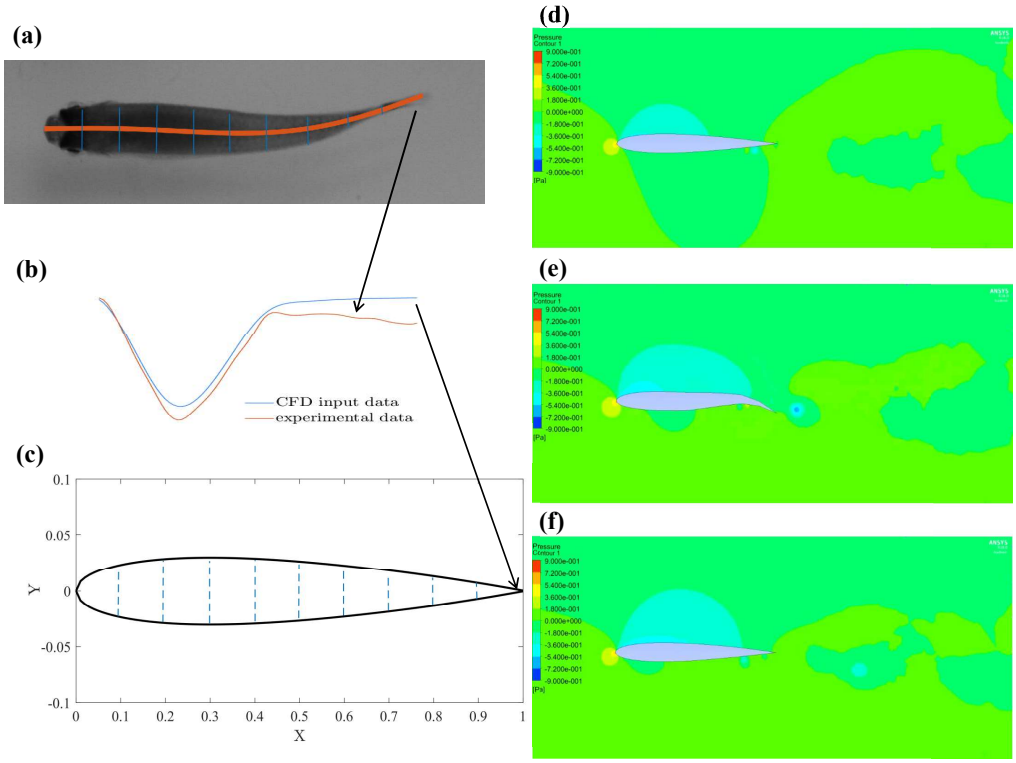

FIGURE 6.2: (a), (b) and (c) Procedure of importing fish kinematics from direct observation to NACA0012. For reference, only tail tip kinematics are shown here, but the same procedure is applied at all 10 positions from the fish body to NACA0012. Pressure contour at different intervals of the flapping cycle for the HT mode: (d) $T^* = 0$, (e) $T^* = 0.5$, (f) $T^* = 1$ at $Re = 10{,}000$.

In a large school of individuals, there is frequent occlusion. Therefore, fish cannot be tracked properly via the image processing-based method used in this project. A new approach is required to address the occlusion problem. This can be dealt with by employing model-based and machine learning algorithms to fish tracking. This will be done in future research.

The other key point is that the experimentation with different species and larger group sizes leads to an infinite amount of work, which is of course not possible. We address that matter in the chapter 1 and give some clues on how and when to fix a limit to those experimentations. The future experiments purpose should be the alliance of the different theoretical models of school and what is observed in nature.

Indeed they should be unificated because as we saw in chapter 3, for example, that the fish kinematics depend strongly on swimming velocity. Therefore, there is a

need to use actual kinematics from real experiments into computational simulations and models for actual depiction. An attempt was made here, and we successfully imported the kinematics into the commercial CFD solver ANSYS Fluent. For this purpose, we equally divided the single fish midline into 10 different parts. At each point, the kinematics for one complete cycle was taken, interpolated and fitted into an equation, as shown in Fig. 6.2(a-c). These processed kinematics were then imported into 10 corresponding positions in NACA0012. The motion between two intermediate positions involved linear interpolation, this was successfully implemented and the fig. 6.2(d-f) shows the snapshot of pressure contour for one complete cycle. However, the results are still in a preliminary stage, andfurther detailed analysis will be done in future work.

Appendix A

Supplementary materials to the paper "Synchronisation and collective swimming patterns in fish *Hemigrammus bleheri*"

Fish Pairs	Flow velocity																			
	2.7cm/s		4.1cm/s		5.5cm/s		6.8cm/s		8.2cm/s		9.6cm/s		11cm/s		12.3cm/s		13.7cm/s		15cm/s	
	l	d	l	d	l	d	l	d	l	d	l	d	l	d	l	d	l	d	l	d
Pair1	0.04	0.58	0.02	0.65	0.14	0.40	0.18	0.43	0.10	0.46	0.10	0.59	0.13	0.59	0.10	0.49	0.22	0.62	0.08	0.49
Pair2	0.21	0.55	0.08	0.50	0.22	0.62	0.07	0.63	0.11	0.73	0.13	0.81	0.10	0.60	0.07	0.60	0.07	0.68	0.04	0.60
Pair3	0.14	0.40	0.07	0.47	0.10	0.60	0.34	0.47	0.35	0.68	0.48	0.53	0.37	0.61	0.29	0.69	0.46	0.70	0.35	0.49
Pair4	0.38	0.61	0.18	0.59	0.03	0.67	0.04	0.72	0.08	0.78	0.08	0.78	0.03	0.57	0.04	0.74	0.06	0.67	0.05	0.65
Pair5	0.10	0.63	0.08	0.62	0.22	0.63	0.04	0.75	0.15	0.52	0.03	0.52	0.14	0.77	0.21	0.62	0.10	0.68	0.04	0.61
Pair6	0.01	0.39	0.02	0.43	0.01	0.40	0.11	0.74	0.07	0.46	0.08	0.41	0.09	0.54	0.02	0.63	0.01	0.78	0.01	0.78
Pair7	0.35	0.57	0.32	0.55	0.22	0.55	0.40	0.44	0.22	0.48	0.37	0.55	0.49	0.61	0.39	0.61	0.28	0.61	0.33	0.68

TABLE A.1: Characteristic distance

Fish Pairs	Flow velocity									
	2.7cm/s	4.1cm/s	5.5cm/s	6.8cm/s	8.2cm/s	9.6cm/s	11cm/s	12.3cm/s	13.7cm/s	15cm/s
Pair1	55	60	64	68	74	80	81	83	88	89
Pair2	55	69	71	67	68	72	78	85	91	98
Pair3	55	63	67	69	71	75	85	90	94	100
Pair4	58	64	67	69	72	80	86	88	96	95
Pair5	55	62	67	71	75	85	89	93	98	101
Pair6	69	80	86	82	98	102	104	102	113	117
Pair7	66	68	70	79	80	81	81	87	97	94

TABLE A.2: Number of flapping cycles used for calculating asynchronous and synchronous phase

Fish Pairs	L1/L2
Pair1	**1.11**
Pair2	**1.10**
Pair3	**1.0**
Pair4	**0.98**
Pair5	**1.0**
Pair6	**0.94**
Pair7	**1.0**

TABLE A.3: Fish length ratio

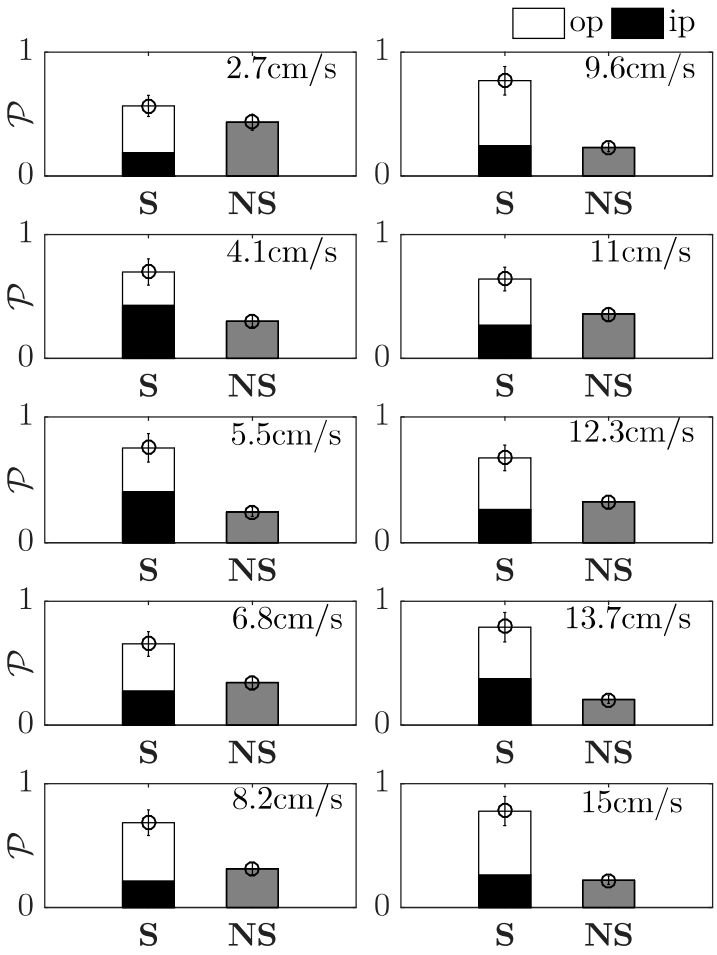

FIGURE A.1: Probability histograms of synchronization of fish pair 1 at different flow velocities. The mean body length of pair1 is 33 mm. The ratio of body length of two fish(L1/L2) is 1.11, where l1 is body length of top fish and L2 is body length of bottom.

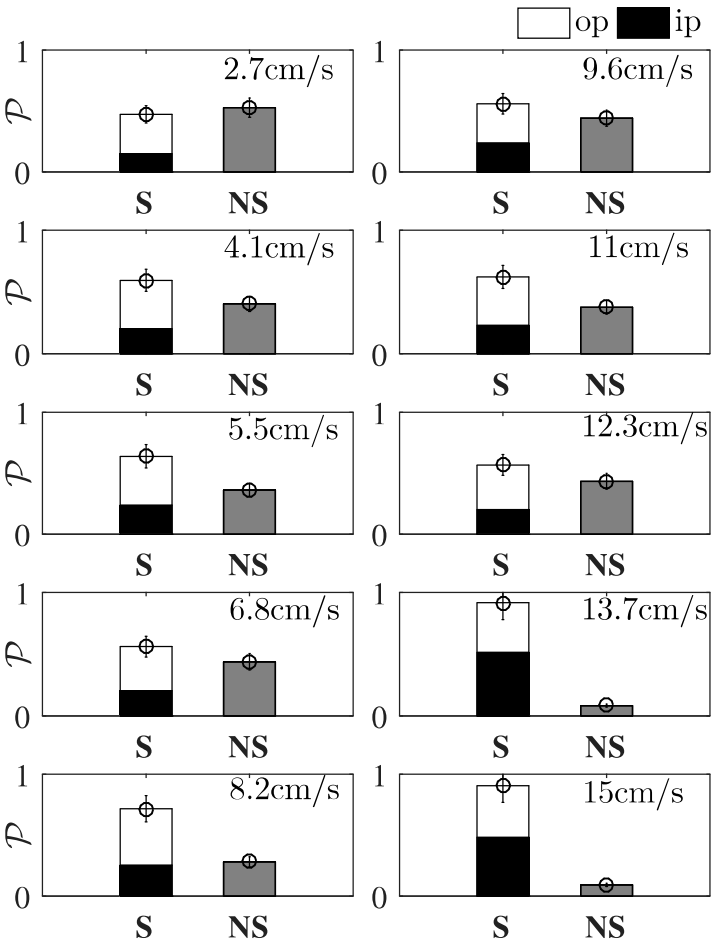

FIGURE A.2: Probability histograms of synchronization of fish pair 2 at different flow velocities: The mean body length of pair2 is 28 mm. The ratio of body length of two fish(L1/L2) is 1.10, where l1 is body length of top fish and L2 is body length of bottom.

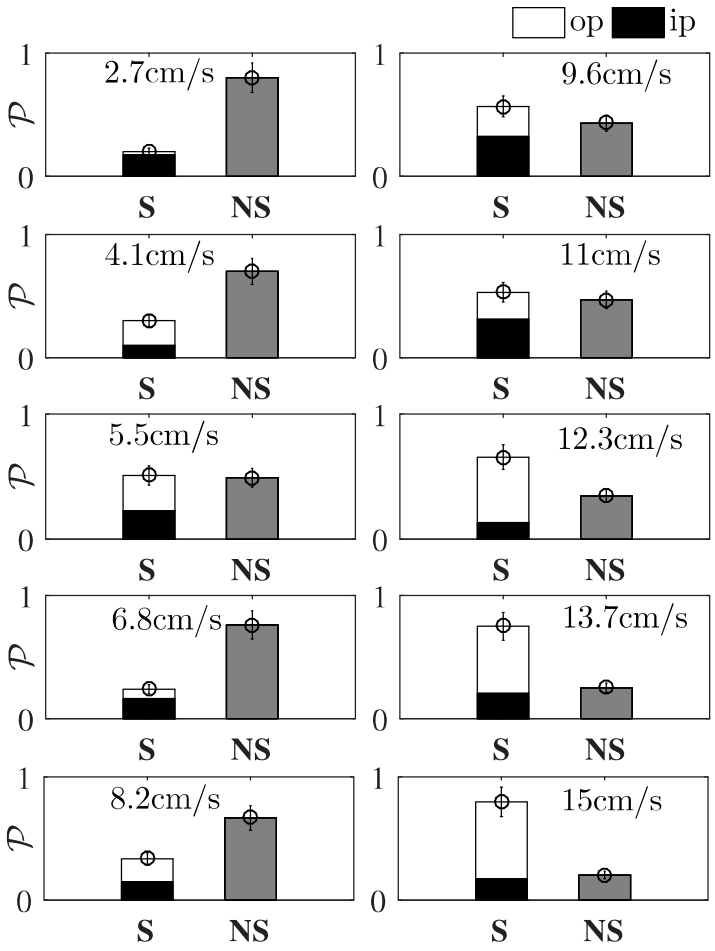

FIGURE A.3: Probability histograms of synchronization of fish pair 3 at different flow velocities. The mean body length of pair3 is 30 mm. The ratio of body length of two fish(L1/L2) is 1.0, where L1 is body length of top fish and L2 is body length of bottom.

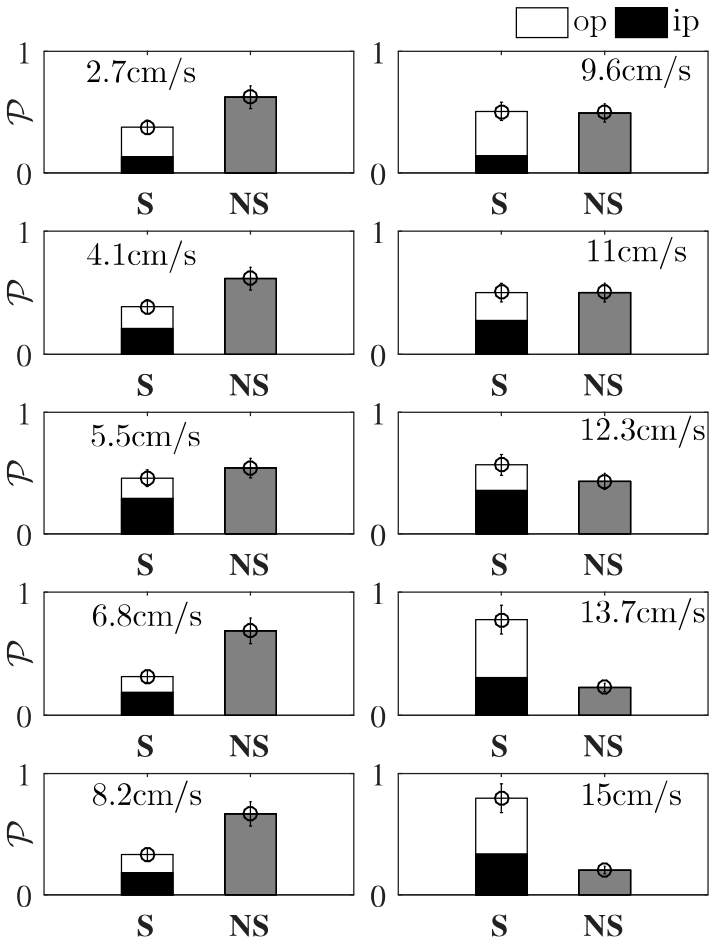

FIGURE A.4: Probability histograms of synchronization of fish pair 4 at different flow velocities. The mean body length of pair4 is 30 mm. The ratio of body length of two fish(L1/L2) is 0.98, where L1 is body length of top fish and L2 is body length of bottom.

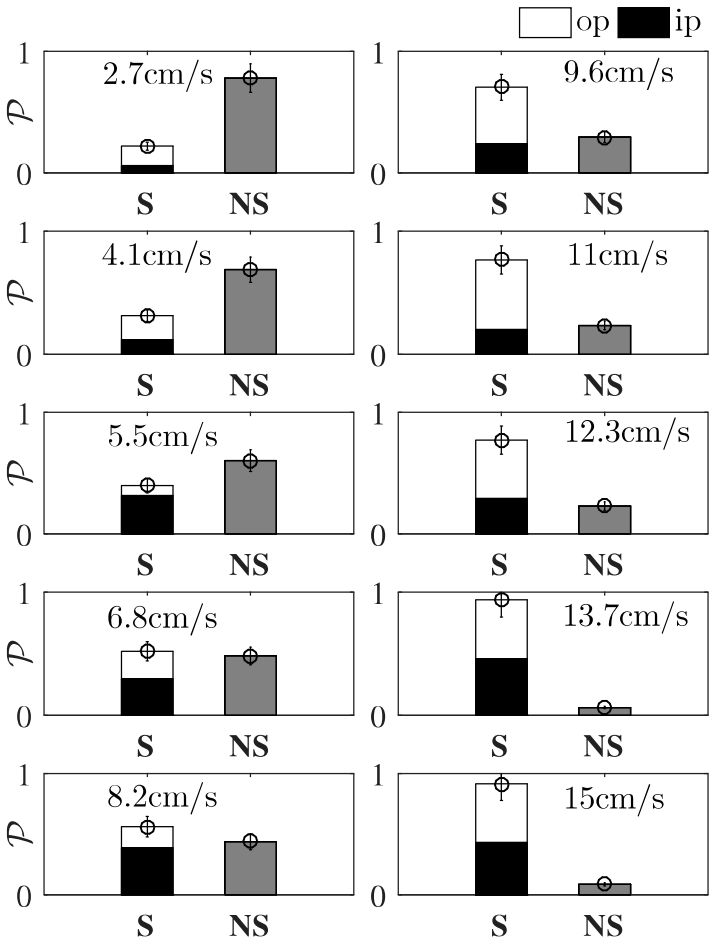

FIGURE A.5: Probability histograms of synchronization of fish pair 5 at different flow velocities. The mean body length of pair5 is 29 mm. The ratio of body length of two fish(L1/L2) is 1.0, where L1 is body length of top fish and L2 is body length of bottom.

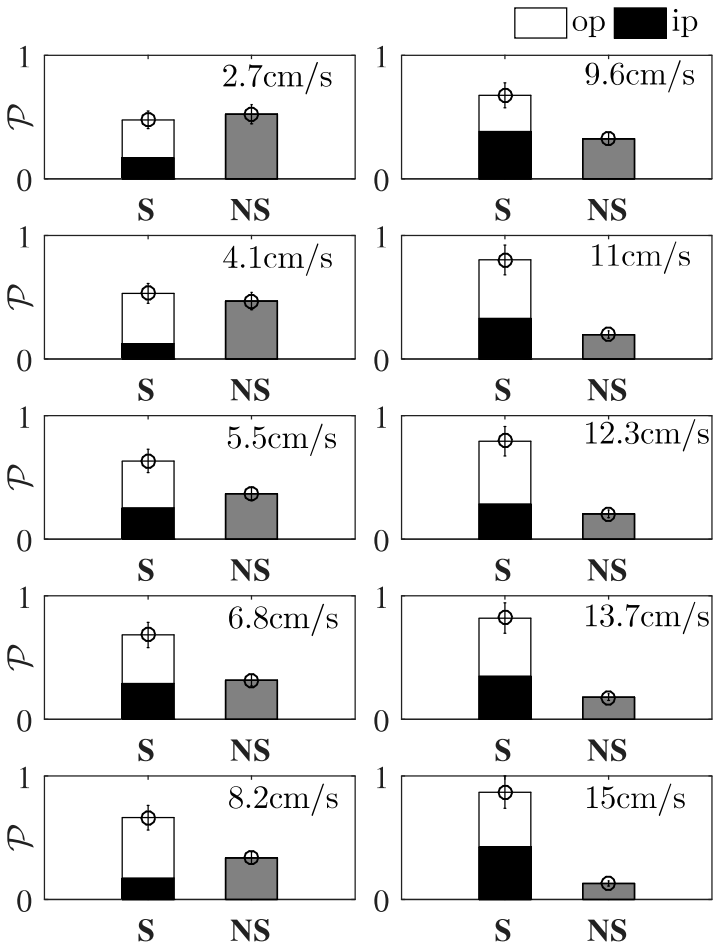

FIGURE A.6: Probability histograms of synchronization of fish pair 6 at different flow velocities. The mean body length of pair6 is 34 mm. The ratio of body length of two fish(L1/L2) is 0.94, where L1 is body length of top fish and L2 is body length of bottom.

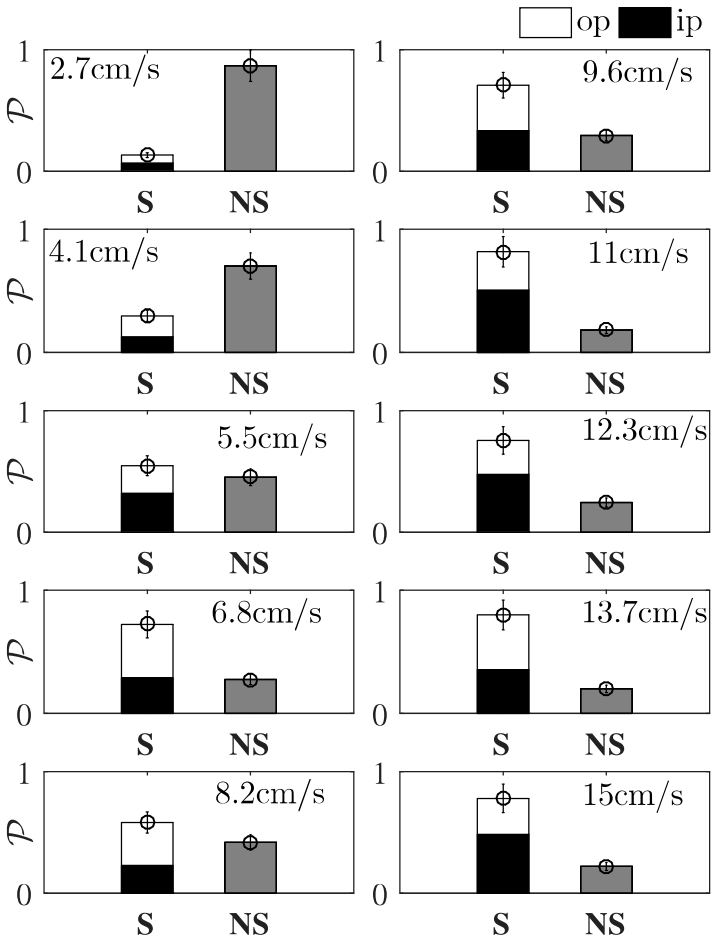

FIGURE A.7: Probability histograms of synchronization of fish pair 7 at different flow velocities. The mean body length of pair7 is 31 mm. The ratio of body length of two fish(L1/L2) is 1.0, where L1 is body length of top fish and L2 is body length of bottom.

Bibliography

[1] Ugo Lopez, Jacques Gautrais, Iain D Couzin, and Guy Theraulaz. “From behavioural analyses to models of collective motion in fish schools”. In: *Interface focus* 2.6 (2012), pp. 693–707.

[2] András Czirók, Albert-László Barabási, and Tamás Vicsek. “Collective motion of self-propelled particles: Kinetic phase transition in one dimension”. In: *Physical Review Letters* 82.1 (1999), p. 209.

[3] Tamás Vicsek and Anna Zafeiris. “Collective motion”. In: *Physics Reports* 517.3 (2012), pp. 71–140.

[4] Andrea Cavagna, Alessio Cimarelli, Irene Giardina, Giorgio Parisi, Raffaele Santagati, Fabio Stefanini, and Massimiliano Viale. “Scale-free correlations in starling flocks”. In: *Proceedings of the National Academy of Sciences* 107.26 (2010), pp. 11865–11870.

[5] Marie Bourjade, Bernard Thierry, Martine Hausberger, and Odile Petit. “Is leadership a reliable concept in animals? An empirical study in the horse”. In: *PloS one* 10.5 (2015), e0126344.

[6] Charles Foley, Nathalie Pettorelli, and Lara Foley. “Severe drought and calf survival in elephants”. In: *Biology Letters* 4.5 (2008), pp. 541–544.

[7] David JT Sumpter, Richard P Mann, and Andrea Perna. “The modelling cycle for collective animal behaviour”. In: *Interface focus* 2.6 (2012), pp. 764–773.

[8] Christos C Ioannou. “Swarm intelligence in fish? The difficulty in demonstrating distributed and self-organised collective intelligence in (some) animal groups”. In: *Behavioural processes* (2016).

[9] Robert E Steele, Charles N David, and Ulrich Technau. “A genomic view of 500 million years of cnidarian evolution”. In: *Trends in genetics* 27.1 (2011), pp. 7–13.

[10] JR Nursall. “The lateral musculature and the swimming of fish”. In: *Journal of Zoology* 126.1 (1956), pp. 127–144.

[11] Johan L Van Leeuwen. “A mechanical analysis of myomere shape in fish”. In: *Journal of Experimental Biology* 202.23 (1999), pp. 3405–3414.

[12] Michael Sfakiotakis, David M Lane, and J Bruce C Davies. “Review of fish swimming modes for aquatic locomotion”. In: *IEEE Journal of oceanic engineering* 24.2 (1999), pp. 237–252.

[13] JJ Magnusson. “Locomotion by Scombroid fishes: hy-dromechanics, morphology, and behaviour”. In: *Fish Physiology* 7 (1978), pp. 240–315.

[14] J Gray. “Studies in animal locomotion”. In: *Journal of experimental biology* 10.1 (1933), pp. 88–104.

[15] P. W. Webb, P. T. Kostecki, and E. D. Stevens. “The Effect of Size and Swimming Speed on Locomotor Kinematics of Rainbow Trout”. In: *Journal of experimental biology* 109 (1984), pp. 77–95.

[16] RG Bottom II, I Borazjani, EL Blevins, and GV Lauder. “Hydrodynamics of swimming in stingrays: numerical simulations and the role of the leading-edge vortex”. In: *Journal of Fluid Mechanics* 788 (2016), pp. 407–443.

[17] MJ Lighthill. “Note on the swimming of slender fish”. In: *Journal of fluid Mechanics* 9.2 (1960), pp. 305–317.

[18] MJ Lighthill. “Aquatic animal propulsion of high hydromechanical efficiency”. In: *Journal of Fluid Mechanics* 44.2 (1970), pp. 265–301.

[19] MJ Lighthill. “Large-amplitude elongated-body theory of fish locomotion”. In: *Proceedings of the Royal Society of London B: Biological Sciences* 179.1055 (1971), pp. 125–138.

[20] T Yao-Tsu Wu. “Hydromechanics of swimming propulsion. Part 3. Swimming and optimum movements of slender fish with side fins”. In: *Journal of Fluid Mechanics* 46.3 (1971), pp. 545–568.

[21] T McMillen and P Holmes. “An elastic rod model for anguilliform swimming”. In: *Journal of mathematical biology* 53.5 (2006), pp. 843–886.

[22] Miguel Piñeirua, Ramiro Godoy-Diana, and Benjamin Thiria. “Resistive thrust production can be as crucial as added mass mechanisms for inertial undulatory swimmers”. In: *Physical Review E* 92.2 (2015), p. 021001.

[23] Gil Iosilevskii. “The undulatory swimming gait of elongated swimmers revisited”. In: *Bioinspiration & Biomimetics* 12.3 (2017), p. 036005.

[24] H Liu and K Kawachi. “A numerical study of undulatory swimming”. In: *Journal of Computational Physics* 155.2 (1999), pp. 223–247.

[25] Stefan Kern and Petros Koumoutsakos. “Simulations of optimized anguilliform swimming”. In: *Journal of Experimental Biology* 209.24 (2006), pp. 4841–4857.

[26] Iman Borazjani, Fotis Sotiropoulos, Eric D Tytell, and George V Lauder. "Hydrodynamics of the bluegill sunfish C-start escape response: three-dimensional simulations and comparison with experimental data". In: *Journal of Experimental Biology* 215.4 (2012), pp. 671–684.

[27] Iman Borazjani and Fotis Sotiropoulos. "Numerical investigation of the hydrodynamics of anguilliform swimming in the transitional and inertial flow regimes". In: *Journal of Experimental Biology* 212.4 (2009), pp. 576–592.

[28] Guido Novati, Siddhartha Verma, Dmitry Alexeev, Diego Rossinelli, Wim M van Rees, and Petros Koumoutsakos. "Synchronisation through learning for two self-propelled swimmers". In: *Bioinspiration & Biomimetics* 12.3 (2017), p. 036001.

[29] Ulrike K Müller, Joris Smit, Eize J Stamhuis, and John J Videler. "How the body contributes to the wake in undulatory fish swimming". In: *Journal of Experimental Biology* 204.16 (2001), pp. 2751–2762.

[30] Eric D Tytell and George V Lauder. "The hydrodynamics of eel swimming". In: *Journal of Experimental Biology* 207.11 (2004), pp. 1825–1841.

[31] Eric D Tytell, Chia-Yu Hsu, Thelma L Williams, Avis H Cohen, and Lisa J Fauci. "Interactions between internal forces, body stiffness, and fluid environment in a neuromechanical model of lamprey swimming". In: *Proceedings of the National Academy of Sciences* 107.46 (2010), pp. 19832–19837.

[32] Richard P Clark and Alexander J Smits. "Thrust production and wake structure of a batoid-inspired oscillating fin". In: *Journal of fluid mechanics* 562 (2006), pp. 415–429.

[33] Daniel Floryan, Tyler Van Buren, Clarence W Rowley, and Alexander J Smits. "Scaling the propulsive performance of heaving and pitching foils". In: *Journal of Fluid Mechanics* 822 (2017), pp. 386–397.

[34] Tyler Van Buren, Nathaniel Wei, Daniel Floryan, and Alexander J Smits. "Swimming speed has little impact on fish-like swimming performance". In: *arXiv preprint arXiv:1707.05608* (2017).

[35] MG Chopra. "Large amplitude lunate-tail theory of fish locomotion". In: *Journal of Fluid Mechanics* 74.1 (1976), pp. 161–182.

[36] Florian T Muijres and David Lentink. "Wake visualization of a heaving and pitching foil in a soap film". In: *Experiments in fluids* 43.5 (2007), pp. 665–673.

[37] Michael S Triantafyllou, Alexandra H Techet, and Franz S Hover. "Review of experimental work in biomimetic foils". In: *IEEE Journal of Oceanic Engineering* 29.3 (2004), pp. 585–594.

[38] GS Triantafyllou, MS Triantafyllou, and MA Grosenbaugh. "Optimal thrust development in oscillating foils with application to fish propulsion". In: *Journal of Fluids and Structures* 7.2 (1993), pp. 205–224.

[39] Douglas A Read, FS Hover, and MS Triantafyllou. "Forces on oscillating foils for propulsion and maneuvering". In: *Journal of Fluids and Structures* 17.1 (2003), pp. 163–183.

[40] Charles Marcus Breder. "The locomotion of fishes". In: *Zoologica* 4 (1926).

[41] John J Videler. *Fish swimming*. Vol. 10. Springer Science & Business Media, 1993.

[42] Iman Borazjani and Fotis Sotiropoulos. "Numerical investigation of the hydrodynamics of carangiform swimming in the transitional and inertial flow regimes". In: *Journal of Experimental Biology* 211.10 (2008), pp. 1541–1558.

[43] Christophe Eloy. "Optimal Strouhal number for swimming animals". In: *Journal of Fluids and Structures* 30 (2012), pp. 205–218.

[44] John Carling, Thelma L Williams, and Graham Bowtell. "Self-propelled anguilliform swimming: simultaneous solution of the two-dimensional Navier-Stokes equations and Newton's laws of motion". In: *Journal of experimental biology* 201.23 (1998), pp. 3143–3166.

[45] Michael S Triantafyllou, GS Triantafyllou, and DKP Yue. "Hydrodynamics of fishlike swimming". In: *Annual review of fluid mechanics* 32.1 (2000), pp. 33–53.

[46] UK Müller, BLE Van Den Heuvel, EJ Stamhuis, and JJ Videler. "Fish foot prints: morphology and energetics of the wake behind a continuously swimming mullet (Chelon labrosus Risso)." In: *Journal of Experimental Biology* 200.22 (1997), pp. 2893–2906.

[47] Iman Borazjani and Mohsen Daghooghi. "The fish tail motion forms an attached leading edge vortex". In: *Proc. R. Soc. B*. Vol. 280. 1756. The Royal Society. 2013, p. 20122071.

[48] Audrey P. Maertens, Amy Gao, and Michael S. Triantafyllou. "Optimal undulatory swimming for a single fish-like body and for a pair of interacting swimmers". In: *Journal of Fluid Mechanics* 813 (2017), 301–345.

[49] Heidi Dewar and J Graham. "Studies of tropical tuna swimming performance in a large water tunnel-Energetics". In: *Journal of Experimental Biology* 192.1 (1994), pp. 13–31.

[50] Ningyu Li, Huanxing Liu, and Yumin Su. "Numerical study on the hydrodynamics of thunniform bio-inspired swimming under self-propulsion". In: *PloS one* 12.3 (2017), e0174740.

[51] MJ Wolfgang, JM Anderson, MA Grosenbaugh, DK Yue, and MS Triantafyllou. "Near-body flow dynamics in swimming fish". In: *Journal of Experimental Biology* 202.17 (1999), pp. 2303–2327.

[52] George V Lauder and Eric D Tytell. "Hydrodynamics of undulatory propulsion". In: *Fish physiology* 23 (2005), pp. 425–468.

[53] RW Blake. "On ostraciiform locomotion". In: *Journal of the Marine Biological Association of the United Kingdom* 57.4 (1977), pp. 1047–1055.

[54] Sam Van Wassenbergh, Klaas van Manen, Tina A Marcroft, Michael E Alfaro, and Eize J Stamhuis. "Boxfish swimming paradox resolved: forces by the flow of water around the body promote manoeuvrability". In: *Journal of The Royal Society Interface* 12.103 (2015), p. 20141146.

[55] Jeffrey A Walker. "Does a rigid body limit maneuverability?" In: *Journal of Experimental Biology* 203.22 (2000), pp. 3391–3396.

[56] Erin L Blevins and George V Lauder. "Rajiform locomotion: three-dimensional kinematics of the pectoral fin surface during swimming in the freshwater stingray Potamotrygon orbignyi". In: *Journal of Experimental Biology* 215.18 (2012), pp. 3231–3241.

[57] Lisa J Rosenberger and Mark W Westneat. "Functional morphology of undulatory pectoral fin locomotion in the stingray Taeniura lymma (Chondrichthyes: Dasyatidae)". In: *Journal of Experimental Biology* 202.24 (1999), pp. 3523–3539.

[58] Frank E Fish, Christian M Schreiber, Keith W Moored, Geng Liu, Haibo Dong, and Hilary Bart-Smith. "Hydrodynamic performance of aquatic flapping: efficiency of underwater flight in the manta". In: *Aerospace* 3.3 (2016), p. 20.

[59] Tony J Pitcher, Brian L Partridge, and CS Wardle. "A blind fish can school". In: *Science* 194.4268 (1976), pp. 963–965.

[60] Karine Faucher, Eric Parmentier, Christophe Becco, Nicolas Vandewalle, and Pierre Vandewalle. "Fish lateral system is required for accurate control of shoaling behaviour". In: *Animal Behaviour* 79.3 (2010), pp. 679–687.

[61] Evelyn Shaw. "Schooling fishes: the school, a truly egalitarian form of organization in which all members of the group are alike in influence, offers substantial benefits to its participants". In: *American Scientist* 66.2 (1978), pp. 166–175.

[62] CW Glass, CS Wardle, and WR Mojsiewicz. “A light intensity threshold for schooling in the Atlantic mackerel, Scomber scombrus”. In: *Journal of Fish Biology* 29.sA (1986), pp. 71–81.

[63] Ahmad Dagamseh, Remco Wiegerink, Theo Lammerink, and Gijs Krijnen. “Imaging dipole flow sources using an artificial lateral-line system made of biomimetic hair flow sensors”. In: *Journal of the Royal Society interface* 10.83 (2013), p. 20130162.

[64] Horst Bleckmann and Randy Zelick. “Lateral line system of fish”. In: *Integrative zoology* 4.1 (2009), pp. 13–25.

[65] Brian L Partridge and Tony J Pitcher. “The sensory basis of fish schools: relative roles of lateral line and vision”. In: *Journal of comparative physiology* 135.4 (1980), pp. 315–325.

[66] DS Pavlov and AO Kasumyan. “Patterns and mechanisms of schooling behavior in fish: a review”. In: *Journal of Ichthyology* 40.2 (2000), S163.

[67] Brian L. Partridge. “Internal dynamics and the interrelations of fish in schools”. In: *Journal of comparative physiology* 144.3 (1981), pp. 313–325. ISSN: 1432-1351.

[68] Brian L Partridge. “The structure and function of fish schools”. In: *Scientific american* 246.6 (1982), pp. 114–123.

[69] M Zheng, Y Kashimori, O Hoshino, K Fujita, and T Kambara. “Behavior pattern (innate action) of individuals in fish schools generating efficient collective evasion from predation”. In: *Journal of theoretical biology* 235.2 (2005), pp. 153–167.

[70] Z Zhang, AJ Gil, O Hassan, and K Morgan. “Feeding Behavior of Murmansk Herring in School and out of School in Aquarium Conditions”. In: *Tr. Murm. Morsk. Biol. Inst.* 2.2 (1962), pp. 254–259.

[71] AE Magurran and JA Bendelow. “Conflict and co-operation in White Cloud Mountain minnow schools”. In: *Journal of Fish Biology* 37.1 (1990), pp. 77–83.

[72] Manabu Shiraishi, Nobuyuki Azuma, and Ichiro Aoki. “Large schools of Japanese sardines, Sardinops melanostictus, mate in single pair units at night”. In: *Environmental biology of fishes* 45.4 (1996), pp. 405–409.

[73] II Girsa and Yu E Lapin. “BEHAVIORAL RHYTHMS OF SOME FISHES OF KANDALAKSHA BAY, WHITE SEA”. In: *BIOLOGIYA MORYA-MARINE BIOLOGY* 5 (1985), pp. 55–57.

[74] Penelope J Watt, Stephen F Nottingham, and Stephen Young. “Toad tadpole aggregation behaviour: evidence for a predator avoidance function”. In: *Animal behaviour* 54.4 (1997), pp. 865–872.

[75] William D Hamilton. “Geometry for the selfish herd”. In: *Journal of theoretical Biology* 31.2 (1971), pp. 295–311.

[76] Ian Vine. “Risk of visual detection and pursuit by a predator and the selective advantage of flocking behaviour”. In: *Journal of Theoretical Biology* 30.2 (1971), pp. 405–422.

[77] Steven V Viscido and David S Wethey. “Quantitative analysis of fiddler crab flock movement: evidence for ‘selfish herd’behaviour”. In: *Animal behaviour* 63.4 (2002), pp. 735–741.

[78] Asa Johannesen, Alison M Dunn, and Lesley J Morrell. “Prey aggregation is an effective olfactory predator avoidance strategy”. In: *PeerJ* 2 (2014), e408.

[79] Anne E Magurran. “Population differentiation without speciation”. In: *Philosophical Transactions of the Royal Society of London B: Biological Sciences* 353.1366 (1998), pp. 275–286.

[80] David A Reznick, Heather Bryga, and John A Endler. “Experimentally induced life-history evolution in a natural population”. In: *Nature* 346.6282 (1990), p. 357.

[81] M Huizinga, CK Ghalambor, and DN Reznick. “The genetic and environmental basis of adaptive differences in shoaling behaviour among populations of Trinidadian guppies, Poecilia reticulata”. In: *Journal of evolutionary biology* 22.9 (2009), pp. 1860–1866.

[82] FCW Olson. “The survival value of fish schooling”. In: *Journal du Conseil* 29.1 (1964), pp. 115–116.

[83] Bernard O Koopman. “The theory of search. II. Target detection”. In: *Operations research* 4.5 (1956), pp. 503–531.

[84] SRStJ Neill and Jonathan M Cullen. “Experiments on whether schooling by their prey affects the hunting behaviour of cephalopods and fish predators”. In: *Journal of Zoology* 172.4 (1974), pp. 549–569.

[85] TJ Pitcher. “Behaviour of Teleost Fishes.” In: *Fish and Fisheries Series* (1993).

[86] Tony J Pitcher and Christopher J Wyche. “Predator avoidance behaviour of sand-eel schools: why schools seldom split”. In: *Predators and prey in fishes* 54 (1983), pp. 193–204.

[87] Tony J Pitcher. “Functions of shoaling behaviour in teleosts”. In: (1986), pp. 294–337.

[88] E Ranta and V Kaitala. “School size affects individual feeding success in three-spined sticklebacks (Gastevosteus aculeatus L.)” In: *Journal of Fish Biology* 39.5 (1991), pp. 733–737.

[89] Troy A Baird, Clifford H Ryer, and Bori L Olla. “Social enhancement of foraging on an ephemeral food source in juvenile walleye pollock, Theragra chalcogramma”. In: *Environmental Biology of Fishes* 31.3 (1991), pp. 307–311.

[90] Elizabeth G Foster, David A Ritz, Jon E Osborn, and Kerrie M Swadling. “Schooling affects the feeding success of Australian salmon (Arripis trutta) when preying on mysid swarms (Paramesopodopsis rufa)”. In: *Journal of Experimental Marine Biology and Ecology* 261.1 (2001), pp. 93–106.

[91] Ashley J Ward, Stephen Axford, and Jens Krause. “Mixed-species shoaling in fish: the sensory mechanisms and costs of shoal choice”. In: *Behavioral Ecology and Sociobiology* 52.3 (2002), pp. 182–187.

[92] John RG Dyer, Darren P Croft, Lesley J Morrell, and Jens Krause. “Shoal composition determines foraging success in the guppy”. In: *Behavioral Ecology* 20.1 (2009), pp. 165–171.

[93] Meagan N Schrandt and Sean P Powers. “Facilitation and Dominance in a Schooling Predator: Foraging Behavior of Florida Pompano, Trachinotus carolinus”. In: *PloS one* 10.6 (2015), e0130095.

[94] I Aoki. “A simulation study on the schooling mechanism in fish”. In: *Bulletin of the Japanese Society of Scientific Fisheries (Japan)* (1982).

[95] Tamás Vicsek, András Czirók, Eshel Ben-Jacob, Inon Cohen, and Ofer Shochet. “Novel type of phase transition in a system of self-driven particles”. In: *Physical review letters* 75.6 (1995), p. 1226.

[96] Daniel S Calovi, Ugo Lopez, Paul Schuhmacher, Hugues Chaté, Clément Sire, and Guy Theraulaz. “Collective response to perturbations in a data-driven fish school model”. In: *Journal of The Royal Society Interface* 12.104 (2015), p. 20141362.

[97] Geir Huse, Steve Railsback, and A Feronö. “Modelling changes in migration pattern of herring: collective behaviour and numerical domination”. In: *Journal of Fish Biology* 60.3 (2002), pp. 571–582.

[98] William L Romey. “Individual differences make a difference in the trajectories of simulated schools of fish”. In: *Ecological Modelling* 92.1 (1996), pp. 65–77.

[99] Jacques Gautrais, Francesco Ginelli, Richard Fournier, Stéphane Blanco, Marc Soria, Hugues Chaté, and Guy Theraulaz. “Deciphering interactions in moving animal groups”. In: *Plos computational biology* 8.9 (2012), e1002678.

[100] Hiro-Sato Niwa. “Self-organizing dynamic model of fish schooling”. In: *Journal of theoretical Biology* 171.2 (1994), pp. 123–136.

[101] Audrey Filella, François Nadal, Clément Sire, Eva Kanso, and Christophe Eloy. “Hydrodynamic interactions influence fish collective behavior”. In: *arXiv preprint arXiv:1705.07821* (2017).

[102] Iain D Couzin, Jens Krause, Richard James, Graeme D Ruxton, and Nigel R Franks. “Collective memory and spatial sorting in animal groups”. In: *Journal of theoretical biology* 218.1 (2002), pp. 1–11.

[103] Dorílson Silva Cambuí and Alexandre Rosas. “Density induced transition in a school of fish”. In: *Physica A: Statistical Mechanics and its Applications* 391.15 (2012), pp. 3908–3914.

[104] Diana Pita, Bertrand Collignon, José Halloy, and Esteban Fernández-Juricic. “Collective behaviour in vertebrates: a sensory perspective”. In: *Royal Society open science* 3.11 (2016), p. 160377.

[105] Zhong-Hua Tang, Hui Wu, Qing Huang, Lu Kuang, and Shi-Jian Fu. “The shoaling behavior of two cyprinid species in conspecific and heterospecific groups”. In: *PeerJ* 5 (2017), e3397.

[106] Kolbjørn Tunstrøm, Yael Katz, Christos C Ioannou, Cristián Huepe, Matthew J Lutz, and Iain D Couzin. “Collective states, multistability and transitional behavior in schooling fish”. In: *PLoS computational biology* 9.2 (2013), e1002915.

[107] Mattia Gazzola, Andrew A Tchieu, Dmitry Alexeev, Alexia de Brauer, and Petros Koumoutsakos. “Learning to school in the presence of hydrodynamic interactions”. In: *Journal of Fluid Mechanics* 789 (2016), pp. 726–749.

[108] PA Fields. “DECREASED SWIMMING EFFORT IN GROUPS OF PACIFIC MACKEREL (SCOMBER-JAPONICUS)”. In: *American Zoologist*. Vol. 30. 4. AMER SOC ZOOLOGISTS 1041 NEW HAMPSHIRE ST, LAWRENCE, KS 66044. 1990, A134–A134.

[109] J Herskin and JF Steffensen. “Energy savings in sea bass swimming in a school: measurements of tail beat frequency and oxygen consumption at different swimming speeds”. In: *Journal of Fish Biology* 53.2 (1998), pp. 366–376.

[110] CM Breder. “Vortices and fish schools”. In: *Zoologica* 50 (1965), pp. 97–114.

[111] VV Belyayev and GV Zuyev. “Hydrodynamic hypothesis of school formation in fishes”. In: *Problems of Ichthyology* 9 (1969), pp. 578–584.

[112] D Weihs. “Hydromechanics of fish schooling”. In: *Nature* 241.5387 (1973), pp. 290–291.

[113] James C Liao, David N Beal, George V Lauder, and Michael S Triantafyllou. "Fish exploiting vortices decrease muscle activity". In: *Science* 302.5650 (2003), pp. 1566–1569.

[114] James C Liao, David N Beal, George V Lauder, and Michael S Triantafyllou. "The Karman gait: novel body kinematics of rainbow trout swimming in a vortex street". In: *Journal of experimental biology* 206.6 (2003), pp. 1059–1073.

[115] DN Beal, FS Hover, MS Triantafyllou, JC Liao, and GV Lauder. "Passive propulsion in vortex wakes". In: *Journal of Fluid Mechanics* 549 (2006), pp. 385–402.

[116] JJ Allen and AJ Smits. "Energy harvesting eel". In: *Journal of fluids and structures* 15.3-4 (2001), pp. 629–640.

[117] Knut Streitlien, George S Triantafyllou, and Michael S Triantafyllou. "Efficient foil propulsion through vortex control". In: *Aiaa journal* 34.11 (1996), pp. 2315–2319.

[118] R Gopalkrishnan, MS Triantafyllou, GS Triantafyllou, and D Barrett. "Active vorticity control in a shear flow using a flapping foil". In: *Journal of Fluid Mechanics* 274 (1994), pp. 1–21.

[119] BL Partridge and TJ Pitcher. "Evidence against a hydrodynamic function for fish schools". In: *Nature* 279.5712 (1979), pp. 418–419.

[120] CM Breder. "Fish schools as operational structures". In: *Fish. Bull* 74.3 (1976), pp. 471–502.

[121] Nathaniel K Newlands and Tracy A Porcelli. "Measurement of the size, shape and structure of Atlantic bluefin tuna schools in the open ocean". In: *Fisheries Research* 91.1 (2008), pp. 42–55.

[122] Brian L Partridge, Jonas Johansson, and John Kalish. "The structure of schools of giant bluefin tuna in Cape Cod Bay". In: *Environmental Biology of Fishes* 9.3 (1983), pp. 253–262.

[123] Andrew A Fejer. "Porpoises and the bow-riding of ships under way". In: *Nature* 188 (1960), pp. 700–703.

[124] Frank E Fish. "Swimming strategies for energy economy". In: *Fish swimming: an etho-ecological perspective* (2010), pp. 90–122.

[125] TM Williams and WA Friedl. "Travel at low energetic cost by swimming and wave-riding bottlenose dolphins". In: *Nature* 355.6363 (1992), p. 821.

[126] N Bose and J Lien. “Energy absorption from ocean waves: a free ride for cetaceans”. In: *Proceedings of the Royal Society of London B: Biological Sciences* 240.1299 (1990), pp. 591–605.

[127] Mohsen Daghooghi and Iman Borazjani. “The hydrodynamic advantages of synchronized swimming in a rectangular pattern”. In: *Bioinspiration & biomimetics* 10.5 (2015), p. 056018.

[128] CK Hemelrijk, DAP Reid, H Hildenbrandt, and JT Padding. “The increased efficiency of fish swimming in a school”. In: *Fish and Fisheries* 16.3 (2015), pp. 511–521.

[129] Gen-Jin Dong and Xi-Yun Lu. “Characteristics of flow over traveling wavy foils in a side-by-side arrangement”. In: *Physics of fluids* 19.5 (2007), p. 057107.

[130] Daniel Weihs. “The hydrodynamics of dolphin drafting”. In: *Journal of Biology* 3.2 (2004), p. 8.

[131] YI Abdel-Aziz, HM Karara, and Michael Hauck. “Direct linear transformation from comparator coordinates into object space coordinates in close-range photogrammetry”. In: *Photogrammetric engineering & remote sensing* 81.2 (2015), pp. 103–107.

[132] YH Kwon. “KWON3D Motion analysis package 2.1 User’s reference manual”. In: *V-TEK Corporation, Anyang, Korea* (1994).

[133] Tyson L Hedrick. “Software techniques for two-and three-dimensional kinematic measurements of biological and biomimetic systems”. In: *Bioinspiration & Biomimetics* 3.3 (2008), p. 034001.

[134] Jean-Yves Bouguet. “Camera calibration toolbox for matlab”. In: (2004).

[135] Bret W Tobalske, Wendy L Peacock, and KENNETH P Dial. “Kinematics of flap-bounding flight in the zebra finch over a wide range of speeds”. In: *Journal of Experimental Biology* 202.13 (1999), pp. 1725–1739.

[136] Adrian C Gleiss et al. “Convergent evolution in locomotory patterns of flying and swimming animals”. In: *Nature communications* 2 (2011), p. 352.

[137] Frank E Fish, Jennifer F Fegely, and Cindy J Xanthopoulos. “Burst-and-coast swimming in schooling fish (Notemigonus crysoleucas) with implications for energy economy”. In: *Comparative Biochemistry and Physiology Part A: Physiology* 100.3 (1991), pp. 633–637.

[138] Daniel Weihs. “Energetic advantages of burst swimming of fish”. In: *Journal of Theoretical Biology* 48.1 (1974), pp. 215–229.

[139] JJ Videler and D Weihs. “Energetic advantages of burst-and-coast swimming of fish at high speeds”. In: *Journal of Experimental Biology* 97.1 (1982), pp. 169–178.

[140] RW Blake. “Functional design and burst-and-coast swimming in fishes”. In: *Canadian journal of zoology* 61.11 (1983), pp. 2491–2494.

[141] D. Floryan, T. Van Buren, and A. J. Smits. “Forces and energetics of intermittent swimming”. In: *Acta Mechanica Sinica* (2017), p. 1.

[142] MH Chung. “On burst-and-coast swimming performance in fish-like locomotion”. In: *Bioinspiration & biomimetics* 4.3 (2009), p. 036001.

[143] UK Muller, EJ Stamhuis, and JJ Videler. “Hydrodynamics of unsteady fish swimming and the effects of body size: comparing the flow fields of fish larvae and adults”. In: *Journal of Experimental Biology* 203.2 (2000), pp. 193–206.

[144] Matthew J McHenry and George V Lauder. “The mechanical scaling of coasting in zebrafish (Danio rerio)”. In: *Journal of Experimental Biology* 208.12 (2005), pp. 2289–2301.

[145] Guanhao Wu, Yan Yang, and Lijiang Zeng. “Kinematics, hydrodynamics and energetic advantages of burst-and-coast swimming of koi carps (Cyprinus carpio koi)”. In: *Journal of Experimental Biology* 210.12 (2007), pp. 2181–2191.

[146] Paul W Webb. “Form and function in fish swimming”. In: *Sci. Am.* 251 (1984), pp. 58–68.

[147] C. Tudorache, P. Viaenen, R. Blust, and G. De Boeck. “Longer flumes increase critical swimming speeds by increasing burst-glide swimming duration in carp Cyprinus carpio, L.” In: *Journal of Fish Biology* 71.6 (Dec. 2007), pp. 1630–1638.

[148] P. W. Webb. “The biology of fish swimming”. In: *Mechanics and physiology of animal swimming*. Ed. by L. Maddock, Q. Bone, and J. M. V. Rayner. Cambridge University Press, 1994.

[149] I. Ashraf, R. Godoy-Diana, J. Halloy, B. Collignon, and B. Thiria. “Synchronization and collective swimming patterns in fish (Hemigrammus bleheri)”. In: *Journal of the Royal Society Interface* 13 (2016), p. 20160734.

[150] I. Ashraf, H. Bradshaw, T.-T. Ha, J. Halloy, R. Godoy-Diana, and B. Thiria. “Simple phalanx pattern leads to energy saving in cohesive fish schooling”. In: *Proceedings of the National Academy of Sciences* 114.36 (Aug. 2017), pp. 9599–9604.

[151] D. S. Calovi, A. Litchinko, V. Lecheval, U. Lopez, A. Pérez Escudero, H. Chaté, C. Sire, and G. Theraulaz. "Disentangling and modeling interactions in fish with burst-and-coast swimming". In: *arXiv preprint arXiv:1703.03801* (2017).

[152] S. L. Katz and R. E. Shadwick. "Curvature of swimming fish midlines as an index of muscle strain suggests swimming muscle produces net positive work". In: *Journal of Theoretical Biology* 193.2 (1998), pp. 243–256.

[153] J. L. van Leeuwen, M. J. M. Lankheet, H. A. Akster, and J. W. M. Osse. "Function of red axial muscles of carp (Cyprinus carpio): recruitment and normalized power output during swimming in different modes". In: *Journal of Zoology* 220.1 (1990), pp. 123–145.

[154] Delfinn Tan, Paul Patton, and Sheryl Coombs. "Do blind cavefish have behavioral specializations for active flow-sensing?" In: *Journal of Comparative Physiology A* 197.7 (2011), pp. 743–754.

[155] Guy Martel and Lawrence M Dill. "Influence of movement by coho salmon (Oncorhynchus kisutch) parr on their detection by common mergansers (Mergus merganser)". In: *Ethology* 99.1-2 (1995), pp. 139–149.

[156] Donald L Kramer and Robert L McLaughlin. "The behavioral ecology of intermittent locomotion". In: *American Zoologist* 41.2 (2001), pp. 137–153.

[157] Karla E Feitl, Victoria Ngo, and Matthew J McHenry. "Are fish less responsive to a flow stimulus when swimming?" In: *Journal of Experimental Biology* 213.18 (2010), pp. 3131–3137.

[158] TJ Pitcher, AE Magurran, and IJ Winfield. "Fish in larger shoals find food faster". In: *Behavioral Ecology and Sociobiology* 10.2 (1982), pp. 149–151.

[159] Mattia Gazzola, Philippe Chatelain, Wim M Van Rees, and Petros Koumoutsakos. "Simulations of single and multiple swimmers with non-divergence free deforming geometries". In: *Journal of Computational Physics* 230.19 (2011), pp. 7093–7114.

[160] Brian L Partridge, Tony Pitcher, J Michael Cullen, and John Wilson. "The three-dimensional structure of fish schools". In: *Behavioral Ecology and Sociobiology* 6.4 (1980), pp. 277–288.

[161] MATTHEW J McHenry, Charles A Pell, and JH Long. "Mechanical control of swimming speed: stiffness and axial wave form in undulating fish models". In: *Journal of Experimental Biology* 198.11 (1995), pp. 2293–2305.

[162] Graham K Taylor, Robert L Nudds, and Adrian LR Thomas. "Flying and swimming animals cruise at a Strouhal number tuned for high power efficiency". In: *Nature* 425.6959 (2003), p. 707.

[163] Andreas Huth and Christian Wissel. “The simulation of fish schools in comparison with experimental data”. In: *Ecological modelling* 75 (1994), pp. 135–146.

[164] Ari Z Zivotofsky and Jeffrey M Hausdorff. “The sensory feedback mechanisms enabling couples to walk synchronously: An initial investigation”. In: *Journal of neuroengineering and rehabilitation* 4.1 (2007), p. 28.

[165] Niek R van Ulzen, Claudine JC Lamoth, Andreas Daffertshofer, Gün R Semin, and Peter J Beek. “Characteristics of instructed and uninstructed interpersonal coordination while walking side-by-side”. In: *Neuroscience letters* 432.2 (2008), pp. 88–93.

[166] Yoshihiro Miyake. “Interpersonal synchronization of body motion and the Walk-Mate walking support robot”. In: *IEEE Transactions on Robotics* 25.3 (2009), pp. 638–644.

[167] Jinzhou Yuan, David M Raizen, and Haim H Bau. “Gait synchronization in Caenorhabditis elegans”. In: *Proceedings of the National Academy of Sciences* 111.19 (2014), pp. 6865–6870.

[168] T Yao-Tsu Wu. “Swimming of a waving plate”. In: *Journal of Fluid Mechanics* 10.3 (1961), pp. 321–344.

[169] Renato E Mirollo and Steven H Strogatz. “Synchronization of pulse-coupled biological oscillators”. In: *SIAM Journal on Applied Mathematics* 50.6 (1990), pp. 1645–1662.

[170] Steven H Strogatz, Ian Stewart, et al. “Coupled oscillators and biological synchronization”. In: *Scientific American* 269.6 (1993), pp. 102–109.

[171] Michael G Rosenblum, Arkady S Pikovsky, and Jürgen Kurths. “Phase synchronization of chaotic oscillators”. In: *Physical review letters* 76.11 (1996), p. 1804.

[172] V Raspa, C Gaubert, and B Thiria. “Manipulating thrust wakes: a parallel with biomimetic propulsion”. In: *EPL (Europhysics Letters)* 97.4 (2012), p. 44008.

[173] V Raspa, R Godoy-Diana, and B Thiria. “Topology-induced effect in biomimetic propulsive wakes”. In: *Journal of Fluid Mechanics* 729 (2013), pp. 377–387.

[174] Rafaela P Ota, Flávio CT Lima, and Carla S Pavanelli. “A new species of Hemigrammus Gill, 1858 (Characiformes: Characidae) from the rio Madeira and rio Paraguai basins, with a redescription of H. lunatus”. In: *Neotropical Ichthyology* 12.2 (2014), pp. 265–279.

[175] Sheryl Coombs, John Janssen, and Jacqueline F Webb. “Diversity of lateral line systems: evolutionary and functional considerations”. In: *Sensory biology of aquatic animals*. Springer, 1988, pp. 553–593.

[176] Christian Schemmel. “Vergleichende Untersuchungen an den Hautsinnesorganen ober-und unterirdisch lebender Astyanax-Formen”. In: *Zoomorphology* 61.2 (1967), pp. 255–316.

[177] Sara Brin Rosenthal, Colin R Twomey, Andrew T Hartnett, Hai Shan Wu, and Iain D Couzin. “Revealing the hidden networks of interaction in mobile animal groups allows prediction of complex behavioral contagion”. In: *Proceedings of the National Academy of Sciences* 112.15 (2015), pp. 4690–4695.

[178] Ariana Strandburg-Peshkin et al. “Visual sensory networks and effective information transfer in animal groups”. In: *Current Biology* 23.17 (2013), R709–R711.

[179] D. J. T. Sumpter. “The principles of collective animal behaviour”. In: *Philosophical Transactions of the Royal Society B: Biological Sciences* 361.1465 (Jan. 2006), pp. 5–22.

[180] A. C. H. Tsang and E. Kanso. “Dipole Interactions in Doubly Periodic Domains”. In: *Journal of Nonlinear Science* 23.6 (July 2013), pp. 971–991.

[181] Rajat Mittal, Haibo Dong, Meliha Bozkurttas, GeorgeV Lauder, and Peter Madden. “Locomotion with flexible propulsors: II. Computational modeling of pectoral fin swimming in sunfish”. In: *Bioinspiration & Biomimetics* 1.4 (2006), S35.

[182] Z Zhang, AJ Gil, O Hassan, and K Morgan. “The simulation of 3D unsteady incompressible flows with moving boundaries on unstructured meshes”. In: *Computers & Fluids* 37.5 (2008), pp. 620–631.

[183] D Adkins and YY Yan. “CFD simulation of fish-like body moving in viscous liquid”. In: *Journal of Bionic Engineering* 3.3 (2006), pp. 147–153.

[184] Mark V Abrahams and Patrick W Colgan. “Risk of predation, hydrodynamic efficiency and their influence on school structure”. In: *Environmental Biology of Fishes* 13.3 (1985), pp. 195–202.

[185] Douglas M Eggers. “The nature of prey selection by planktivorous fish”. In: *Ecology* 58.1 (1977), pp. 46–59.

[186] Mattia Gazzola, Médéric Argentina, and Lakshminarayanan Mahadevan. “Scaling macroscopic aquatic locomotion”. In: *Nature Physics* 10.10 (2014), p. 758.

[187] N. Vandenberghe, J. Zhang, and S. Childress. "Symmetry breaking leads to forward flapping flight". In: *Journal of Fluid Mechanics* 506 (2004), pp. 147–155.

[188] R Quian Quiroga, A Kraskov, T Kreuz, and Peter Grassberger. "Performance of different synchronization measures in real data: a case study on electroencephalographic signals". In: *Physical Review E* 65.4 (2002), p. 041903.

[189] Andrew Clarke and Nadine M Johnston. "Scaling of metabolic rate with body mass and temperature in teleost fish". In: *Journal of Animal Ecology* 68.5 (1999), pp. 893–905.

[190] JL Johansen, R Vaknin, John Fleng Steffensen, and P Domenici. "Kinematics and energetic benefits of schooling in the labriform fish, striped surfperch Embiotoca lateralis". In: *Marine Ecology Progress Series* 420 (2010), pp. 221–229.

[191] Shaun S Killen, Stefano Marras, John F Steffensen, and David J McKenzie. "Aerobic capacity influences the spatial position of individuals within fish schools". In: *Proc. R. Soc. B*. Vol. 279. 1727. The Royal Society. 2012, pp. 357–364.

[192] C Lowe. "Metabolic rates of juvenile scalloped hammerhead sharks (Sphyrna lewini)". In: *Marine Biology* 139.3 (2001), pp. 447–453.

[193] Stefano Marras, Shaun S Killen, Jan Lindström, David J McKenzie, John F Steffensen, and Paolo Domenici. "Fish swimming in schools save energy regardless of their spatial position". In: *Behavioral ecology and sociobiology* 69.2 (2015), pp. 219–226.

[194] Maria Faldborg Steinhausen, John Fleng Steffensen, and Niels Gerner Andersen. "Tail beat frequency as a predictor of swimming speed and oxygen consumption of saithe (Pollachius virens) and whiting (Merlangius merlangus) during forced swimming". In: *Marine Biology* 148.1 (2005), p. 197.

[195] DM Webber, RG Boutilier, SR Kerr, and MJ Smale. "Caudal differential pressure as a predictor of swimming speed of cod (Gadus morhua)". In: *Journal of Experimental Biology* 204.20 (2001), pp. 3561–3570.

[196] DM Webber, GP McKinnon, and G Claireaux. "Evaluating Differential Pressure in the European Sea Bass (Dicentrarchus labrax) as a Telemetered Index of Swimming Speed". In: *Electronic tagging and tracking in marine fisheries*. Springer, 2001, pp. 297–313.

[197] Mukul Shrivastava, Malhar Malushte, Amit Agrawal, and Atul Sharma. "CFD Study on Hydrodynamics of Three Fish-Like Undulating Hydrofoils in Side-by-Side Arrangement". In: *Fluid Mechanics and Fluid Power–Contemporary Research*. Springer, 2017, pp. 1443–1451.

List of Figures

1.1 Examples of collective motion: (a) Fish milling, (b) the entrance crater to a nest of the ant (*Messor barbarus*), (c) traffic flow in Paris, (d) a bifurcation in a Pharaoh's ant trail, (e) mexican wave at an American football game, (f) a band of marching locusts [7]. 2
1.2 Fins and features of a fish [12]. Together, the anal and dorsal fins are referred to as median fins, whereas pectoral and pelvic fins are referred to as paired fins. 4
1.3 Average forces acting on a fish. 5
1.4 Propulsion mechanisms in aquatic swimming. (a) Thrust generation by the added-mass (reactive) mechanism. (b) Thrust generation by the lift-based (circulatory, vorticity) mechanism. F_A is the added-mass force, θ is the angle between the propulsive element and swimming direction, F_T is the thrust force and F_L is the lateral force [16]. 6
1.5 Classification of the BCF Mode[12] 7
1.6 (a) Bénard–von Karman (BvK) vortex street behind a circular cylinder and (b) reverse Bénard–von Karman (rBvK) vortex street behind a steady swimming fish. The average velocity profile, u, of the wake of a two-dimensional (2D) cylinder (c) average velocity profile, u, of wake of a 2D steady swimming fish [43]. 8
1.7 Kinematics of different BCF modes of swimming. (a) Anguilliform mode based on Anguilla, (b) Subcarangiform mode based on Lepomis, (c) Carangiform mode based on Scomber, and (d) Thunniform mode based on Euthynnus. (e) Midline envelope of Anguilliform swimming, (f) Midline envelope of subcarangiform swimming, (g) Midline envelope of Carangiform swimming, and (h) Midline envelope of thunniform swimming. The swimming speed is 1.8 BL/s [52]. 11
1.8 (a) Lateral line system in a fish, (b) canal neuromast (CN) and (c) superficial neuromast (SN) [63]. 13
1.9 Evolution of antipredator behaviour in Trinidadian guppies [79]. Males are represented by black circles, while females are represented by white circles. 16
1.10 Behavioural zones in a fish school. REP is the repulsion zone, ORI is the orientation zone and ATT is the attraction zone; r_r denotes the radius of the repulsion zone, r_a denotes the radii of the attraction zone and r_o denotes the radii of the orientation zone [103]. 18
1.11 Collective motion patterns in fish schools. (a) Swarming, (b) fish school, (c) milling pattern, (d) structure pattern [1]. 18

1.12 Different collective swimming phases observed by Filella et al. [101]. (a) swarming, (b) schooling, (c) milling, (d) turning 20
1.13 Phase diagram using the value of the polarisation P and milling M [101]. 20
1.14 Ideal diamond shape formation according to Weihs [112]. 22
1.15 (A) Cartwheel (also known as mill or torus), (B) surface-sheet, (C) dome or 'packed dome', (D) soldier (also known as phalanx), (E) mixed, (F) ball and (G) oriented shapes[121]. 23
1.16 Enhancement of flow between swimmers in a rectangular pattern due to the channelling effect [127]. 24
1.17 Three-dimensional (3D) wake structure by using q-criterion for a fish school in a rectangular pattern at lateral distances, $w = 0.3$ [127]. This clearly demostrates that the actual 3D wake structure of a fish is far more complex and non-coherent than the two-dimensional (2D) wake structure, as proposed in numerous studies. 25

2.1 Schematic diagram of the swimming channel. An external pump drives the flow, which is directed toward the test section after a convergent ramp and through a honeycomb section to minimise swirling motions. The test section is covered from the top by using acrylic plate. The two side cameras and one top camera is installed to track the fish. 28
2.2 Flow in the channel at the average flow velocity, (a) $U = 2.7cm/s$ and (b) $U = 15cm/s$ respectively. 28
2.3 (a) Velocity profile, u(y), in the x-direction at the mid-height and mid-section of the channel, which is flat and does not change with the flow rate. (b) Turbulence intensity (TI) as a function of the average flow velocity in the channel. It can be seen that the turbulence in the flow remains fairly constant over the flow rate range explored and stays below 5%. 29
2.4 Process of automated fish tracking and midline estimation. 31
2.5 Stereoscopic imaging system for three-dimensional (3D) tracking. . 33
2.6 DLT calibration method in experimental setup. As shown, the images with test pattern are taken at different height of known coordinates. . 35
2.7 Fish tail tip frequency, f and amplitude, A_r estimation. 36
2.8 Phase velocity, v_ϕ estimation. 37
2.9 Burst-and-coast time period estimation: (a) amplitude profile, A_r, (b) velocity profile, $\dot{A}_r$, of tail-beat undulation. 38
2.10 Internal frequency, F_i, estimation. 38

3.1 Midline kinematics (left) and time series of the tail tip amplitude, A_r, (right), for fish swimming at (a) 0.36 BL/s, (b) 1.26 BL/s, and (c) 3.0 BL/s. The burst-and-coast periods, T_B, and, T_C, in a swimming bout of duration, T_P, are indicated: grey bands in the background of the plots correspond to coasting time, white backgrounds correspond to bursting. 43

3.2 (a) Burst-and-coast event period, T_P, (b) duration of bursting with respect to the burst-and-coast event, where 1 means continuous flapping, (c) internal frequency (measured within a burst) and (d) tail-beat amplitude at the rear end of the caudal fin A_r, as a function of the average swimming velocity in body lengths per second. 44
3.3 (a) Curvature at profile, (b) average curvature value & (c) maximum curvature value as a function of swimming velocity, U. 47
3.4 (a) Length scale L_p during bout period (b) Length scale L_c during coast period as a function of swimming velocity, U. 48

4.1 (a): Example of top visualisation of two swimming fish. The school pattern is defined by the two characteristic length scales d and l, representing the distance to the nearest neighbour(s) and the shift between leading and following individuals, respectively. (b): superimposed instantaneous swimming kinematics (middle lines) extracted from the visualisation. The black lines are the spatial envelop fitted with the analytical function $A(x) = A_r \exp \alpha(x-1)$ [22]. The head of the fish is located on the right, the tip of the caudal fin on the left. 51
4.2 (a) Averaged beating frequency, f, and amplitude,A, (inset) for both top and bottom fish as a function of the swimming velocity averaged over the seven pairs studied. As can be seen here, fish frequencies are very close to each other and evolves linearly with U. L is the fish body length. (b) Strouhal number $St = \langle f \rangle \langle A \rangle / U$ and phase velocity v_ϕ (inset) as a function of the swimming speed U. (c) Typical lengths l and d defining the swimming pattern of a tandem of individuals as a function of the swimming speed. Again, the values are averaged over the seven pairs studied. The results show a constant value for both lengths, setting in average, a single spatial ordering for the tandem. . 53
4.3 Top: The two different state of synchronisation observed for a pair of swimming *H. bleheri*. The OP state corresponds to a configuration where both fish swim out-of-phase (a), the IP state to a configuration where both fish swim in-phase (b). 55
4.4 Two typical caudal fin tip kinematics for respectively slow (2.7 cm.s^{-1}, (a)) and fast (15 cm.s^{-1}, (b)) swimming velocities. Top and bottom fish are represented by blue and red lines, respectively. Phase difference plot for swimming velocities 2.7 cm s^{-1}, (b) and 15 cm s^{-1}, (d) respectively. 56

4.5 (a) Cumulated probability histograms of synchronisation over seven different fish pairs at different flow velocities. In each frame, the left bar represents the percentage of time where the fish were synchronised (**S**), in phase (black fill) or out of phase (white fill), over a 10 second recording of the swimming kinematics. The right bar is the time spent out of synchronisation (**NS**). The time series were analysed using the flapping frequency of one fish as the time base so that fish were considered synchronised at a given time only if they spent the full flapping period synchronised. (b) Plot showing the cumulative probability of synchronised state as a function of swimming speed. 58

4.6 Top row: Illustration of the three most probable swimming patterns for a three fish group of *H. bleheri*. Distances and angles between neighbours are kept constant. (a): two aligned fish are leading the pattern on the sides and the middle fish lies in the back. (b): one fish is leading the pattern on the side, the two other fish are shifted respectively from the other. (c): one fish is leading in the middle of the pattern, two aligned fish follow in the back. Bottom row: (d) occasionally observed schooling pattern evoking the diamond-like arrangement described in [112], two aligned fish are leading the pattern on the sides. This time the third fish is evolving in the wakes of the two firsts, changing the global organisation of the swimming pattern. 59

4.7 (a) Averaged beating frequency for the three fish (top, middle, bottom) as a function of the swimming velocity averaged over the seven trio of individuals studied, and amplitude in the inset. As for the two-fish case, respective frequencies are very close to each other and evolves linearly with U. (b) Strouhal number for the three fish (top, middle, bottom) as a function of the swimming velocity. (c) Typical distance to nearest neighbour and shift lengths l defining the swimming pattern of the trio of individuals as a function of the swimming speed. Again, the values are averaged over the seven pairs studied. . 61

4.8 (a)-(b) Cumulated probability histograms of synchronisation over seven different fish trios at different flow velocities. In each frame, the left bar represents the percentage of time where the fish were synchronised (**S**), in phase (black fill) or out of phase (white fill), over a 10 second recording of the swimming kinematics. The right bar is the time spent out of synchronisation (**NS**). (c) Plot showing the cumulative probability of a synchronised state between (1) top and middle fish and (2) middle and bottom fish, as a function of swimming speed. 62

4.9 The pressure field produced by the undulating midline calculated using Eq. 4.2 is shown in colour for the top fish, illustrating that the maximum of pressure fluctuations occurs before the end of the lateral line of the neighbouring fish (at the root of the caudal fin) because of the pattern chosen by the fish pair. 64

5.1 Characteristic swimming patterns for increasing fish group size at two different swimming speeds. Left column (a), (c), (e) (g): $U = 0.77BL.s^{-1}$. The school pattern is spread downstream with characteristic angles and distances to nearest neighbors (see text). Right column (b), (d), (f) (h): $U = 3.91BL.s^{-1}$. As more effort is required to hold a high swimming regime, the fish reorganize in a compact in-line formation. In this configuration, fish within the group are synchronized with their nearest neighbors, corresponding to collaborative efficient swimming modes. 71

5.2 Statistical properties of the fish schools as a function of swimming speeds over the whole range of cases studied. (a) Variation of the z-position of fish (h_z is the depth normalized by the fish average body height) as a function of swimming speed. Small black dots represent the instantaneous z-position of each fish, whereas orange squares represent average z-position, averaged over all groups. (b) and (c): Probability density of the nearest neighbor distance **NND** for low and high swimming speeds respectively. Insets show the probability density of nearest neighbor angles ϕ. (d): Probability density map of **NND** as a function of the swimming speed. (e): Percentage of occurrences of diamond-shaped **DS** (or T-shaped **TS**) and phalanx-shaped **PS** patterns. High speed swimmers are mainly characterized by phalanx patterns and short **NND** in comparison to low speed regimes. . 73

5.3 (a) Tail flapping frequency f (Hz), and (b) Tail flapping amplitude (non-dimensionalized by fish body length), as a function of the swimming velocity U (in body lengths per second). (c) Transverse Reynolds number, $Re_t = \langle f \rangle \langle A \rangle \langle L \rangle / \langle \nu \rangle$, as a function of the cruising Reynolds number, $Re_U = \langle U \rangle \langle L \rangle / \langle \nu \rangle$. (d) Evolution of the synchronisation parameter $s^* = S/(S+NS)$ that represents the cumulative probability of a synchronized state between nearest neighbors, as a function of the swimming velocity U. (e) Strouhal number, St, as a function of the swimming velocity U. 74

5.4 Examples of time series of the tail tip amplitude for one given individual (fish 2) within the school and its two nearest neighbors (fish 1 and fish 3). (a): For low swimming speed and (b): high swimming speed. The in-phase (IP) and out-of-phase (OP) swimming regimes are also shown. Evolution of the phase difference Υ between fish 2 and its two nearest neighbors (fish 1 and fish 3) showing (c) a non-synchronized state (NS) at low swimming speed and (d) strongly synchronized state (S) at high swimming speeds. The insets in (d) show zooms in the case of synchronised swimming that are either around 0 (for in-phase synchronization) or π (for out-of-phase synchronization). 75

6.1 Fish school of size , $N = 19$, at swimming velocities of (a) $U = 1BL/s$ and (b) $U = 3.5BL/s$. 84

6.2 (a), (b) and (c) Procedure of importing fish kinematics from direct observation to NACA0012. For reference, only tail tip kinematics are shown here, but the same procedure is applied at all 10 positions from the fish body to NACA0012. Pressure contour at different intervals of the flapping cycle for the HT mode: (d) $T^* = 0$, (e) $T^* = 0.5$, (f) $T^* = 1$ at $Re = 10,000$ 85

A.1 Probability histograms of synchronization of fish pair 1 at different flow velocities. The mean body length of pair1 is 33 mm. The ratio of body length of two fish(L1/L2) is 1.11, where l1 is body length of top fish and L2 is body length of bottom. 89

A.2 Probability histograms of synchronization of fish pair 2 at different flow velocities: The mean body length of pair2 is 28 mm. The ratio of body length of two fish(L1/L2) is 1.10, where l1 is body length of top fish and L2 is body length of bottom. 90

A.3 Probability histograms of synchronization of fish pair 3 at different flow velocities. The mean body length of pair3 is 30 mm. The ratio of body length of two fish(L1/L2) is 1.0, where L1 is body length of top fish and L2 is body length of bottom. 91

A.4 Probability histograms of synchronization of fish pair 4 at different flow velocities. The mean body length of pair4 is 30 mm. The ratio of body length of two fish(L1/L2) is 0.98, where L1 is body length of top fish and L2 is body length of bottom. 92

A.5 Probability histograms of synchronization of fish pair 5 at different flow velocities. The mean body length of pair5 is 29 mm. The ratio of body length of two fish(L1/L2) is 1.0, where L1 is body length of top fish and L2 is body length of bottom. 93

A.6 Probability histograms of synchronization of fish pair 6 at different flow velocities. The mean body length of pair6 is 34 mm. The ratio of body length of two fish(L1/L2) is 0.94, where L1 is body length of top fish and L2 is body length of bottom. 94

A.7 Probability histograms of synchronization of fish pair 7 at different flow velocities. The mean body length of pair7 is 31 mm. The ratio of body length of two fish(L1/L2) is 1.0, where L1 is body length of top fish and L2 is body length of bottom. 95

List of Tables

A.1 Characteristic distance 87
A.2 Number of flapping cycles used for calculating asynchronous and synchronous phase 87
A.3 Fish length ratio 88